Arctic Report Card 2018

Effects of persistent Arctic warming continue to mount

2018 Headlines

Effects of persistent Arctic warming continue to mount

Continued warming of the Arctic atmosphere and ocean are driving broad change in the environmental system in predicted and, also, unexpected ways. New emerging threats are taking form and highlighting the level of uncertainty in the breadth of environmental change that is to come.

Video

Highlights

- **Surface air temperatures** in the Arctic continued to warm at twice the rate relative to the rest of the globe. Arctic air temperatures for the past five years (2014-18) have exceeded all previous records since 1900.
- In the **terrestrial system**, atmospheric warming continued to drive broad, long-term trends in declining terrestrial **snow cover**, melting of the **Greenland Ice Sheet** and **lake ice**, increasing summertime Arctic **river discharge**, and the expansion and greening of Arctic tundra **vegetation**.
- Despite increase of vegetation available for grazing, herd populations of **caribou and wild reindeer** across the Arctic tundra have declined by nearly 50% over the last two decades.
- In 2018 Arctic **sea ice** remained younger, thinner, and covered less area than in the past. The 12 lowest extents in the satellite record have occurred in the last 12 years.
- Pan-Arctic observations suggest a long-term decline in **coastal landfast sea ice** since measurements began in the 1970s, affecting this important platform for hunting, traveling, and coastal protection for local communities.
- Spatial patterns of late summer **sea surface temperatures** are linked to regional variability in sea-ice retreat, regional air temperature, and advection of waters from the Pacific and Atlantic oceans.
- In the Bering Sea region, **ocean primary productivity** levels in 2018 were sometimes 500% higher than normal levels and linked to a record low sea ice extent in the region for virtually the entire 2017/18 ice season.
- Warming Arctic Ocean conditions are also coinciding with an expansion of **harmful toxic algal blooms** in the Arctic Ocean and threatening food sources.
- **Microplastic contamination** is on the rise in the Arctic, posing a threat to seabirds and marine life that can ingest debris.

Conservation of Arctic Flora and Fauna

December 2018

www.arctic.noaa.gov/Report-Card

Citing the complete report:
Osborne, E., J. Richter-Menge, and M. Jeffries, Eds., 2018: Arctic Report Card 2018, https://www.arctic.noaa.gov/Report-Card.

Citing an essay (for example):
Mudryk, L., R. Brown, C. Derksen, K. Luojus, B. Decharme, and S. Helfrich, 2018: Terrestrial Snow Cover [in Arctic Report Card 2018], https://www.arctic.noaa.gov/Report-Card.

Table of Contents

Executive Summary

E. Osborne[1], J. Richter-Menge[2], M. Jeffries[3]

[1]National Oceanic and Atmospheric Administration, Arctic Research Program, Silver Spring, MD, USA
[2]University of Alaska Fairbanks, Institute of Northern Engineering, Fairbanks, AK, USA
[3]Cold Regions Research and Engineering Laboratory of the Engineer Research and Development Center, U.S. Army Corps of Engineers, Hanover, NH, USA

In its 13th year, NOAA's Arctic Report Card (www.arctic.noaa.gov/Report-Card) reflects on a range of land, ice, and ocean observations made throughout the Arctic during the 2018 calendar year. A series of 14 essays written by more than 80 scientists from 12 countries are included in the 2018 Arctic Report Card. As in previous years, this update highlights the changes that continue to occur in, and among, the physical and biological components of the Arctic environmental system.

In 2018, surface air temperatures in the Arctic continued to warm at roughly twice the rate relative to the rest of the globe, a phenomenon that has been termed "Arctic Amplification." The year 2018 was the second warmest year on record in the Arctic since 1900 (after 2016), at +1.7° C relative to the long-term average (1981–2010). Arctic air temperatures for the past five years (2014–18) have exceeded all previous records since 1900. Growing atmospheric warmth in the Arctic results in a sluggish and unusually wavy jet stream that coincided with abnormal weather events in both the Arctic and mid-latitudes. Notable extreme weather events coincident with deep waves in the jet stream include the heat wave at the North Pole in autumn 2017, a swarm of severe winter storms in the eastern United States in 2018, and the extreme cold outbreak in Europe in March 2018 known as "the Beast from the East."

Continued warming of Arctic atmospheric temperatures in 2018 is an indicator of both regional and global climate change and a driver of broad Arctic environmental change. In the terrestrial system, atmospheric warming continued to drive broad, long-term trends in declining terrestrial snow cover, melting of the Greenland Ice Sheet and lake ice, increasing summertime Arctic river discharge, and the expansion and greening of Arctic tundra vegetation. Despite the growth of vegetation available for grazing land animals, herd populations of caribou and wild reindeer across the Arctic tundra have declined by nearly 50% over the last two decades.

As a result of atmosphere and ocean warming, the Arctic is no longer returning to the extensively frozen region of recent past decades. In 2018 Arctic sea ice remained younger, thinner, and covered less area than in the past. The wintertime maximum sea ice extent measured in March of 2018 was the second lowest in the 39-year record, following only 2017. For the satellite record (1979–present), the 12 lowest sea ice extents have occurred in the last 12 years. The disappearance of the older and thicker classes of sea ice are leaving an ice pack that is more vulnerable to melting in the summer, and liable to move unpredictably. When scientists began measuring Arctic ice thickness in 1985, 16% of the ice pack was very old (i.e., multiyear) ice. In 2018, old ice constituted less than 1% of the ice pack, meaning that very old Arctic ice has declined by 95% in the last 33 years. The pace and extent of the changes to summer sea ice cover, along with regional air temperatures and advection of waters from the Pacific and Atlantic oceans, are linked to the spatial patterns of late summer sea surface temperature. August mean sea surface temperatures in 2018 show statistically significant warming trends for 1982–2018 in most regions of the Arctic Ocean that are ice-free in August.

Later sea ice freeze-up and earlier ice break-up also have important implications for the extent and thickness of coastal landfast ice. This seasonal form of ice hardens and fastens to the coast. The direct connection to the coast makes landfast ice the most accessible form of sea ice and the one most often encountered by people. This ice platform is used for hunting and travel and plays a critical role buffering the coastal communities against the erosive action of strong winter storms. Pan-Arctic observations suggest a long-term decline in landfast ice since measurements began in the 1970s. Broad observations of Chukchi-bounded landfast ice along the North Slope of Alaska suggest an extent that is half as far offshore in the 2000s compared to the 1970s. A 16-year time series of landfast ice thickness within this region near Utqiaġvik (formerly Barrow) reveal a 30-cm thinning of ice since the year 2000.

One of the more remarkable features of Arctic sea ice in 2018 was the dearth of ice in the Bering Sea, which was at a record low extent for virtually the entire 2017/18 ice season. The reduced sea ice coverage and early break-up of ice had a profound effect on ocean primary productivity in 2018, particularly in the Bering Sea region where productivity levels were sometimes 500% higher than normal levels. Warming Arctic Ocean conditions are also coinciding with an expansion of harmful algae species responsible for toxic algal blooms in the Arctic Ocean. Considerable concentrations of algal toxins have been found in the tissues of Arctic clams, seals, walrus, and whales and other marine organisms. Impacts of the anticipated continued expansion of harmful algal blooms will be significant in a region where traditional monitoring programs for toxins in shellfish, fish, or other food sources are not feasible due to remote and expansive coastlines.

Another emerging threat of marine microplastics is taking form in the Arctic. A recent global survey of marine microplastics revealed that concentrations in the remote Arctic Ocean are higher than all other ocean basins in the world. Particularly high levels of microplastics are found in the Greenland and Barents seas in the northeastern Atlantic sector of the Arctic and point to the transportation and delivery of marine debris through global thermohaline ocean circulation. The handful of existing monitoring programs in the Arctic show microplastics contamination has increased over the last decade and pose a threat to seabirds and marine life that can become entangled or ingest debris.

The collective results reported in the 2018 Arctic Report Card show that the effects of persistent Arctic warming continue to mount. Continued warming of the Arctic atmosphere and ocean are driving broad change in the environmental system in predicted and, also, unexpected ways. New and rapidly emerging threats are taking form and highlighting the level of uncertainty in the breadth of environmental change that is to come. Long-term monitoring programs are critical to our understanding of baseline conditions and the magnitude and frequency of the changes that are being delivered to the Arctic. Such understanding is central to the livelihood of communities that call the Arctic home as well as the rest of the globe, which is already experiencing the changes and implications of a warming and melting Arctic.

Acknowledgments

Financial support for the Arctic Report Card is provided by the Arctic Research Program in the NOAA Climate Program Office. Preparation of Arctic Report Card 2018 was directed by the NOAA Arctic Research Program, with editorial assistance by researchers from the University of Alaska Fairbanks (via research sponsored by the Cooperative Institute for Alaska Research with funds from the NOAA Administration under cooperative agreement NA13OAR4320056 with the University of Alaska) and in kind support from the Office of Naval Research and the Cold Regions Research and Engineering Laboratory of the Engineer Research and Development Center, U.S. Army Corps of Engineers. The 14 contributions to Arctic Report Card 2018, representing the collective effort of an international team of

81 researchers in 12 countries, are based on published and ongoing scientific research. Independent peer review of the scientific content of Arctic Report Card 2018 was facilitated by the Arctic Monitoring and Assessment (AMAP) Program of the Arctic Council.

December 3, 2018

Surface Air Temperature

J. E. Overland[1], E. Hanna[2], I. Hanssen-Bauer[3], S. -J. Kim[4], J. E. Walsh[5], M. Wang[6], U. S. Bhatt[7], R. L. Thoman[8]

[1]NOAA/Pacific Marine Environmental Laboratory, Seattle, WA, USA
[2]School of Geography and Lincoln Centre for Water and Planetary Health, University of Lincoln, Lincoln, UK
[3]Norwegian Meteorological Institute, Blindern, Oslo, Norway
[4]Korea Polar Research Institute, Incheon, Republic of Korea
[5]International Arctic Research Center, University of Alaska Fairbanks, Fairbanks, AK, USA
[6]Joint Institute for the Study of the Atmosphere and Ocean, University of Washington, Seattle, WA, USA
[7]Geophysical Institute, University of Alaska Fairbanks, Fairbanks, AK, USA
[8]NOAA, National Weather Service, Alaska Region, Anchorage, AK, USA

Highlights

- The average annual surface air temperature over land north of 60° N for October 2017-September 2018 was the second warmest (after 2015-16) in the observational record beginning in 1900. Arctic temperatures for the past five years (2014-18) all exceed previous records.
- Arctic air temperature continues to increase at double the rate of the global mean air temperature increase.
- Relatively warm autumn, winter and spring months were related to an influx of heat and moisture from the subarctic, facilitated by north-south wavy jet stream patterns.
- During summer, neutral temperature anomalies occurred across the central Arctic Ocean and, like summer 2016 and 2017, did not support rapid summer sea ice and ice sheet loss.

Arctic surface air temperature is an indicator of both regional and global climate change. Although there are year-to-year and regional differences in air temperatures driven by natural variability, the magnitude, year-to-year persistence, and Arctic-wide character of recent temperature increases is a major indicator of global climate change and the concentration of atmospheric greenhouse gases (Overland, 2009; Notz and Stroeve, 2016). Warming atmospheric temperatures also act as the driver of broader Arctic change in the terrestrial and ocean spheres. A linear relationship between global temperature change and Arctic sea ice area decline and suggest direct forcing (Mahlstein and Knutti, 2012). Tundra and glacier responses also appear as forced changes from temperature increases. We report on the spatial and temporal variability of Arctic air temperatures during the period October 2017 through September 2018, the 12-month period since the end of the previous reporting period in Arctic Report Card 2017.

Mean Annual Land Surface Air Temperature

At +1.7° C, the mean annual surface air temperature (SAT) anomaly for October 2017-September 2018 for land stations north of 60° N is the second highest value (after 2016) in the record starting in 1900 (**Fig. 1**). Currently, the Arctic is warming at more than twice the rate of global mean temperatures; a phenomenon known as Arctic Amplification (**Fig. 1**). Recorded annual mean Arctic temperatures over the past five years (2014-18) all exceed previous records.

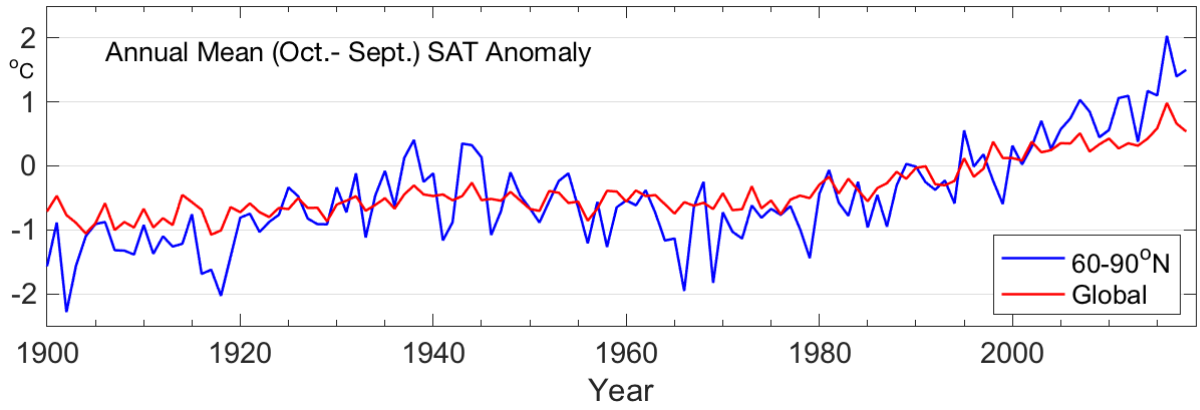

Fig. 1. Arctic (land stations north of 60° N) and global mean annual land surface air temperature (SAT) anomalies (in °C) for the period 1900-2018 relative to the 1981-2010 mean value. Note that there were few stations in the Arctic, particularly in northern Canada, before 1940. Source: CRUTEM4 dataset, which is available at www.cru.uea.ac.uk/cru/data/temperature/.

Currently there is no consensus on understanding the full reasons for Arctic amplification. Proposed mechanisms for Arctic amplification include: reduced summer albedo due to sea ice and snow cover loss; the increase of total water vapor content in the Arctic atmosphere; changes in cloudiness, and changes in pollution (Pithan and Mauritsen, 2014; Kim et al., 2017; Acosta Navarro et al., 2016; Dufour et al., 2016).

Air Temperature Variation

Seasonal air temperature variations are divided into autumn 2017 (October, November, December [OND]), and winter (January, February, March [JFM]), spring (April, May, June [AMJ]), and summer (July, August, September [JAS]) of 2018 (**Fig. 2**). These seasonal SAT divisions are chosen to coincide with the seasonal cycles of key Arctic variables: summer sea ice minimum occurs in September and autumn cooling continues through December.

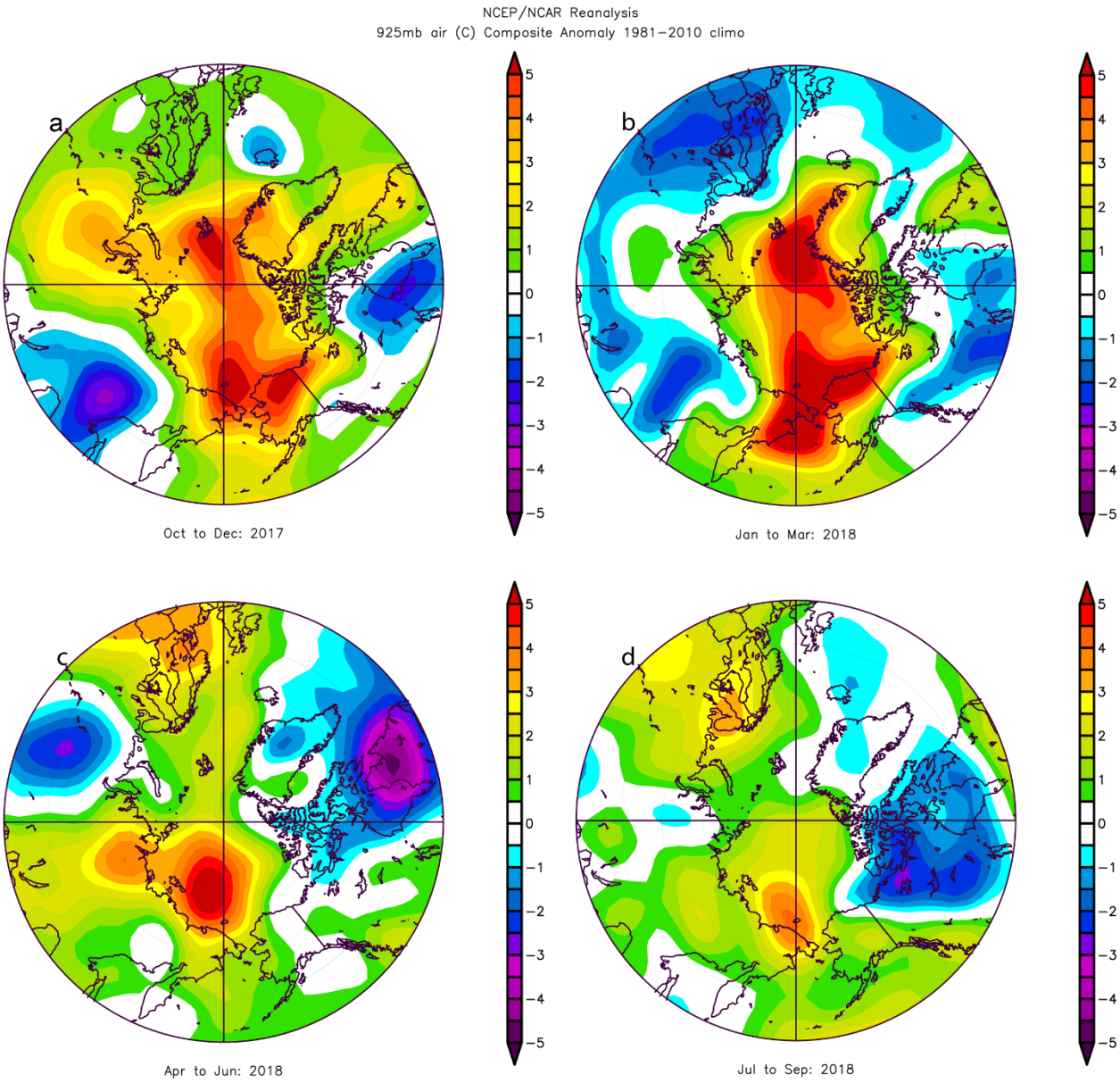

Fig. 2. Seasonal anomaly patterns for near-surface air temperatures (in °C) relative to the baseline period 1981-2010 in autumn 2017 (top left), winter 2018 (top right), spring 2018 (bottom left), and summer 2018 (bottom right). Temperature anomalies are from slightly above the surface layer (at 925 mb level) to emphasize large spatial patterns rather than local features. Data for this and the following figures are available from NOAA/ESRL, Boulder, CO, at https://www.esrl.noaa.gov/psd/.

All autumn, winter and spring months showed extensive central Arctic warm temperatures, often more than +4° C above the long-term norms (1981-2010). Large scale weather patterns in the central Arctic, such as the Arctic Oscillation (AO), were generally weak, while those of the subarctic (North Atlantic Oscillation [NAO] and Pacific North American [PNA]) had large values and month to month variability. As a result, large amounts of heat and moisture were transported northward into the Arctic. These weather patterns contributed to especially warm conditions between Greenland and Svalbard and in the Chukchi Sea. Summer 2018, similar to 2016 and 2017, had near-average air temperatures (relative to the 1981-

2010 climatology) associated with low pressure systems and extensive cloudiness. Details about the seasonal air temperature variations in 2018 are provided below.

Autumn 2017 (OND). A broad swath of extreme warm temperature anomalies (> +4° C) stretched across the central Arctic (**Fig. 2a**). The warmest temperature extremes, north of Bering Strait and near the North Pole on the Atlantic side, were due to a combination of local heating from extensive open water and advection of warm air from the Pacific and Atlantic oceans (see subarctic weather patterns, below). Over the land area, the extreme warm temperature anomalies over a large portion eastern Russia made the autumn 2017 the warmest season observed (**Fig. 2a**). The North Slope and western Alaska had the warmest autumn of record (since 1925). In Svalbard the temperature anomaly relative to 1981-2010 was +5° C. Eastern Asia and eastern North America had extensive spells of cold weather in December.

Winter 2018 (JFM). Winter continued with a similar central Arctic and regional temperature pattern as autumn (**Fig. 2b**), but the temperature anomaly over most of the land area tended to be near neutral. The northern Bering Sea and Svalbard were particularly warm, and contributed to low sea ice (see essay on *Sea Ice*). The temperature anomaly over Svalbard in January and February exceeded +7° C at most stations. Europe had particularly cold conditions in March, referred to as the "beast from the east." Finland and Norway had the coldest March during the last 5 years, northern Greenland was warm in February, and the UK had the coldest March day in 100 years.

Spring 2018 (AMJ). Spring (**Fig. 2c**) showed warm temperature anomalies especially in the East Siberian Sea, as also seen during 2017. This regional warming supported early sea ice loss in the Chukchi Sea (see essay on *Sea Ice*). Europe was particularly warm, while Iceland had cold and rainy conditions (Trausti Jonsson, Icelandic Met Office, pers. comm.) In May 2018, the mean temperature in Finland of +11.6° C was the highest in the instrumental record (dating from the early 1900s), which exceeds the previous record from 1963 by 0.5° C (Timo Vihma, Finnish Meteorological Institute, pers. comm.). The mean May temperature for Norway was the highest in the time series which starts in 1900, and 1.7° C above the previous record (from 2013). May 2018 was also record warm at all regular Svalbard meteorological stations, including the composite series from Longyearbyen, starting in 1898 (Nordli et al., 2014).

Summer 2018 (JAS). Like summer 2016 and 2017, summer 2018 contrasted with the warm conditions observed in much of the previous decade (**Fig. 2d**). Neutral anomalies occurred across the central Arctic in summer 2018, which did not support continued overall rapid summer sea ice loss (see essay on *Sea Ice*). The July temperature anomalies for the Spitsbergen stations Longyearbyen and Ny-Alesund were below +1° C, while the precipitation was record high. The east Siberian and Beaufort Seas were 3° C colder in July 2018 than in 2017. June and July 2018 Greenland temperatures were typically within 0.5 to 1° C over the long-term (1961-90) monthly means; not a notably warm summer by recent standards (see essay on *Greenland*). Scandinavia and eastern Asia had extensive warm spells. In July, the average temperature anomaly for Norway was +4° C while the precipitation anomaly was -40%. Norway and Sweden had extensive forest fires. Seoul in eastern Asia experienced a heat wave with 39° C during August.

Geopotential Heights and Resulting Regional Temperature Patterns

Atmospheric temperatures and pressures in 2018 provided additional evidence in support of Arctic-mid-latitude weather connections (see Frostbites essay on *Mid-latitude Weather*).

Warm temperature conditions in the Arctic in autumn 2017 through spring 2018 had a contribution from southerly winds (from the south) that advected warm moist air into the Arctic from the Atlantic and Pacific. This transport of warm, moist air was related to an active subarctic jet stream weather pattern that formed due to weak Arctic Oscillation (AO) conditions in the central Arctic during October through April (http://www.cpc.ncep.noaa.gov/products/precip/CWlink/daily_ao_index/ao.shtml). Weather patterns in the subarctic driven by the North Atlantic Oscillation (NAO) and Pacific North American (PNA) climate modes were active in 2018. The NAO was strongly positive December through June (except March), which resulted in deep Icelandic low pressures that drove a strong southerly wind pattern extending into the Arctic. These hemispheric atmospheric patterns are characterized by their wavy nature around a latitude circle and are quantified by the number of wave features at a given time along a latitudinal path.

Figure 3a shows the persistent pattern in the geopotential height field (used to characterize atmospheric wind circulation) for autumn months. Winds tend to follow the contours of geopotential heights counter-clockwise around low values. Autumn is characterized by a wave number three pattern (**Fig. 3a**) shown by the three centers of low geopotential height (dark purple regions). The southerly winds on the east side of each low geopotential height region brought warm air into the Arctic (north of Barents Sea, over Alaska, and on the west side of Greenland). From December 2017 to early January 2018, cold air from the Arctic was delivered to eastern Canada and USA resulting in extreme cold spells (**Fig. 3a**; see essay on *Mid-latitude Weather*). The rest of 2018 has shown greater month-to-month variability in wavy weather patterns.

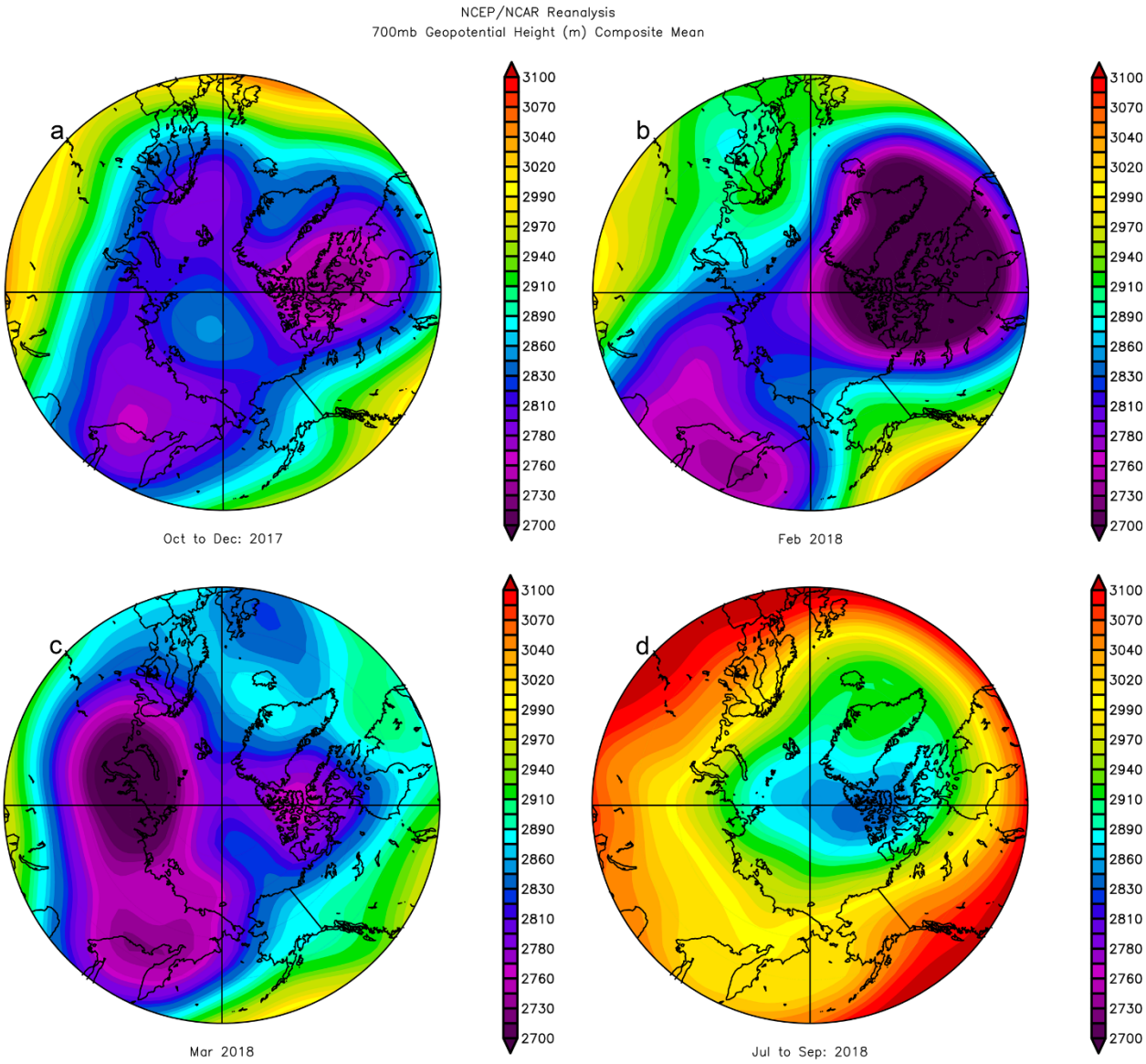

Fig. 3. The geopotential height pattern at 700hPa for selected 2017-18 months. a) autumn showing a wave number 3 atmospheric pattern, b) February 2018 with southerly flow from the Pacific to Bering Sea, which contributes to the warm anomalies there, c) a low geopotential height center in Europe and east Asia during March, d) low geopotential heights over the Arctic Ocean and subarctic North Atlantic characterized summer (July to September).

In February, there was a reduction in low pressure zones and a shift to a wave number two pattern (**Fig 3b**). Strong warm winds from the south over the Bering Sea related to a strong wavy jet stream pattern over Alaska that greatly retarded sea ice extent (see essay on *Sea Ice*) and moved warm air northward along the date line into the central Arctic. In March (**Fig. 3c**) the large scale pattern shifted to a wave number one pattern with low geopotential heights over Asia and western Russia and higher geopotential heights over North America and Greenland. The gradient between geopotential heights in central Eurasia and Scandinavia produced strong northerly winds and severe cold weather over Europe, a weather abnormality called the "Beast from the East" (see essay on *Mid-latitude Weather*).

Summer was characterized by low geopotential heights in the central Arctic (**Fig 3d**), which prevented atmospheric mid-latitude heat from penetrating into the central Arctic. This condition in summer 2018

differed from previous years and associated low sea-ice summers and contributed to a slowing of the sea ice loss in summer 2018 (see essay on *Sea Ice*). Low central Arctic pressure also resulted in widespread cloud cover as seen in satellite observations that limited the solar heating of the lower atmosphere in the central Arctic. Again, this is a pattern differed from recent previous years and was instead similar to the predominant pattern in 1996, which was a high summer sea ice extent year.

References

Acosta Navarro, J. C., V. Varma, I. Riipinen, Ø. Seland, A. Kirkevåg, H. Struthers, T. Iversen, H. -C. Hansson, and A. M. L. Ekman, 2016: Amplification of Arctic warming by past air pollution reductions in Europe. *Nat. Geosci.*, 9, 277-281.

Dufour, A., O. Zolina, and S. K. Gulev, 2016: Atmospheric moisture transport to the Arctic. *J. Clim.*, 29, 5061-5081.

Kim, B. -M., S. -W. Son, S. -K. Min, J. -H. Jeong, S. -J. Kim, X. Zhang, T Shim, and J. -H. Yoon, 2014: Weakening of the stratospheric polar vortex by Arctic sea-ice loss. *Nat. Commun.*, 5, 4646, doi: 10.1038/ncomms5646.

Kim, B. -M., J. -Y. Hong, S. -Y. Jun, X. Zhang, H. Kwon, S. -J. Kim, J. -H. Kim, S. -W. Kim, and H. -K. Kim, 2017: Major cause of unprecedented Arctic warming in January 2016: Critical role of Atlantic windstorm. *Sci. Rep.*, 7, 40051, doi: 10.1038/srep40051.

Mahlstein, I., and R. Knutti, 2012: September Arctic sea ice predicted to disappear near 2° C global warming above present. *J. Geophys. Res. Atmos.*, 117, D06104, doi: 10.1029/2011JD016709.

Nordli, Ø., R. Przybylak, A. E. J. Ogilvie, and K. Isaksen, 2014: Long-term temperature trends and variability on Spitsbergen: The extended Svalbard Airport temperature series, 1898-2012. *Polar Res.*, 33(1), 21349, doi: 10.3402/polar.v33.21349.

Notz, D., and J. Stroeve, 2016: Observed Arctic sea-ice loss directly follows anthropogenic CO_2 emission. *Science*, 354, 747-750, doi: 10.1126/science.aag2345.

Overland, J. E., 2009: The case for global warming in the Arctic, in *Influence of Climate Change on the Changing Arctic and Sub-Arctic Conditions.* J. C. J. Nihoul and A. G. Kostianoy, Eds., Springer, pp. 13-23.

Pithan, F., and T. Mauritsen, 2014: Arctic amplification dominated by temperature feedbacks in contemporary climate models. *Nat. Geosci.*, 7, 181-184, doi: 10.1038/ngeo2071.

November 23, 2018

Terrestrial Snow Cover

L. Mudryk[1], R. Brown[1], C. Derksen[1], K. Luojus[2], B. Decharme[3], S. Helfrich[4]

[1]Climate Research Division, Environment and Climate Change Canada, Canada
[2]Arctic Research Centre, Finnish Meteorological Institute, Finland
[3]Centre National de Recherches Météorologiques, France
[4]NOAA/NESDIS Center for Satellite Applications and Research, USA

Highlights

- Snow accumulation during the 2017/18 winter was well above average across the Eurasian Arctic, consistent with an early start to the snow season. North American Arctic snow accumulation was near normal until May and June when what snow remained was generally deeper than usual for the time of year.
- Snow cover extent for Eurasia was above average during April, slightly above average for May, and below average by June (relative to the 1981-2010 average). This month-to-month change is consistent with unusually high early spring accumulation combined with rapid late spring snow loss.
- Despite relatively high spring snow accumulation and snow cover extent over the Arctic during the previous two spring seasons, long-term trends remain negative.

Snow covers the Arctic land surface (land areas north of 60° N) for up to 9 months each year, and influences the surface energy budget, ground thermal regime, and freshwater budget of the Arctic. Snow also interacts with vegetation, affects biogeochemical activity, and influences migration and access to forage for wildlife, with consequences for ecosystems. Previous assessments in the Arctic Report Card using a combination of data from satellites and snow models show that over the past 15 years snow has melted from the land surface earlier in the spring (April, May, June) with a shallower snowpack compared to past decades. Inter-annual variability within these trends is high due to competing influences of temperature and precipitation.

Snow across the Arctic land surface can be characterized using three variables: how much area is covered by snow (snow cover extent - SCE), how long snow continuously remains on the land surface (snow cover duration - SCD), and how much water is stored in solid form by the snowpack (a function of the snow depth and density, commonly expressed as snow water equivalent - SWE).

SCE anomalies (relative to the 1981-2010 climatology) for the Arctic in spring 2018 were computed separately for the North American and Eurasian sectors of the Arctic. Anomalies were derived from the NOAA snow chart climate data record, which extends from 1967 to present (maintained at Rutgers University; Estilow et al., 2015; http://climate.rutgers.edu/snowcover/; **Fig. 1a-c**). Eurasian Arctic spring SCE in 2018 was above average in April, only slightly positive in May, and by June the anomalies were negative with respective to the historical average. SCE anomalies over the North American Arctic were negative for May and June but did not approach the series of record-breaking low SCE values observed in recent years.

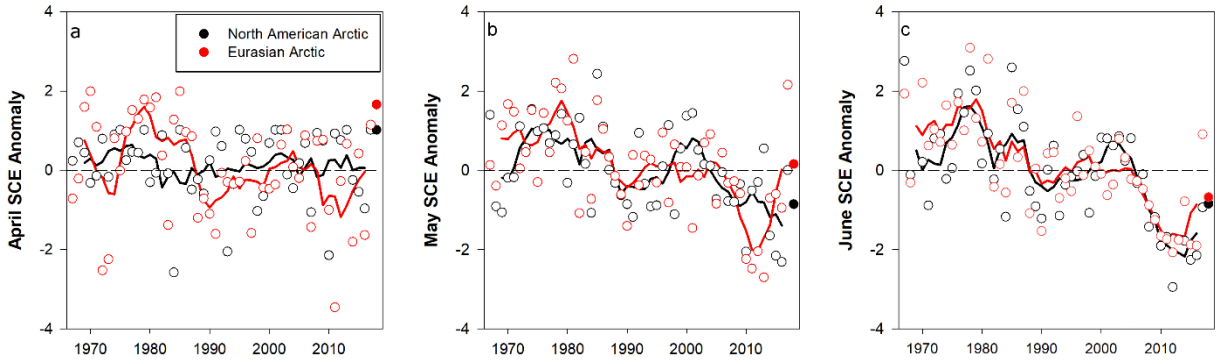

Fig. 1. Monthly snow cover extent (SCE) for Arctic land areas (>60° N) for (a) April, (b) May, and (c) June from 1967 to 2016. Anomalies are relative to the average for 1981-2010 and standardized (each observation differenced from the mean and divided by the standard deviation and thus unitless). Solid black and red lines depict 5-yr running means for North America and Eurasia, respectively. Filled circles are used to highlight 2018 anomalies. Source: NOAA snow chart Climate Data Record (CDR).

SCD anomalies (**Fig. 2**) were derived from the NOAA daily Interactive Multisensor Snow and Ice Mapping System (IMS) snow cover product (Helfrich et al., 2007). The IMS data are used to determine SCD due to the increased temporal and spatial resolution of the product. Snow cover onset (**Fig. 2a**) was normal to slightly earlier than normal over most of the Arctic. Snow-off (**Fig. 2b**) was slightly later than normal over large regions of Eurasia and over Alaska but slightly earlier over the central Canadian Arctic.

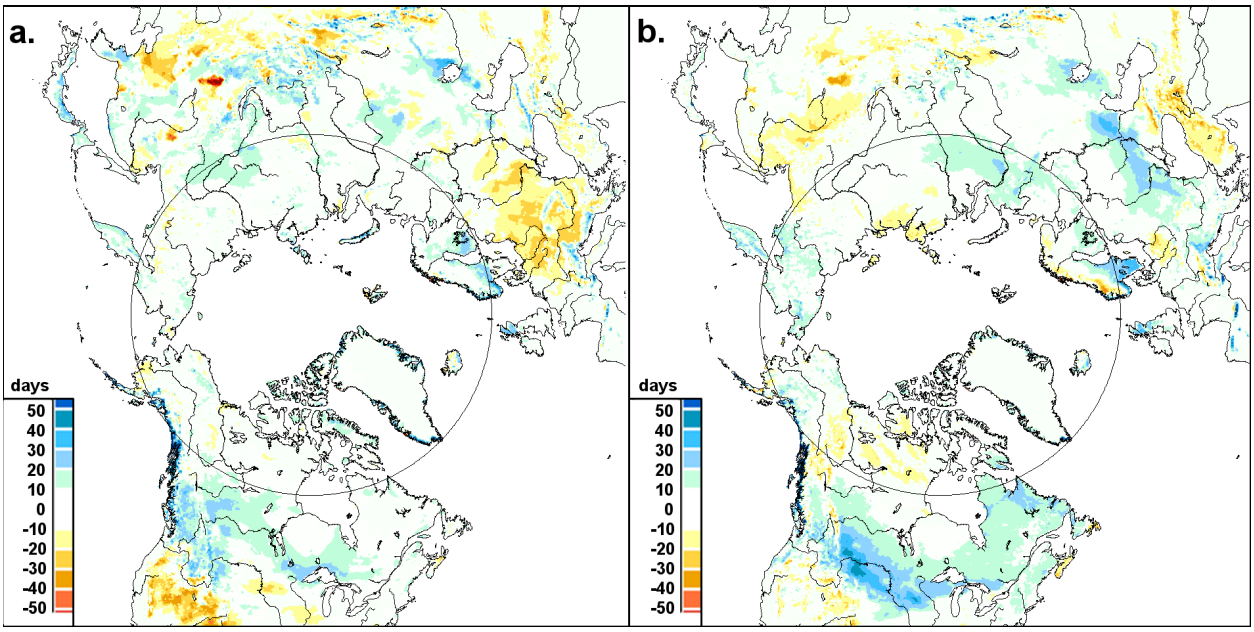

Fig. 2. Snow cover duration (SCD, in days) anomalies (difference from 1998-2010 mean) for the 2017/18 snow year: (a) snow onset (Aug-Jan); and (b) snow melt (Feb-Jul). The grey circle marks the latitude 60° N; land north of this defines Arctic land areas considered in this study. Source: NOAA IMS data record.

Snow depth anomalies (**Fig. 3**) were derived from the Canadian Meteorological Centre (CMC) daily gridded global snow depth analysis (Brasnett, 1999). The CMC snow depth product relies on air temperature analyses and precipitation forecasts but also includes assimilation of in situ snow depth

observations. This type of product is required to obtain hemispheric estimates of snow depths as in situ observations are too temporally and spatially sparse to be representative. These data indicate that in the 2017/18 snow season, anomalously high snow depths in the Arctic and subarctic boreal zone of Eurasia were established in November 2017 (not shown) and persisted throughout the winter. As a result, April 2018 Eurasian Arctic anomalies averaged 60% above normal and remained above average through June 2018. The North American Arctic saw a mix of positive and negative snow depth anomalies in March and April 2018, but what snow remained by May and June 2018 was generally deeper than average for the time of year.

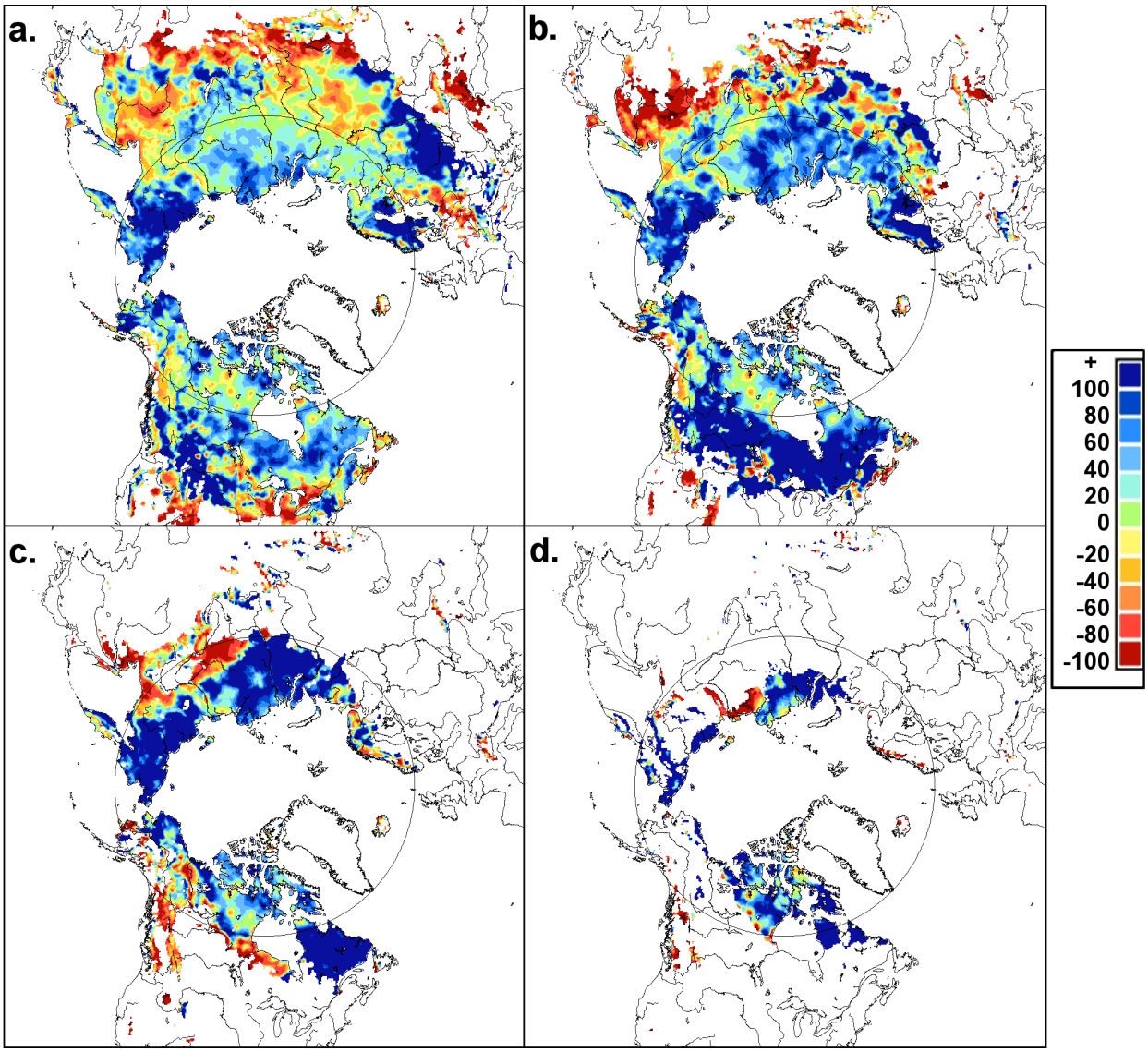

Fig. 3. Snow depth anomaly (% of the 1999-2017 average) in 2018 for (a) March, (b) April, (c) May, and (d) June. The grey circle marks the latitude 60° N. Source: CMC snow depth analysis.

Four products were utilized to generate a multi-dataset SWE anomaly time series (1981-2018) for April (typically the month of maximum SWE across the Arctic; **Fig. 4**): (1) modern atmospheric reanalysis (The Modern-Era Retrospective Analysis for Research and Applications version 2; MERRA-2; Reichle et al., 2017); (2) reconstructed snow accumulation driven by ERA-interim meteorology with the temperature index model described by Brown et al. (2003); (3) the physical snowpack model Crocus (Brun et al.,

2013); and (4) the European Space Agency GlobSnow product derived through a combination of satellite passive microwave data and climate station observations (Takala et al., 2011). As for snow depth, analyses of this type are required to obtain representative gridded estimates of SWE; several products were used in order to characterize their spread. SWE estimates for 2018 indicated the highest amount of SWE since 1981 over the Eurasian Arctic, consistent with the high Arctic snow depth anomalies seen in the CMC analysis. North American Arctic SWE anomalies varied slightly among the products, but on average were close to normal.

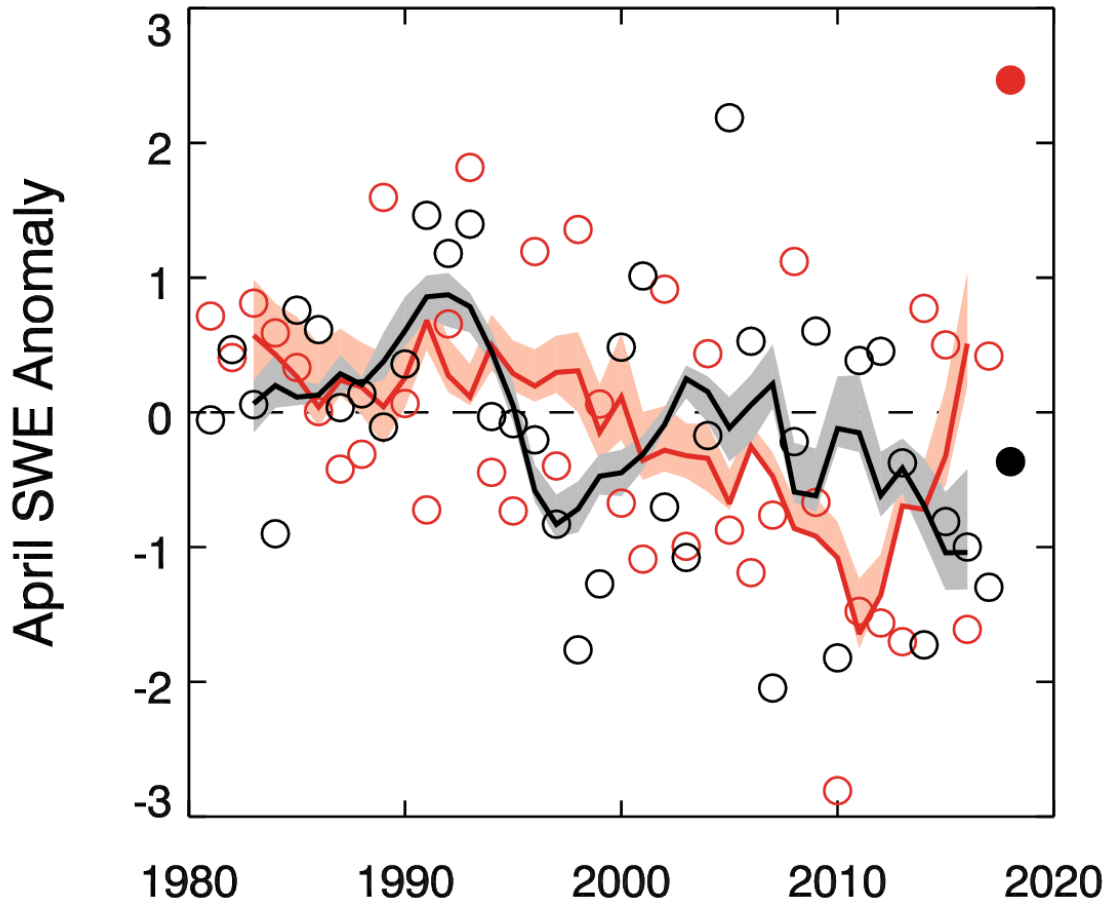

Fig. 4. Mean April SWE anomalies for Arctic land areas calculated for North American (black) and Eurasian (red) sectors of the Arctic. Anomalies are relative to the average for 1981-2010 and standardized (each observation differenced from the mean and divided by the standard deviation and thus unitless). Filled circles are used to highlight 2018 anomalies. Solid black and red lines depict 5-yr running means for North America and Eurasia, respectively; the spread among the running means for individual datasets is shown in shading. Source: suite of four independent snow analyses as described in text.

In summary, snow accumulation during the 2017/18 winter was well above average across the Eurasian Arctic (**Figs. 3** and **4**) with the highest level of Eurasian Arctic SWE seen since 1981. This is consistent with an early start to the snow season (and hence a longer period over which accumulation occurred;

Fig. 2) and suggests the occurrence of above-average winter snowfall. Snow accumulation over the North American Arctic was close to normal in March and April with remaining regions of anomalously deep snow by May and June. The above average snow accumulation remaining in late spring (May and June) may have contributed to above average river discharge seen over both continents (see essay on *River Discharge*). During early spring, the above average snow accumulation was also expressed as positive SCE anomalies in April, but snow cover extent reduced quickly during May and June (reflected in the transition to negative SCE anomalies over both North America and Eurasia; **Fig. 1**). Where snow remained on the ground in these months, it was unusually deep, as indicated by strongly positive snow depth anomalies in the CMC product (**Fig. 3**).

Despite anomalously high SCE during the 2017 melt season and anomalously high SWE during the 2018 melt season (both primarily observed over the Eurasian continent), long-term trends for both SCE and SWE remain negative. The trends in Arctic SCE over the 1981-2018 period are -0.1%/decade, -3.4%/decade, and -14.9%/decade for April, May, and June, respectively. The April trend in Arctic SWE over the 1981-2018 period is -2.5%/decade, yielding a decrease of about 10% over the entire Arctic since 1981. The loss of spring snow cover in June is approximately the same magnitude as September sea ice extent loss. April SWE trends (near the timing of Arctic SWE maximum) are weaker because they are less sensitive to temperature increases than SCE and more strongly influenced by precipitation trends.

References

Brasnett, B., 1999: A global analysis of snow depth for numerical weather prediction. *J. Appl. Meteorol.*, 38, 726-740.

Brown, R., B. Brasnett, and D. Robinson, 2003: Gridded North American monthly snow depth and snow water equivalent for GCM evaluation. *Atmos.-Ocean.*, 41, 1-14.

Brun, E., V. Vionnet, A. Boone, B. Decharme, Y. Peings, R. Valette, F. Karbou, and S. Morin, 2013: Simulation of Northern Eurasian local snow depth, mass, and density using a detailed snowpack model and meteorological reanalyses. *J. Hydrometeorol.*, 14, 203-219, doi: 10.1175/JHM-D-12-012.1.

Estilow, T. W., A. H. Young, and D. A. Robinson, 2015: A long-term Northern Hemisphere snow cover extent data record for climate studies and monitoring. *Earth Syst. Sci. Data*, 7, 137-142.

Helfrich, S., D. McNamara, B. Ramsay, T. Baldwin, and T. Kasheta, 2007: Enhancements to, and forthcoming developments in the Interactive Multisensor Snow and Ice Mapping System (IMS). *Hydrol. Process.*, 21, 1576-1586.

Reichle, R., C. Draper, Q. Liu, M. Girotto, S. Mahanama, R. Koster, and G. De Lannoy, 2017: Assessment of MERRA-2 land surface hydrology estimates. *J. Clim.*, 30, 2937-2960, doi: 10.1175/JCLI-D-16-0720.1.

Takala, M., K. Luojus, J. Pulliainen, C. Derksen, J. Lemmetyinen, J. -P. Kärnä, and J. Koskinen, 2011: Estimating northern hemisphere snow water equivalent for climate research through assimilation of space-borne radiometer data and ground-based measurements. *Remote Sens. Environ.*, 115, 3517-3529.

November 28, 2018

Greenland Ice Sheet

M. Tedesco[1,2], J. E. Box[3], J. Cappelen[4], R. S. Fausto[3], X. Fettweis[5], J. K. Andersen[3], T. Mote[6], C. J. P. P. Smeets[7], D. van As[3], R. S. W. van de Wal[7]

[1]Lamont Doherty Earth Observatory of Columbia University, Palisades, NY, USA
[2]NASA Goddard Institute of Space Studies, New York, NY, USA
[3]Geological Survey of Denmark and Greenland, Copenhagen, Denmark
[4]Danish Meteorological Institute, Copenhagen, Denmark
[5]University of Liege, Liege, Belgium
[6]Department of Geography, University of Georgia, Athens, Georgia, USA
[7]Institute for Marine and Atmospheric Research Utrecht, Utrecht University, Utrecht, The Netherlands

Highlights

- Estimates of the spatial extent of melt across the Greenland ice sheet (GrIS) were unexceptional for most of the summer (i.e., June, July, August) melt season of 2018.
- Surface ice mass balance for the 2017/18 season was below or near the long-term mean (relative to the period 1961-90), consistent with a snow cover that survived late into the spring and average/low surface melting during summer.
- Summer 2018 albedo (a measure of surface reflectivity), averaged over the whole ice sheet, tied with the record high set in 2000 for the 2000-18 period. Relatively high albedo was associated with the reduced surface melting and extended survival of the snow cover, which reduced the exposure of darker, bare ice.
- Surface air temperatures set new high records in winter (up to +14.4° C above the mean) and low records in summer (-46.3° C at Summit).

The Greenland ice sheet plays a crucial role on our planet and in the Arctic. The high albedo (i.e., the fraction of incident solar radiation reflected by a surface) of the ice sheet contributes to modulating the amount of solar energy absorbed by the Earth and controls atmospheric circulation because of its location and topography. Moreover, Greenland represents a major contributor to current and projected sea level rise, through surface runoff and calving.

Surface Melting

Estimates of the spatial extent of melt across the Greenland ice sheet (GrIS) were unexceptional for most of summer melt season of 2018. Observations derived from brightness temperatures (a measure of a body's natural radiance) measured by the Special Sensor Microwave Imager/Sounder (SSMIS) passive microwave radiometer (e.g., Mote, 2007; Tedesco et al., 2013), indicated that melt extent exceeded (i.e., conditions were warmer) by one standard deviation in early June and again briefly in late July and early August (**Fig. 1a**). During the middle of the season, from mid-June to mid-July, the spatial extent of melting remained largely within the interquartile range of the 1981-2010 mean. The spatial extent of melt for the period of June, July, and August (JJA) 2018 was above average on only 26% of the summer days. During the same period of 2017, another low melt year, only 16% of days were above the average. Surface melt reached its maximum extent in 2018 (44%) on 31 July (**Fig. 1a**), compared to an average maximum extent of 39.8% (standard deviation of 14.9%) over the summer. Compared to

previous summers, melt duration was within ±5 days of the mean for most of the ice sheet. There were notable exceptions in the southwest portion and along a thin margin in the northeast of the ice sheet, where melting was more frequent than the 1981-2010 mean (**Fig. 1b**) by more than 5 days.

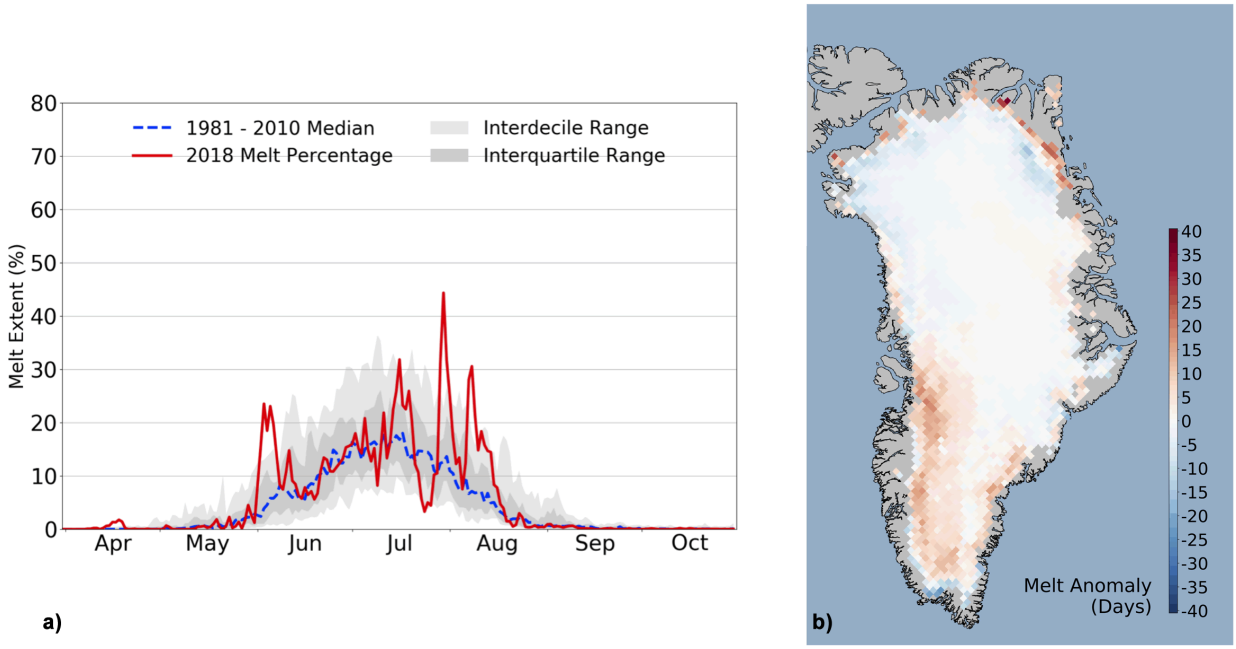

Fig. 1. a) SSMIS-derived surface melt area as a percentage of the ice sheet area during 2018 (solid red), in addition to the 1981-2010 average (dashed blue) and interdecile and interquartile ranges (shaded) b) melt anomaly (in number of melting days) with respect to the 1981-2010 period during the summer of 2018 estimated from spaceborne passive microwave observations.

Surface Ice Mass Balance

Net ice ablation (i.e., loss) in 2018, measured at 18 Program for Monitoring of the Greenland Ice Sheet (PROMICE, https://www.promice.dk/home.html) sites, was on average the lowest during the 2008-18 observational period (**Fig. 2a**). The southern and northern Greenland ice sheet margin (sites KPC: 79.91° N, 24.08° W; THU: 76.39° N, 68.26° W; and QAS: 61.03° N, 46.84° W) experienced the most negative anomalies (least ablation) spanning 1.3-1.9 standard deviations below the 2008-18 mean, while ablation at the other sites was within 1 standard deviation. The observed ablation values from the lower PROMICE stations, referenced to the 1961-90 climate-standard period, showed that anomalies at the KPC and THU sites were the most negative (least ablation), beyond methodological uncertainty (van As et al., 2016). Only two of eight sites (NUK: 64.48° N, 49.53° W and KAN: 67.12° N, 50.18° W) experienced above-average ablation, though not beyond methodological uncertainty.

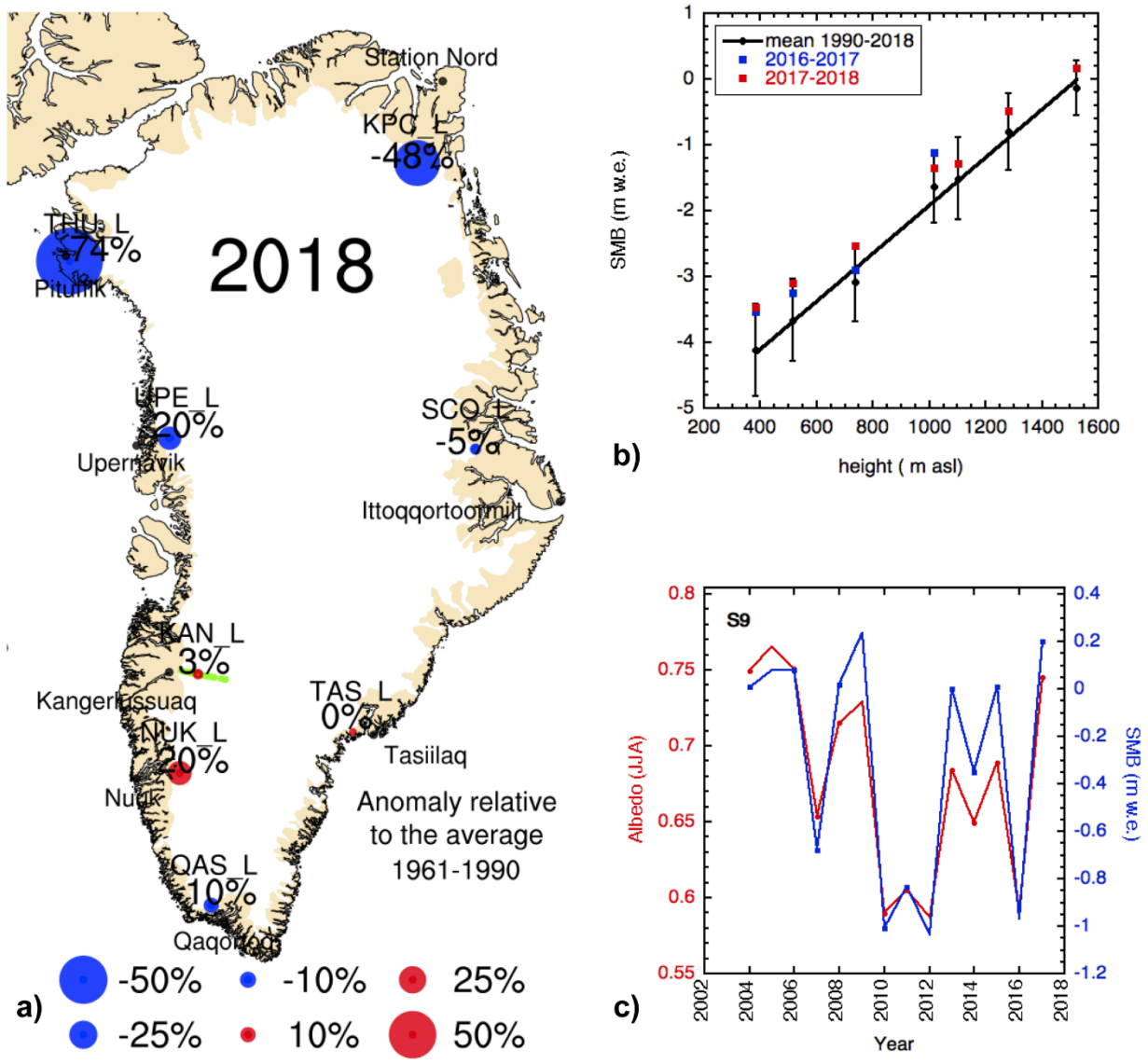

Fig. 2. a) Ablation anomalies for 2018 at lower ("L") PROMICE weather station sites over the Greenland ice sheet ablation area, referenced to the 1961-90 period following the approach by van As et al. (2016). b) The surface mass balance as a function of elevation along the K-transect (shown as a green line nearby the KAN_L station) for the period 2017-18 and the mean over the period 1990-2018. The error bars are the standard deviation over the period 1990-2018. c) Summer surface mass balance (blue) and albedo (red) at the S9 station (67° 03' N, 48° 13' W, ~1500 m above sea level) along the K-transect.

The mass balance year 2017/18 along the K-transect (van de Wal et al., 2012) is characterized by moderate ablation over the entire ablation region (e.g., where net mass loss occurs). All sites show a surface mass balance within one standard deviation from the 1990-2018 mean, with a tendency of ablation being below the mean (**Fig. 2b**). The average surface mass balance over the K-transect for 2017/18 is nearly identical to the average over the season 2016/17. Overall, surface ice mass balance for the 2017/18 season was below or near the long-term mean (relative to the period 1961-90), consistent with a snow cover that survived late into the spring and average/low surface melting during summer.

Total Ice Mass Balance

GRACE satellite data can be used to estimate monthly changes in the total mass of the Greenland ice sheet, as done in the past (e.g., Tedesco et al., 2017). However, the NASA GRACE mission, which started in 2002, ended in October 2017. Hence, there are no data available on the total mass balance for the 2017/18 season. The GRACE Follow On (GRACE-FO, https://gracefo.jpl.nasa.gov/) mission was launched on 22 May 2018. Data acquired since its launch are currently under review for quality control. The May 2018 launch means that no data are available from space between October 2017 and May 2018. Processing of the GRACE-FO dataset will provide estimates of total mass change anomalies for the summer of 2018 and will be calibrated to data acquired by GRACE.

Albedo

The summer (JJA) 2018 albedo averaged over the whole Greenland ice sheet was 81.7% (**Fig. 3a**), as estimated from the Moderate Resolution Imaging Spectroradiometer (MODIS; after Box et al., 2017). The 2018 summer albedo is tied with 2000 for the highest value recorded during the 19-year MODIS period of observation (i.e., 2000-18). The months of June and July had record high albedo. The high albedo anomalies along most of the coastline (**Fig. 3b**) are consistent with reduced melting in summer 2018, which resulted in late surviving snow over the darkest bare ice areas. The minimum average summer albedo was recorded in 2012 (76.8%), the year of record maximum melt extent. Albedos have been relatively high since 2012. Consistently with MODIS estimates, measurements at the S9 K-transect station show higher than usual albedo values (**Fig. 2c**), which are also strongly correlated with the surface mass balance values measured at the same location. In summary, summer 2018 albedo, averaged over the whole ice sheet, was relatively high for the 2000-18 period, matching the value of the record high set in 2000.

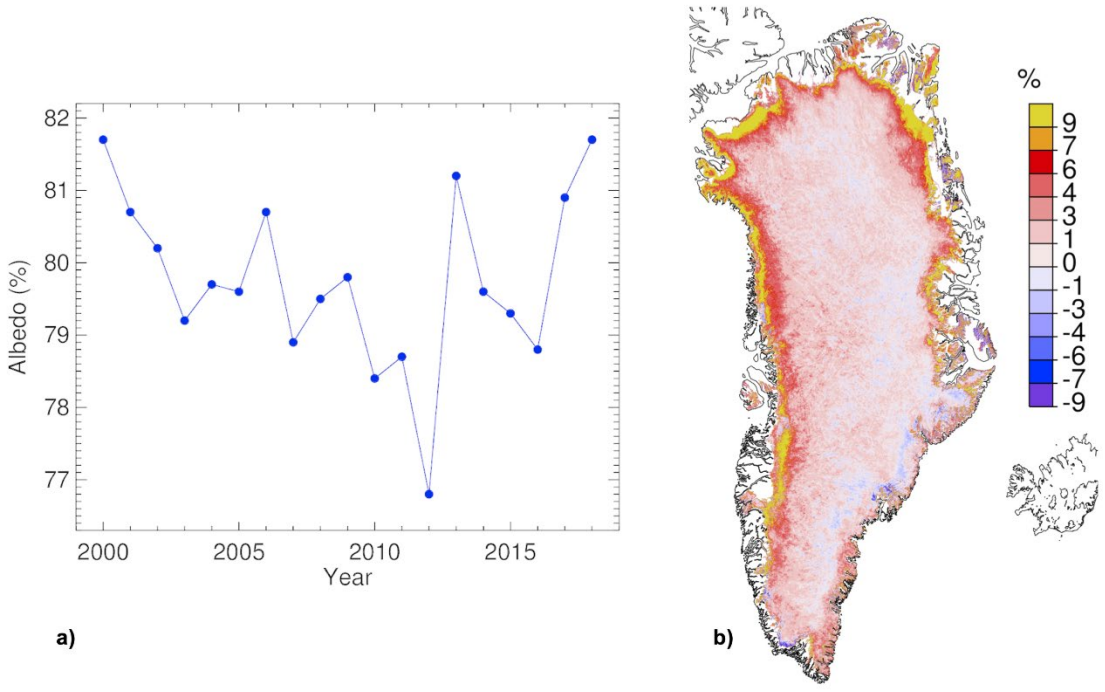

Fig. 3. (a) Time series summer (JJA) albedo averaged over the entire ice sheet. (b) Map of the summer 2018 albedo anomaly relative to the 2000-2009 reference period.

Surface Air Temperature

Measurements at 20 weather stations of the Danish Meteorological Institute (DMI, Cappelen, in prep.) indicate widespread above or near-average air temperatures for autumn 2017 and winter 2017/18, relative to the average for the period 1981-2010. Some record highs were set for winter and also in some individual winter months (**Table 1**). At Station Nord, the world's northernmost station, temperatures at Kap Morris Jesup were remarkably warm in February, reaching up to +14.4° C above the mean; an absolute temperature of +6.2° C was reached on 25 February. Spring 2018 was generally near average except in some places along eastern Greenland, where temperatures were above normal. Summer 2018 was generally colder or near average. A new record-breaking high temperature of +17° C was measured at Kap Morris Jesup on 3 August, surpassing the previous one of +15.4° C set on 5 August 1991. At Summit, the highest point on the ice cap, autumn 2018 was the third warmest, after 1993 and 2002. A new record-breaking cold temperature record, -46.3° C, was measured at Summit on 9 May, close to the previous one of -45.6° C set on 1 May.

Table 1. Surface temperature anomalies [°C] and z-scores at twenty DMI stations for the periods of autumn 2017 (SON), winter (DJF) 2017-2018, spring (MAM) 2018 and summer (JJA) 2018. Station names, together with the year in which observations began and the corresponding coordinates are also reported, along with the years when maximum and minimum records were set. Highlighted text indicates the stations and periods when a new record was set.

Station Name, Start Year, Latitude, Longitude		SON 2017	DJF 17/18	MAM 2018	JJA 2018
Pituffik/Thule AFB 1948, 76.5° N, 68.8° W	Anomaly [°C]	1.4	2.7	-0.9	-0.4
	z-score	0.9	0.9	-0.8	-0.4
	Max Year	2010	1986	1953	1957
	Min Year	1964	1949	1992	1996
Station Nord 1961, 81.6° N, 16.7° W	Anomaly [°C]	2.2	6.3	0.6	-1.1
	z-score	1.2	2.7	0.6	-0.8
	Max Year	2016	**2018**	2006	2003
	Min Year	1989	1967	1961	1970
Upernavik 1873, 72.8° N, 56.1° W	Anomaly [°C]	0.7	2.2	-0.2	-1.6
	z-score	0.7	0.7	-0.2	-0.7
	Max Year	2010	1947	1932	2012
	Min Year	1917	1983	1896	1873
Kangerlussuaq 1949, 67.0° N, 50.7° W	Anomaly [°C]	0.7	-0.2	-0.2	-0.2
	z-score	0.4	-0.2	-0.1	-0.5
	Max Year	2010	1986	2016	1960
	Min Year	1982	1983	1993	1983
Ilulissat 1807, 69.2° N, 51.1° W	Anomaly [°C]	0.5	1.0	0.5	-1.6
	z-score	0.8	0.6	0.3	-0.7
	Max Year	2010	1929	1847	1960
	Min Year	1837	1863	1813	1863
Aasiaat 1958, 68.7° N, 52.8° W	Anomaly [°C]	0.8	1.8	0.9	-0.8
	z-score	0.9	0.2	0.3	-0.7
	Max Year	2010	2010	2016	2012
	Min Year	1986	1984	1993	1972
Nuuk 1784, 64.2° N, 51.7° W	Anomaly [°C]	0.6	-0.8	0.4	0.2
	z-score	0.8	-0.1	0.1	0.3
	Max Year	2010	2010	1932	2012
	Min Year	1811	1818	1802	1819
Paamiut 1958, 62.0° N, 49.7° W	Anomaly [°C]	1.0	0.4	0.1	0.2
	z-score	0.9	-0.1	0.0	0.2
	Max Year	2010	2010	2005	2010
	Min Year	1982	1984	1993	1969

Station Name, Start Year, Latitude, Longitude		SON 2017	DJF 17/18	MAM 2018	JJA 2018
Ivittuut/Narsarsuaq 1873, 61.2° N, 45.4° W	Anomaly [°C]	0.9	0.3	0.1	-0.8
	z-score	0.9	0.2	-0.1	-0.3
	Max Year	2010	2010	2010	2016
	Min Year	1874	1984	1989	1873
Qaqortoq 1807, 60.7° N, 46.1° W	Anomaly [°C]	0.7	-0.2	-0.3	-0.4
	z-score	1.0	0.2	-0.3	-0.2
	Max Year	2010	2010	1932	1929
	Min Year	1874	1863	1811	1811
Danmarkshavn 1949, 76.8° N, 18.7° W	Anomaly [°C]	4.4	5.0	-0.4	-0.9
	z-score	2.6	2.5	-0.1	-1.2
	Max Year	2016	**2018**	1976	2016
	Min Year	1971	1967	1966	1955
Ittoqqortoormiit 1949, 70.5° N, 22.0° W	Anomaly [°C]	3.6	3.7	1.7	-0.6
	z-score	2.2	1.7	1.2	0.4
	Max Year	2016	2014	1996	2016
	Min Year	1951	1966	1956	1955
Tasiilaq 1895, 65.6° N, 37.6° W	Anomaly [°C]	1.6	1.8	0.9	0.2
	z-score	1.5	1.1	0.5	0.0
	Max Year	1941	1929	1929	2016
	Min Year	1917	1918	1899	1983
Prins Christian Sund 1958, 60.1° N, 42.2° W	Anomaly [°C]	1.3	-0.5	0.1	0.3
	z-score	1.4	-0.4	0.1	0.1
	Max Year	2010	2010	2005	2010
	Min Year	1982	1993	1989	1970
Summit 1991, 72.6° N, 38.5° W	Anomaly [°C]	2.7	-0.8	0.0	0.3
	z-score	1.2	-0.2	0.0	0.1
	Max Year	2002	2010	2016	2012
	Min Year	2009	1993	1992	1992

Consistent with net ablation observations and with DMI measurements, summer temperatures were below the 2008-18 average at all PROMICE sites by more than one standard deviation along the northern, north-western, and north-eastern slopes. July 2018 was the coldest in the 2008-18 period along the northern, north-western, and southern ice sheet ablation area. Out of all Jan-Aug 2018 station-months, 28% of monthly temperatures were more than one standard deviation below average, and only 3% were over one standard deviation above average.

Marine Terminating Glaciers

Marine-terminating glaciers are the outlets by which the Greenland ice sheet discharges ice mass to the ocean. When in balance, the rate of iceberg calving (by area) is balanced by the seaward ice flow. Glacier area measurements have been measured by Sentinel-2, LANDSAT and ASTER satellite imagery since 1999 (Box and Hansen, 2015). The 2017/18 net area change of the 47 surveyed glaciers, relative to the previous year, is +4.1 km^2 and stands alone as the only year in the survey with an area gain (**Fig. 4a**). The next closely ranked year is 2006/07, when the net loss was -19.8 km^2. The 2017/18 annual area change is 113.8 km^2 less than the annual area loss per year averaged over the 19-year period of record (-109.7 km^2 per year, 1999/2000 to 2017/18). Among the surveyed glaciers (**Fig. 4b**), 21 retreated and 12 advanced. The area changes at the remaining 14 glaciers were within ±0.2 km^2. The largest single glacier area change in 2017/18 was an area loss at the Northwest Greenland Humboldt Glacier (-13.3 km^2), followed by Kangerlussuaq Glacier (-8.1 km^2) in East Greenland). Meanwhile, Petermann Glacier advanced (+19.1 km^2), similar to the previous year (+11.5 km^2). Greenland's largest ice producer, Jakobshavn Glacier, continued its retreat by losing a front area of 2.6 km^2 relative to the previous year. Helheim Glacier advanced 10.6 km^2.

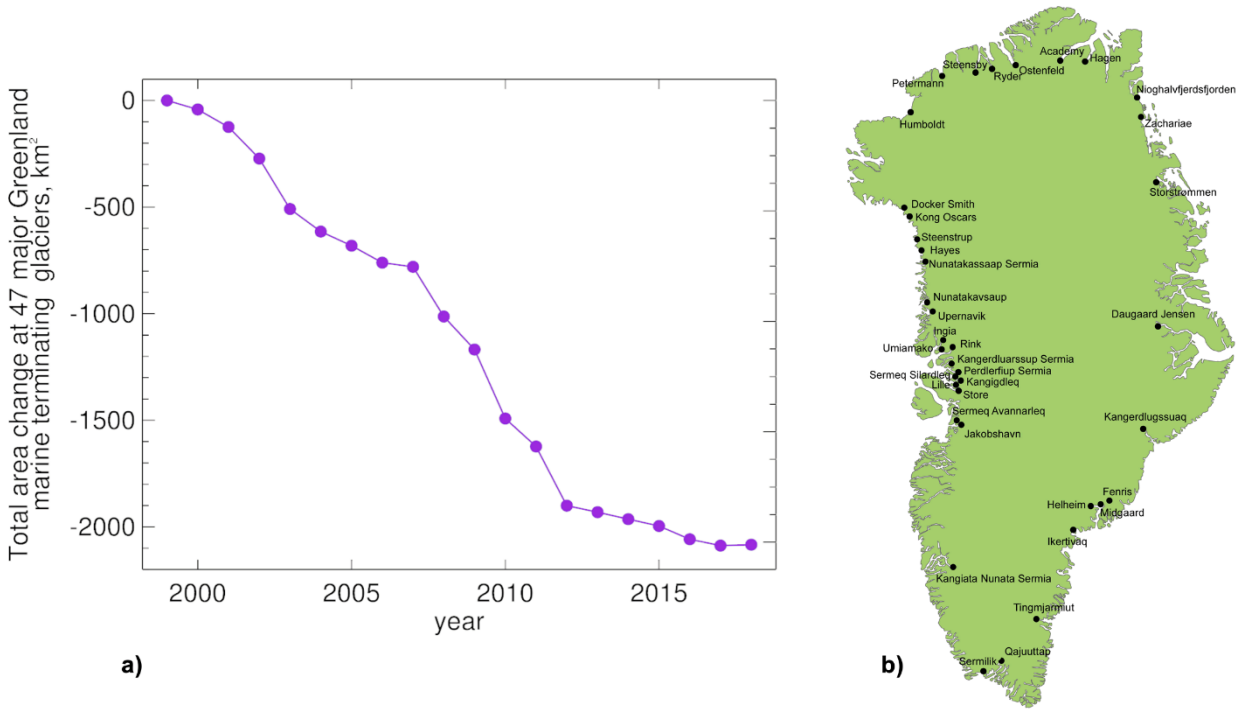

Fig. 4. a) Cumulative net area change (km^2) at the 47 marine-terminating glaciers of the Greenland ice sheet (after Box and Hansen, 2015) b) Location of the marine-terminating glaciers used in this study.

References

Box, J. E., and K. Hansen, 2015: Survey of Greenland glacier area changes. *PROMICE Newsletter*, 8, December 2015, http://promice.org/Newsletter.html.

Box, J. E., D. van As, and K. Steffen, 2017: Greenland, Canadian and Icelandic land ice albedo grids (2000-2016). *Geol. Surv. Den. Greenl. Bull.*, 38, 53-56.

Cappelen, J. (Ed.), 2019: Greenland - DMI Historical Climate Data Collection 1784-2018. DMI Report 19. (in preparation)

Mote, T., 2007: Greenland surface melt trends 1973-2007: Evidence of a large increase in 2007. *Geophys. Res. Lett.*, 34, L22507.

Nghiem, S. V., D. K. Hall, T. L. Mote, M. Tedesco, M. R. Albert, K. Keegan, C. A. Shuman, N. E. DiGirolamo, and G. Neumann, 2012: The extreme melt across the Greenland ice sheet in 2012. *Geophys. Res. Lett.*, 39, L20502, doi: 10.1029/2012GL053611.

Tedesco, M., X. Fettweis, T. Mote, J. Wahr, P. Alexander, J. Box, and B. Wouters, 2013: Evidence and analysis of 2012 Greenland records from spaceborne observations, a regional climate model and reanalysis data. *Cryosphere*, 7, 615-630.

Tedesco, M., J. E. Box, J. Cappelen, R. S. Fausto; X. Fettweis, K. Hansen, T. Mote, I. Sasgen, C. J. P. P. Smeets, D. van As, R. S. W. van de Wal, and I. Velicogna, 2017: Greenland Ice Sheet [in Arctic Report Card 2017], https://www.arctic.noaa.gov/Report-Card.

van As, D., R. S. Fausto, J. Cappelen, R. S. W. Van de Wal, R. J. Braithwaite, H. Machguth, and PROMICE project team, 2016: Placing Greenland ice sheet ablation measurements in a multi-decadal context. *Geol. Surv. Den. Greenl. Bull.*, 35, 71-74.

van de Wal, R. S. W., W. Boot, C. J. P. P. Smeets, H. Snellen, M. R. van den Broeke, and J. Oerlemans, 2012: Twenty-one years of mass balance observations along the K-transect, West-Greenland. *Earth Syst. Sci. Data*, 4, 31-35, doi: 10.5194/essd-4-31-2012.

November 14, 2018

Sea Ice

D. Perovich[1], W. Meier[2], M. Tschudi[3], S. Farrell[4], S. Hendricks[5], S. Gerland[6], C. Haas[5], T. Krumpen[5], C. Polashenski[1,7], R. Ricker[5], M. Webster[8]

[1]Thayer School of Engineering, Dartmouth College, Hanover, NH, USA
[2]National Snow and Ice Data Center, Boulder, CO, USA
[3]Aerospace Engineering Sciences, University of Colorado, Boulder, CO, USA
[4]NOAA Earth System Science Interdisciplinary Center, University of Maryland, College Park, MD, USA
[5]Alfred Wegener Institute, Helmholtz Centre for Polar and Marine Research, Bremerhaven, Germany
[6]Norwegian Polar Institute, Fram Centre, Tromsø, Norway
[7]ERDC - CRREL, 72 Lyme Road, Hanover, NH, USA
[8]NASA Goddard Space Flight Center, Greenbelt, MD, USA

Highlights

- The Arctic sea ice cover continues the declining trends in the summer maximum and winter minimum extents. In 2018, the summer extent was the sixth lowest and the winter extent was the second lowest in the satellite record (1979-2018).
- There was the dearth of ice in the Bering Sea through the 2017/18 ice growth season.

Sea Ice Extent

Arctic sea ice cover varies substantially over the year, with end-of-winter ice cover generally being two to three times as large as at the end of summer. Sea ice is an important element of the Arctic system: (1) acting as a barrier between the underlying ocean and the atmosphere, (2) limiting the amount of absorbed solar energy during the summer due to its high albedo, (3) providing a habitat for biological activity, and (4) limiting human access to the Arctic Ocean. Sea ice extent has been monitored by passive microwave instruments on satellite platforms since 1979, providing a 39-year long perspective on changing coverage over the last several decades. The months of March and September are of particular interest in sea ice time-series because they represent typical Arctic sea ice maximum and minimum extents, respectively. **Figure 1** maps monthly average ice extents in March and September 2018.

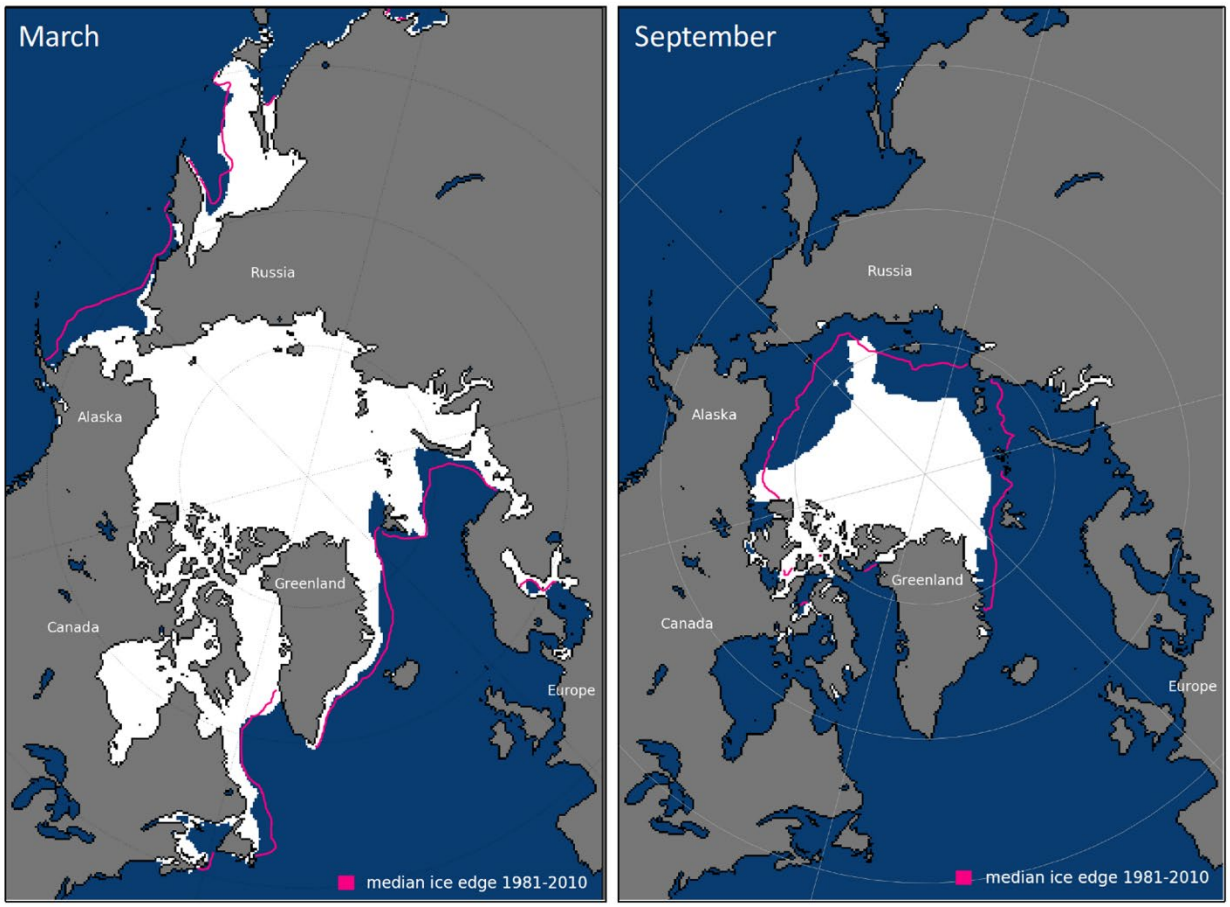

Fig. 1. Average monthly sea ice extent in March (left) and September (right) 2018 illustrate the respective winter maximum and summer minimum extents. The magenta line indicates the median ice extents in March and September, respectively, during the period 1981-2010. Maps are from NSIDC at http://nsidc.org/data/seaice_index/ (Fetterer et al., 2012).

Sea ice extent estimates are based on products from by the National Snow and Ice Data Center (NSIDC) Sea Ice Index (Fetterer et al., 2012) from NASA gridded sea ice concentration fields (Cavalieri et al., 1996; Maslanik and Stroeve, 1999; Meier et al., 2012). The sea ice cover reached a winter maximum value extent of 14.48 million km^2, on 17 March 2018. This was 7.3% below the 1981-2010 average and was the second lowest maximum extent recorded. The past four years (2015-18) have the four lowest maximums in the satellite record. The sea ice cover reached a minimum annual extent of 4.59 million km^2 on 19 September and 23 September 2018. This was tied for the sixth lowest extent of the satellite record with 2008 and 2010 and was 1.63 million km^2 (26%) less than the 1981-2010 average minimum ice extent. The 12 lowest extents in the satellite record have occurred in the last 12 years. The September ice extent has not returned to pre-2007 levels. The minimum occurred nine days later than the 1981-2010 median minimum date of 14 September and the 23 September minimum ties with 1997 for the latest minimum.

Observations of Arctic sea ice extent have shown decreasing trends in all months and virtually all regions (Meier et al., 2012). The September monthly average trend for the entire Arctic Ocean is now -12.8% per decade relative to the 1981-2010 average (**Fig. 2**). Trends are smaller during March (-2.7% per decade),

but the decrease is statistically significant. In 2018, 9.89 million km^2 of ice was lost between the March maximum and September minimum extent.

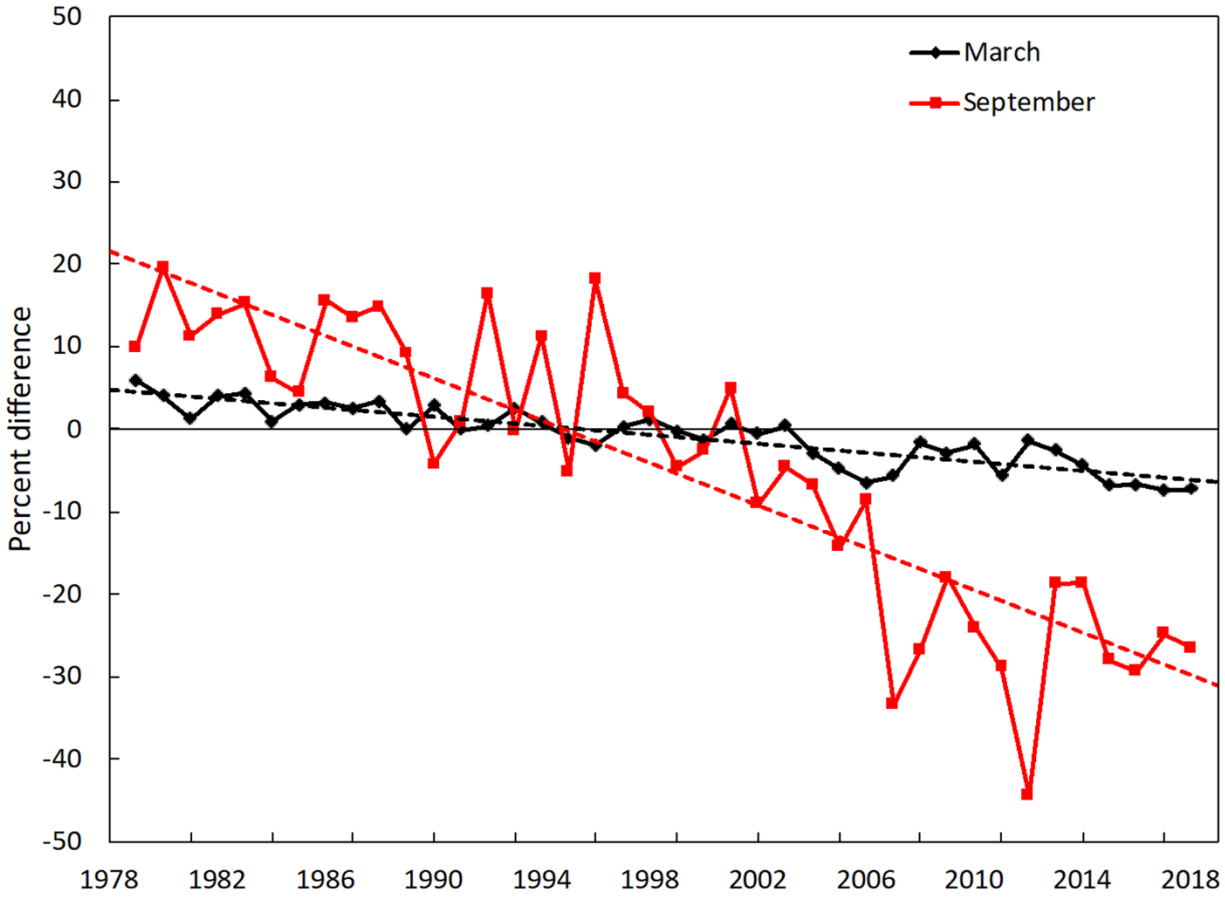

Fig. 2. Time series of ice extent anomalies in March (the month of maximum ice extent) and September (the month of minimum ice extent). The anomaly value for each year is the difference (in %) in ice extent relative to the mean values for the period 1981-2010. The black and red lines are least squares linear regression lines. The slopes of these lines indicate ice losses of -2.7 ± 0.5% and 12.8 ± 2.3% per decade in March and September, respectively. Both trends are significant at the 99% confidence level.

A notable feature of the 2018 summer melt season was the dispersed nature of parts of the ice cover. In particular, the pattern of sea ice loss resulted in an isolated patch of ice along the Alaskan coast that persisted through the summer despite being a few hundred kilometers from the main ice pack. In addition, a narrow band of ice extending from the main ice pack into the East Siberian Sea persisted through the summer. Both of these features were likely the result of concentrations of multiyear ice surrounded by thinner first-year ice.

Age of the Sea Ice

The age of sea ice is another descriptor of the state of the sea ice cover that serves as an indicator of physical ice properties, such as surface roughness, melt pond coverage and thickness (Tschudi et al., 2016) (**Fig.3**). The age of the ice is determined using satellite observations and drifting buoy records to

track ice parcels over several years (Tschudi et al., 2010; Maslanik et al., 2011). This method has been used to provide a record of the age of the ice since the early 1980s (Tschudi et al., 2015).

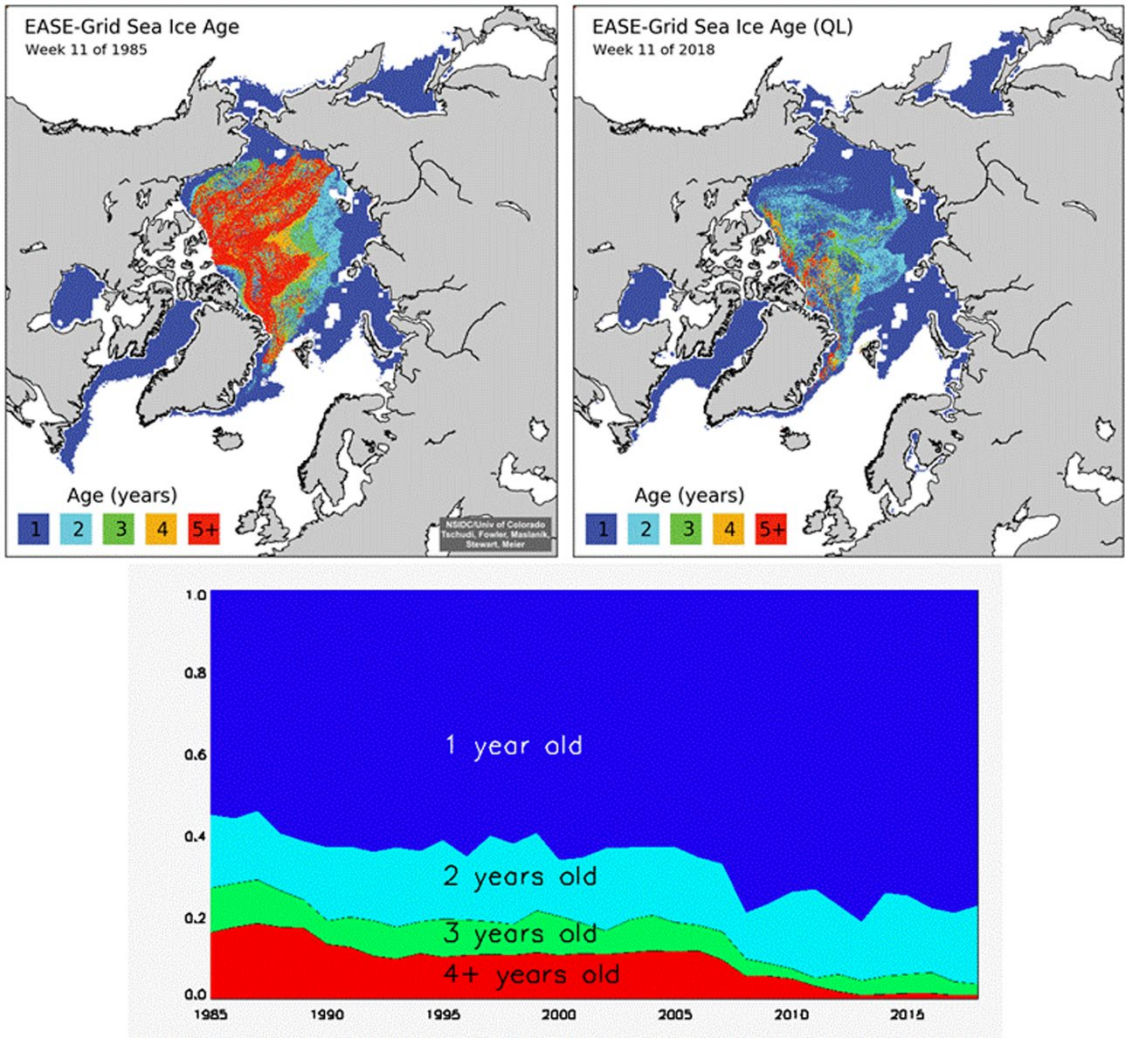

Fig. 3. Sea ice age coverage map for (a) March 1985 and b) March 2018. (c) Sea ice age coverage by year, 1985-2018.

Older ice tends to be thicker and is thus more resilient to changes in atmospheric and oceanic heat content compared to younger, thinner ice. The oldest ice (>4 years old) continues to make up a small fraction of the Arctic ice pack in March, when the sea ice extent has been at its maximum in most years of the satellite record. In 1985, the oldest ice comprised 16% of the ice pack (**Fig. 3a**), whereas in March of 2018 old ice only constituted 0.9% of the ice pack (**Fig.3b**). Therefore, the oldest ice extent declined from 2.54 million km^2 in March 1985 to 0.13 million km^2 in March 2018, representing a 95% reduction.

First-year ice now dominates the ice cover, comprising ~77% of the March 2018 ice pack compared to about 55% in the 1980s. Given that older ice tends to be thicker, the sea ice cover has transformed from a strong, thick pack in the 1980s to a more fragile, younger. thinner, and more mobile pack in recent years (**Fig. 3c**). The thinner, younger ice is more vulnerable to melting out in the summer and has contributed to the decreasing trend in the minimum ice extent.

Sea Ice Thickness

The ESA CryoSat-2 radar altimeter completed its 8th year of operation since its launch in 2010, providing large-scale sea ice thickness observations between October and April (Laxon et al., 2013). The recent launch of NASA's ICESat-2, a laser-based altimeter, will enhance large-scale measurements of sea ice thickness.

The CryoSat-2 observed a mean sea-ice thickness of 2.14 meters in the Arctic Basin (see insert in **Fig. 4b**) at the end of the 2017/18 winter season in April. This value is marginally lower than the average value measured over in the 2010-18 CryoSat-2 record (2.19 m), which ranges from 2.03 m to 2.29 m thickness. **Figure 4a** shows the mean sea-ice thickness anomaly for the winter of 2017/18 and indicates that thicknesses were above average in the East Siberian Sea shelf areas, coinciding with an elevated rate of ice convergence in early winter. In general, the eastern part of the Arctic basin shows above-average thicknesses with thinner ice in Fram Strait, Beaufort Sea, and Bering Strait.

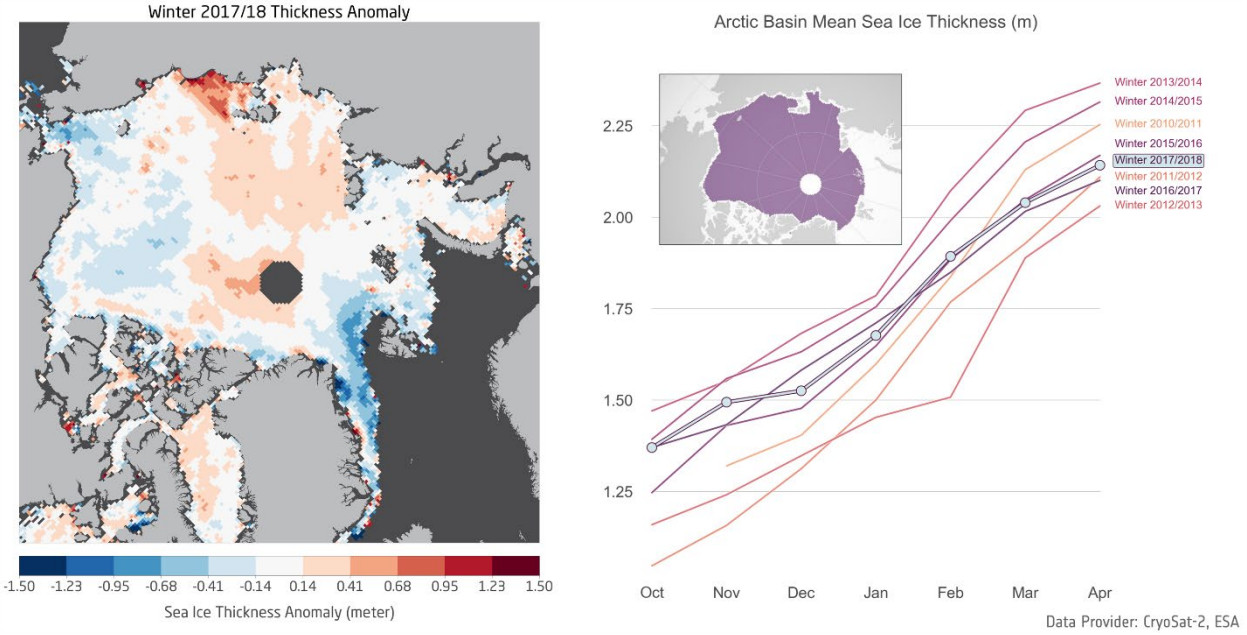

Fig. 4. (a) Mean sea-ice thickness anomaly for the winter season of October 2017 to 2018. Positive values indicate higher thicknesses than the mean winter sea-ice thickness in the CryoSat-2 data record of 2010 to 2018. (b) Monthly mean sea ice thickness in the Central Arctic Basin (shaded area in map) for all winter seasons of the CryoSat-2 data record. (Data source: AWI CryoSat sea ice product, www.seaiceportal.de).

The evolution of monthly mean thickness in comparison to the previous winters is shown in **Fig. 4b**. The thickness increase from October 2017 through April 2018 was less than normal, resulting in a relative decline in mean thicknesses over the winter. Ice volume estimates representative of ice extent and concentration in the central Arctic verify the below average ice volume gain over this interval. The total volume gain amounted to only 7.31 thousand km^3 compared to the 2010-18 average of 7.73 thousand km^3.

Snow Depth

Snow depth plays an important role in the evolution of the sea ice cover, acting as a thermal insulator and an excellent reflector of sunlight. It is also critical to the derivation of ice thickness from CryoSat-2 and IceSat-2. Snow depth distributions measured during March and April 2018 from NASA's Operation IceBridge show a spatial gradient of thick snow on multiyear ice north of Greenland and the Canadian Archipelago and thin snow on seasonal ice in the Beaufort and Chukchi seas (**Fig. 5**). Field observations in the Beaufort Sea showed an average snow depth of 12 cm and 39 cm on first-year and multiyear ice, respectively.

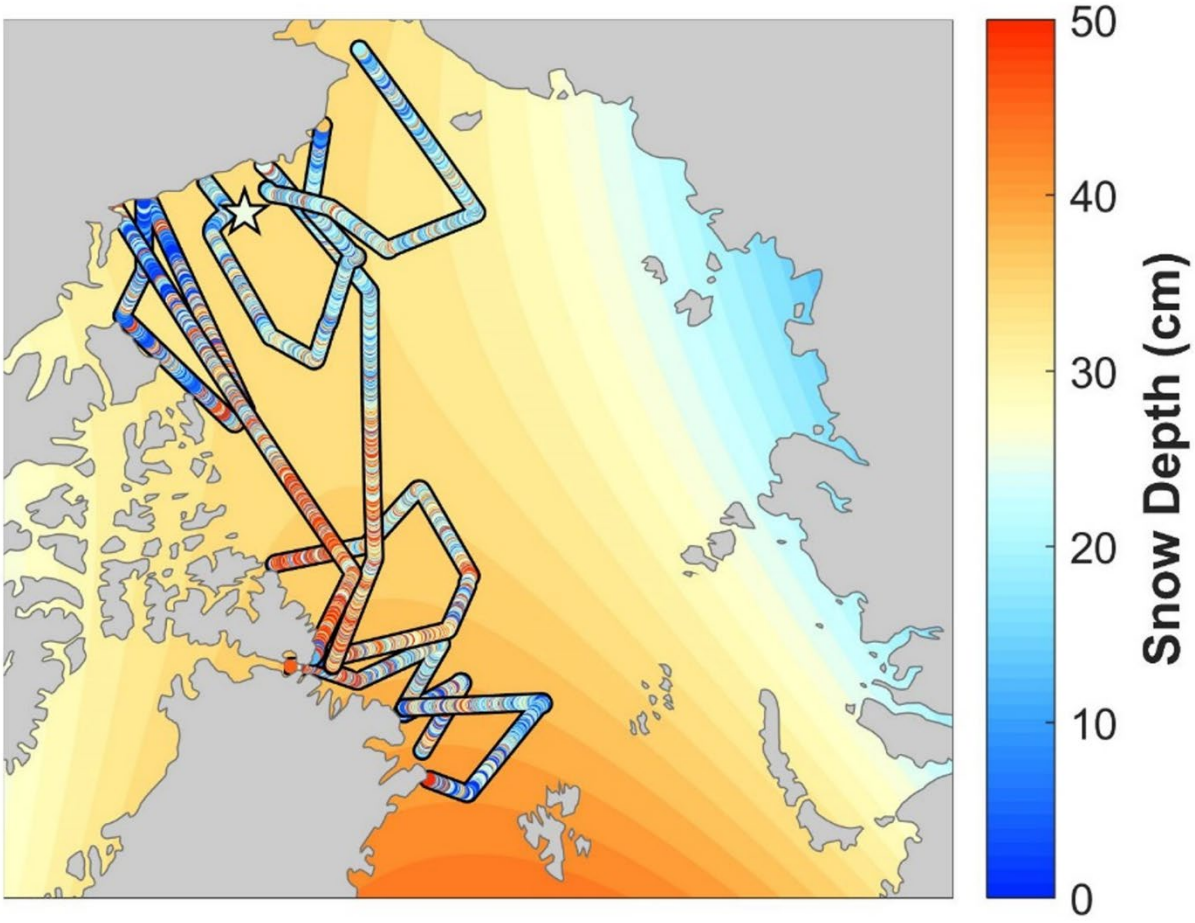

Fig. 5. Track of snow depth measurements made by NASA IceBridge. The background is snow climatology from Warren et al. (1999).

Winter Bering Sea

One of the more remarkable features of Arctic sea ice over the past year was the dearth of ice in the Bering Sea through the 2017-18 ice growth season. The Bering Sea supports a vibrant sea ice-ecosystem with abundant seals, birds, and other pelagic species that critically depend on the timing of sea ice formation and retreat. It is also an important commercial fishing region. Ice typically begins to form in the Bering around the beginning of October, expands through the winter and then melts away through the spring. By the end of June most or all of the Bering ice has typically melted out (**Fig. 6**).

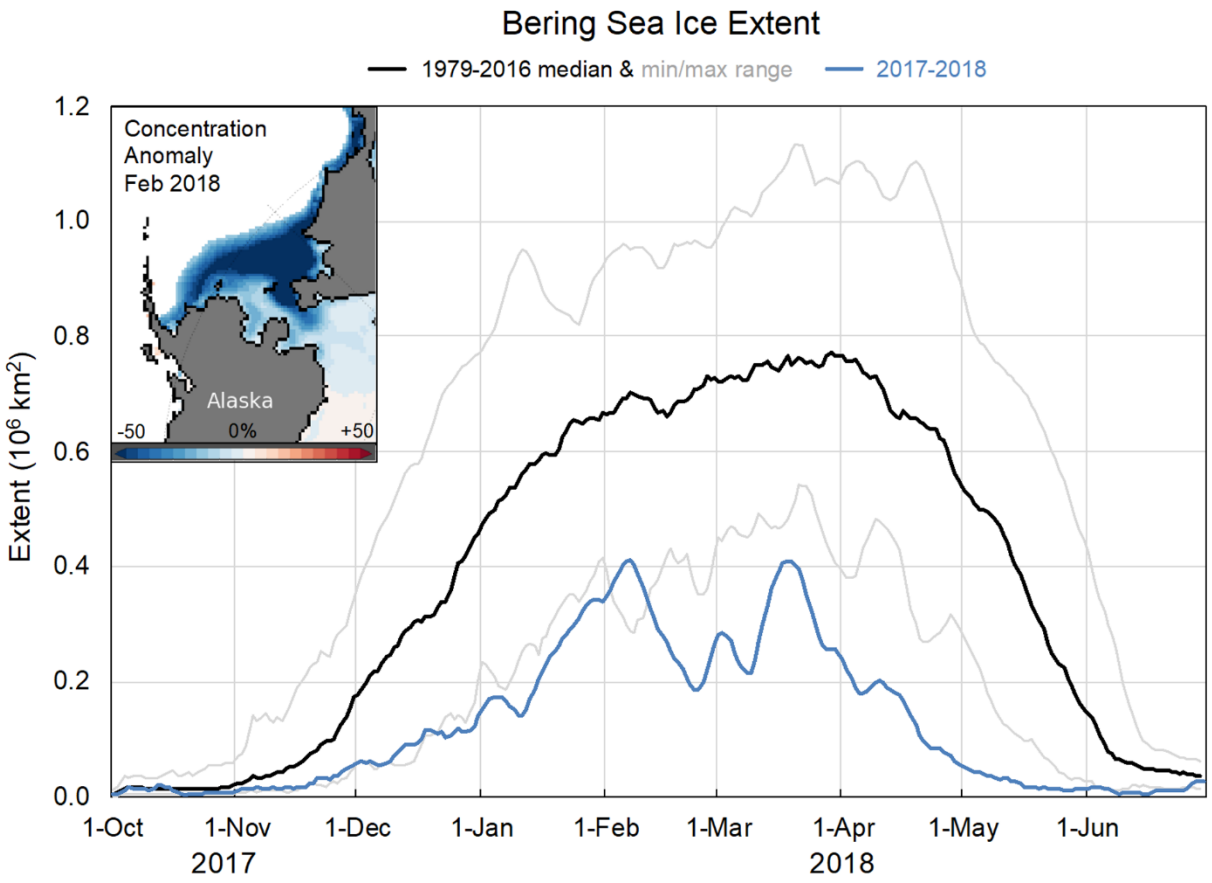

Fig. 6. Bering Sea ice extent for the 2017/18 ice growth season (in blue) and the 1979-2016 median (black) and minimum and maximum ranges (gray shading). Data are from the NSIDC Sea Ice Index (https://nsidc.org/data/seaice_index/).

For virtually the entire 2017-2018 Bering Sea ice season, the extent was at a record low (**Fig. 6a**). During February, typically the height of the winter season, the Bering Sea actually lost significant ice cover. From 7 February to 23 February 2018, ice extent decreased by ~215,000 km^2, dropping from ~59% to only ~26% of normal (relative to the 1979-2016 median). The Bering Sea ice cover remained extremely low until mid-March, when extent increased over a couple of weeks, though it still remained at record low levels until the season spring decline began.

Anomalously warm sea surface temperatures (SSTs) persisted in the Bering Sea from September 2017 through 2018 (NOAA's Optimum Interpolation Version 2 SST: https://www.esrl.noaa.gov/psd/map/clim/sst.shtml) and air temperatures were also well above average (NCEP/NCAR Reanalysis: https://www.esrl.noaa.gov/psd/cgi-bin/data/composites/printpage.pl). A key factor in the low Bering Sea ice was persistent southerly circulation that brought warm air and surface waters from the south and pushed sea ice that formed northward (see essay on *Surface Air Temperature*). Moorings measuring ocean currents and heat fluxes detected very warm water in the region in summer 2017, which likely pre-conditioned the waters for a late start to the freeze-up season (see essay on *Sea Surface Temperature*). The low winter and spring ice conditions allowed for early absorption of solar insolation by the ocean and warming of the surface waters. These warm ocean waters may have contributed to early summer ice loss in 2018 in the Chukchi and Beaufort seas, as the

ocean heat melted ice. However, the ice loss in Chukchi slowed during July during a period of cool air temperatures in the region.

References

Cavalieri, D. J., C. L. Parkinson, P. Gloersen, and H. J. Zwally, 1996, updated yearly: Sea Ice Concentrations from Nimbus-7 SMMR and DMSP SSM/I-SSMIS Passive Microwave Data, Version 1. Boulder, CO USA. NASA National Snow and Ice Data Center Distributed Active Archive Center, doi: 10.5067/8GQ8LZQVL0VL.

Fetterer, F., K. Knowles, W. Meier, and M. Savoie, 2002, updated 2012: Sea Ice Index, National Snow and Ice Data Center. Digital media, Boulder, CO.

Laxon, S. W., K. A. Giles, A. L. Ridout, D. J. Wingham, R. Willatt, R. Cullen, R. Kwok, A. Schweiger, J. Zhang, C. Haas, S. Hendricks, R. Krishfield, N. Kurtz, S. Farrell, and M. Davidson, 2013: CryoSat-2 estimates of Arctic sea ice thickness and volume. *Geophys. Res. Lett.*, 40, 732-737, doi: 10.1002/grl.50193.

Maslanik, J., and J. Stroeve, 1999, updated daily: Near-Real-Time DMSP SSMIS Daily Polar Gridded Sea Ice Concentrations, Version 1. Boulder, Colorado USA. NASA National Snow and Ice Data Center Distributed Active Archive Center, doi: 10.5067/U8C09DWVX9LM.

Maslanik, J., J. Stroeve, C. Fowler, and W. Emery, 2011: Distribution and trends in Arctic sea ice age through spring 2011. *Geophys. Res. Lett.*, 38, L13502, doi: 10.1029/2011GL047735.

Meier, W. N., J. Stroeve, A. Barrett, and F. Fetterer, 2012: A simple approach to providing a more consistent Arctic sea ice extent time series from the 1950s to present. *Cryosphere*, 6, 1359-1368, doi: 10.5194/tc-6-1359-2012.

Tschudi, M. A., J. C. Stroeve, and J. S. Stewart, 2016: Relating the age of Arctic sea ice to its thickness, as measured during NASA's ICESat and IceBridge Campaigns. *Remote Sens.*, 8(6), 457, doi: 10.3390/rs8060457.

Tschudi, M. A., C. Fowler, J. A. Maslanik, and J. A. Stroeve, 2010: Tracking the movement and changing surface characteristics of Arctic sea ice. *IEEE J. Sel. Top. Appl. Earth Obs. Remote Sens.*, 3, 536-540, doi: 10.1109/JSTARS.2010.2048305.

Tschudi, M., C. Fowler, and J. Maslanik, 2015: EASE-Grid Sea Ice Age, Version 2. NASA National Snow and Ice Data Center Distributed Active Archive Center, Boulder, CO, doi: 10.5067/1UQJWCYPVX61.

Warren, S., I. Rigor, N. Untersteiner, V. F. Radionov, N. N. Bryazgin, Y. I. Aleksandrov, and R. Colony, 1999: Snow depth on Arctic sea ice. *J. Clim.*, 12, 1814-1829.

November 13, 2018

Sea Surface Temperature

M. -L. Timmermans[1], C. Ladd[2]

[1]Yale University, New Haven, CT, USA
[2]Pacific Marine Environmental Laboratory, NOAA, Seattle, WA, USA

Highlights

- August mean sea surface temperatures (SSTs) show statistically significant warming trends for 1982-2018 in most regions of the Arctic Ocean that are ice-free in August.
- Spatial patterns of August 2018 SST anomalies relative to the 1982-2010 August mean are linked to regional variability in sea-ice retreat, regional air temperature, and advection of waters from the Pacific and Atlantic oceans.
- Northern Barents Sea August mean SSTs show statistically significant cooling trends for 1982-2018, a result of sea ice conditions and ocean heat transport unique to this region.

Summer sea surface temperatures (SST) in the Arctic Ocean are driven mainly by the amount of incoming solar radiation absorbed by the sea surface. Solar warming of the Arctic surface ocean is influenced by the distribution of sea ice (with greater warming occurring in ice-free regions), cloud cover, water color, and upper-ocean stratification. In the Barents and Chukchi seas, there is an additional source of ocean heat contributed by the advection of warm water from the North Atlantic and North Pacific oceans, respectively. Arctic SSTs are an essential indicator of the role of the ice-albedo feedback mechanism in any given melt season. As the area of sea ice cover decreases, more incoming solar radiation is absorbed by the ocean and the warmer ocean, in turn, melts more sea ice. In addition, marine ecosystems are influenced by SST, which affects timing and developmental cycles of primary and secondary production as well as available habitat for individual species.

SST data presented here are from the NOAA Optimum Interpolation (OI) SST Version 2 product (OISSTv2), which is a blend of in situ and satellite measurements from December 1981 to present (Reynolds et al., 2002, 2007). Compared to in situ temperature measurements, the OISSTv2 product showed average correlations of about 80%, with an overall cold SST bias of -0.02° C (Stroh et al., 2015). August SSTs provide the most appropriate representation of Arctic Ocean summer SSTs because they are not affected by the cooling and subsequent sea-ice growth that typically takes place in the latter half of September.

Mean SSTs in August 2018 in ice-free regions ranged from ~0° C in some regions to as high as +11° C in the southern Chukchi and Barents seas (**Fig. 1a**). Compared to the 1982-2010 August mean, anomalously warm SSTs in August 2018 (around 1-3° C warmer than the 1982-2010 average) were observed in the Beaufort, Chukchi, Laptev, and southern Barents seas (**Fig. 1b**). Anomalously warm SSTs on the ice-free side of the 2018 August mean sea-ice edge are linked to anomalously early local sea ice retreat, which facilitated direct solar heating of the exposed surface waters (**Fig. 1b**). Conversely, the southern boundary of the Beaufort Sea in 2018 was marked by anomalously cool August SSTs (around 1-2° C cooler than the 1982-2010 average). These low SSTs are associated with unusually cool August 2018 air temperatures along the entire southern Beaufort Sea (see essay on *Surface Air Temperature*) and the persistence of sea ice in the region, maintained by northerly August winds in the region (see essay on *Sea Ice*). These factors were distinct from August 2017 conditions (milder air temperatures were

recorded in August 2017; Arctic Report Card 2017 Surface Air Temperature), with the entire Beaufort Sea region exhibiting cooler August SSTs (up to 3.5° C cooler) in 2018 compared to 2017 (**Fig. 1c**).

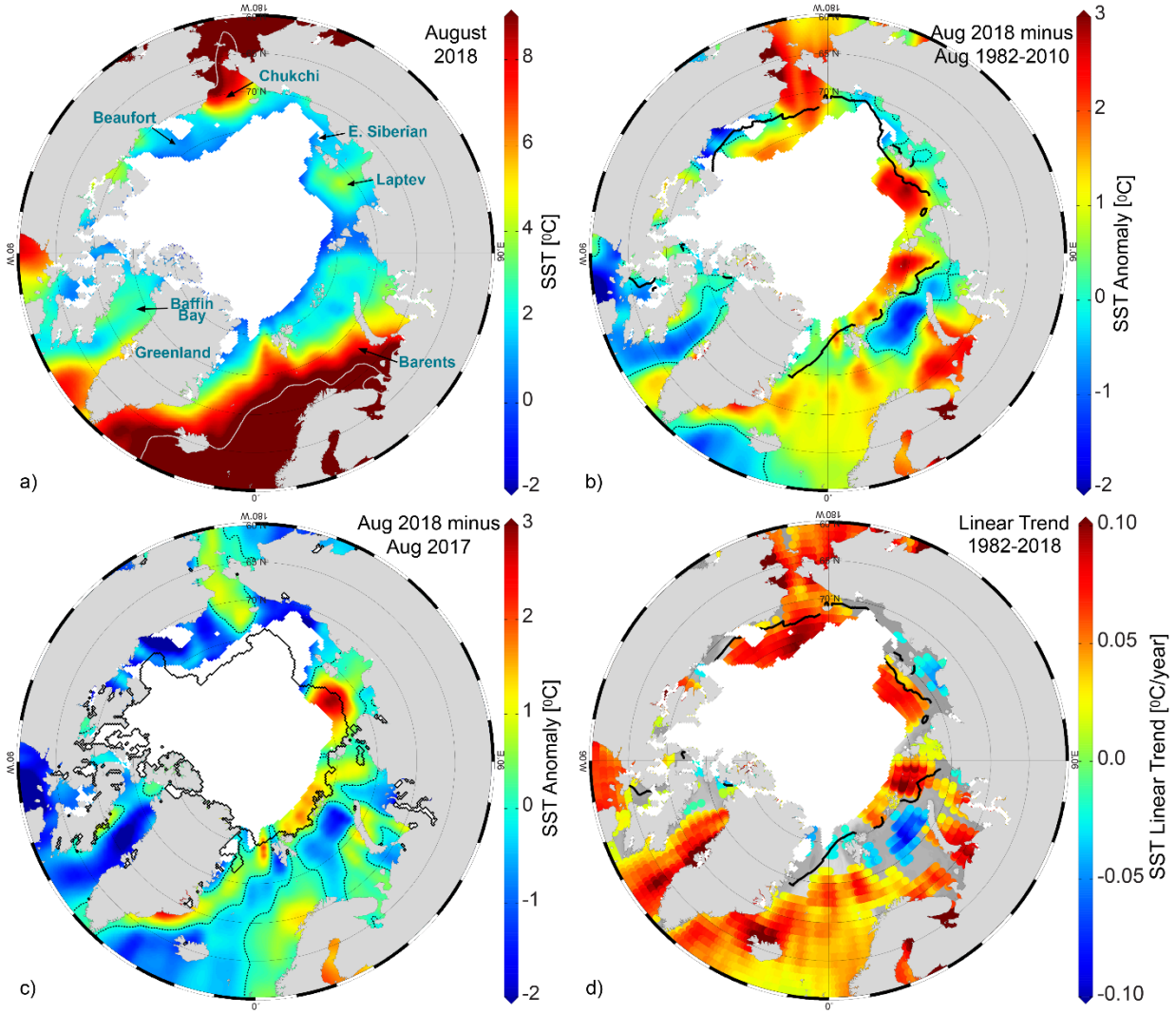

Fig. 1. (a) Mean SST (°C) in Aug 2018. White shading is the Aug 2018 mean sea ice extent (shown in each panel), and gray contours indicate the 10° C SST isotherm. (b) SST anomalies (°C) in Aug 2018 relative to the Aug 1982-2010 mean (the dotted black contour indicates zero anomaly). The black line indicates the median ice edge for Aug 1982-2010. (c) SST anomalies (°C) in Aug 2018 relative to Aug 2017. The black line indicates the median ice edge for Aug 2017. (d) Linear SST trend (°C yr^{-1}) for Aug of each year from 1982-2018. The trend is only shown for values that are significant at the 95% confidence interval; the region is gray otherwise. The black line indicates the median ice edge for Aug 1982-2010. (Sources: SST data are from the NOAA OISSTv2; sea ice extent and ice-edge data are from NSIDC Sea Ice Index, Version 3, Fetterer et al., 2017.)

Mean August SSTs from 1982-2018 show warming trends over much of the Arctic Ocean; statistically significant (at the 95% confidence interval) linear warming trends of up to +1° C $decade^{-1}$ are observed (**Figs. 1d** and **2**). These warming trends coincide with declining trends in summer sea-ice extent (including late-season freeze-up and early melt, e.g., Parkinson, 2014), increased solar absorption (e.g., Timmermans et al., 2018), and increased vertical ocean heat transport (e.g., Lind et al., 2018). A marked exception to the prevalent August SST warming trend is the cooling trend (-0.06±0.03° C/yr) in the

northern Barents Sea (**Figs. 1d** and **2**). Related to this, the northern Barents Sea exhibited notably cool August 2018 SSTs, characterized by temperatures 1-2° C cooler than the 1982-2010 average (**Fig. 1b**), with August 2018 SSTs also around 1°C cooler than August 2017 (**Fig. 1c**). A statistically significant cooling trend in the northern Barents Sea is only observed for the months of August and September, with most other months (January to June) characterized by statistically significant warming trends (+0.03±0.01 °C/yr) over the same region. The result is that annually-averaged northern Barents Sea SSTs exhibit a warming trend (see e.g., Barton et al., 2018). A coupled ice-ocean numerical model study reveals subtle variability in spatial and seasonal trends in the Barents Sea region that appears to depend upon the interplay between sea-ice changes, local solar absorption and lateral ocean heat transport (Long and Perrie, 2017). These complex relationships in this important Arctic gateway region merit further study.

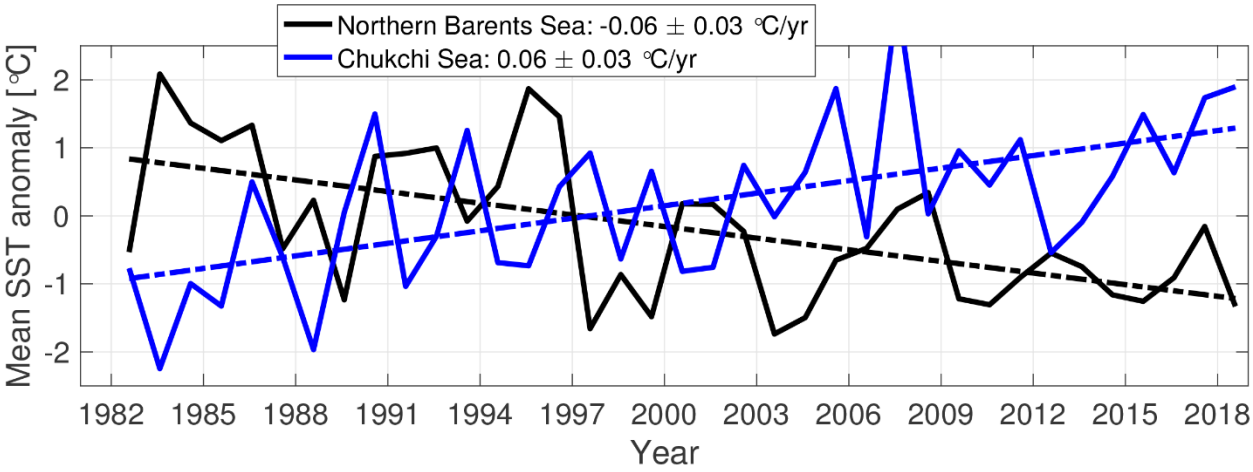

Fig. 2. Area-averaged SST anomalies (°C) for August of each year relative to the 1982-2010 August mean for the Chukchi Sea region (68-74° N, 180-200° E) and the northern Barents Sea region (76.4-79.4° N, 38-60° E). The dashed lines show the linear SST trends (over the period shown). Numbers in the legend correspond to linear trends in °C year^{-1} (with 95% confidence intervals).

References

Barton, B. I., Y. Lenn, and C. Lique, 2018: Observed Atlantification of the Barents Sea causes the Polar Front to limit the expansion of winter sea ice. *J. Phys. Oceanogr.*, 48, 1849-1866, doi: 10.1175/JPO-D-18-0003.1.

Fetterer, F., K. Knowles, W. Meier, M. Savoie, and A. K. Windnagel, 2017, updated daily: Sea Ice Index, Version 3. Boulder, Colorado USA. NSIDC: National Snow and Ice Data Center, doi: 10.7265/N5K072F8.

Lind, S., R. B. Ingvaldsen, and T. Furevik, 2018: Arctic warming hotspot in the northern Barents Sea linked to declining sea-ice import. *Nat. Clim. Change*, 8(7), 634-639, doi: 10.1038/s41558-018-0205-y.

Long, Z., and W. Perrie, 2017: Changes in ocean temperature in the Barents Sea in the twenty-first century. *J. Clim.*, 30, 5901-5921, doi: 10.1175/JCLI-D-16-0415.1.

Parkinson, C. L., 2014: Spatially mapped reductions in the length of the Arctic sea ice season. *Geophys. Res. Lett.*, 41, 4316-4322, doi: 10.1002/2014GL060434.

Reynolds, R. W., N. A. Rayner, T. M. Smith, D. C. Stokes, and W. Wang, 2002: An improved in situ and satellite SST analysis for climate. *J. Clim.*, 15, 1609-1625.

Reynolds, R. W., T. M. Smith, C. Liu, D. B. Chelton, K. S. Casey, and M. G. Schlax, 2007: Daily high-resolution-blended analyses for sea surface temperature. *J. Clim.*, 20, 5473-5496. (Data available at https://www.esrl.noaa.gov/psd/data/gridded/data.noaa.oisst.v2.html.)

Stroh, J. N., G. Panteleev, S. Kirillov, M. Makhotin, and N. Shakhova, 2015: Sea-surface temperature and salinity product comparison against external in situ data in the Arctic Ocean. *J. Geophys. Res. Oceans*, 120, 7223-7236, doi: 10.1002/2015JC011005.

Timmermans, M. -L., J. Toole, R. Krishfield, 2018: Warming of the interior Arctic Ocean linked to sea ice losses at the basin margins. *Sci. Adv.*, 4(8) eaat6773, doi: 10.1126/sciadv.aat6773.

November 13, 2018

Arctic Ocean Primary Productivity: The Response of Marine Algae to Climate Warming and Sea Ice Decline

K. E. Frey[1], J. C. Comiso[2], L. W. Cooper[3], J. M. Grebmeier[3], L. V. Stock[2]

[1]Graduate School of Geography, Clark University, Worcester, MA, USA
[2]Cryospheric Sciences Laboratory, NASA Goddard Space Flight Center, Greenbelt, MD, USA
[3]Chesapeake Biological Laboratory, University of Maryland Center for Environmental Science, Solomons, MD, USA

Highlights

- Satellite estimates of ocean primary productivity (i.e., the rate at which marine algae transform dissolved inorganic carbon into organic material) were higher in 2018 (relative to the 2003-17 mean) for three of the nine investigated regions (the Eurasian Arctic, Bering Sea, and Baffin Bay).
- All regions continue to exhibit positive trends over the 2003-18 period, with the strongest trends for the Eurasian Arctic, Barents Sea, Greenland Sea, and North Atlantic.
- The regional distribution of relatively high (low) chlorophyll-*a* concentrations can often be associated with a relatively early (late) breakup of sea ice cover.

Autotrophic single-celled algae living in the sea ice (ice algae) and water column (phytoplankton) are the main primary producers in the Arctic Ocean. Through photosynthesis, they transform dissolved inorganic carbon into organic material. Consequently, primary production provides a key ecosystem service by providing energy to the entire food web in the oceans. The global oceans play a significant role in global carbon budgets via photosynthesis, contributing approximately half of Earth's net annual photosynthesis with ~10-15% of this production occurring on the continental shelves alone (Müller-Karger et al., 2005). Primary productivity is strongly dependent upon light availability and the presence of nutrients, and thus is highly seasonal in the Arctic. In particular, the melting and retreat of sea ice during spring are strong drivers of primary production in the Arctic Ocean and its adjacent shelf seas owing to enhanced light availability and stratification (Barber et al., 2015; Leu et al., 2015; Ardyna et al., 2017). Recent declines in Arctic sea ice extent (see the essay on *Sea Ice*) have contributed substantially to shifts in primary productivity throughout the Arctic Ocean. However, the response of primary production to sea ice loss has been both seasonally and spatially variable (e.g., Tremblay et al., 2015; Hill et al., 2018).

Here we present satellite-based estimates of algal chlorophyll-*a* (occurring in all species of phytoplankton), based on the color of the ocean, and subsequently provide calculated primary production estimates. These results are shown for ocean areas with less than 15% sea ice concentration and, therefore, do not include production by sea ice algae, open water from within the sea ice pack, or under-ice phytoplankton blooms.

Chlorophyll-*a*

Measurements of the algal pigment chlorophyll (e.g., chlorophyll-*a*) serve as a proxy for the amount of algal biomass present as well as overall plant health. The complete, updated MODIS-Aqua satellite chlorophyll-*a* record for the northern polar region for the years 2003-18 can serve as a time-series against which individual years can be compared. For example, a base period of 2003-17 was chosen to calculate the 2018 anomalies to maximize the length of the short satellite-based time series.

The 2018 data show a distribution of both positive and negative anomalies in chlorophyll-*a* concentrations in a number of locations across the Arctic Ocean region, where patterns are spatially and temporally heterogeneous (**Fig. 1**). These patterns are often associated with the timing of sea ice break-up: positive anomalies tend to occur in regions where the break up is relatively early, while negative anomalies tend to occur in regions where the break up is delayed. The most notable positive anomalies in 2018 occurred during May and June, with relatively high concentrations of chlorophyll-*a* occurring in the northern Barents Sea surrounding Svalbard and along the ice edge in the Greenland Sea (**Fig. 1a, b**). These anomalies are associated with clear declines in sea ice cover in these regions as well (**Fig. 2a, b**). Additional widespread positive anomalies occurred in the Bering Sea in June, which will be discussed in greater detail below. Some of the strongest negative anomalies in chlorophyll-*a* concentrations occurred southeast of Greenland in the Denmark Strait in May and July (**Fig. 1a, c**) and in the Kara Sea in July (**Fig. 1c**). The relatively low chlorophyll-*a* concentrations in the Kara Sea in July are associated with increases in sea ice cover in that region throughout the season (**Fig. 2a-c**).

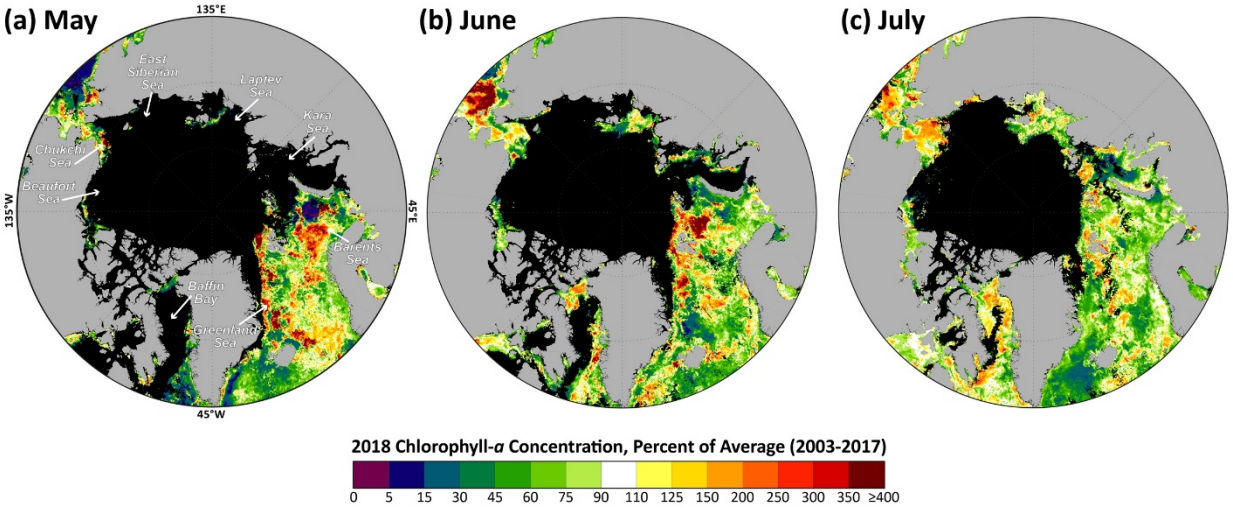

Fig. 1. Mean monthly chlorophyll-a concentrations during 2018, shown as a percent of the 2003-17 average for (a) May, (b) June, and (c) July. Satellite-based chlorophyll-a data across the pan-Arctic region were derived using the MODIS-Aqua Reprocessing 2014.0, OC3 algorithm: http://oceancolor.gsfc.nasa.gov/.

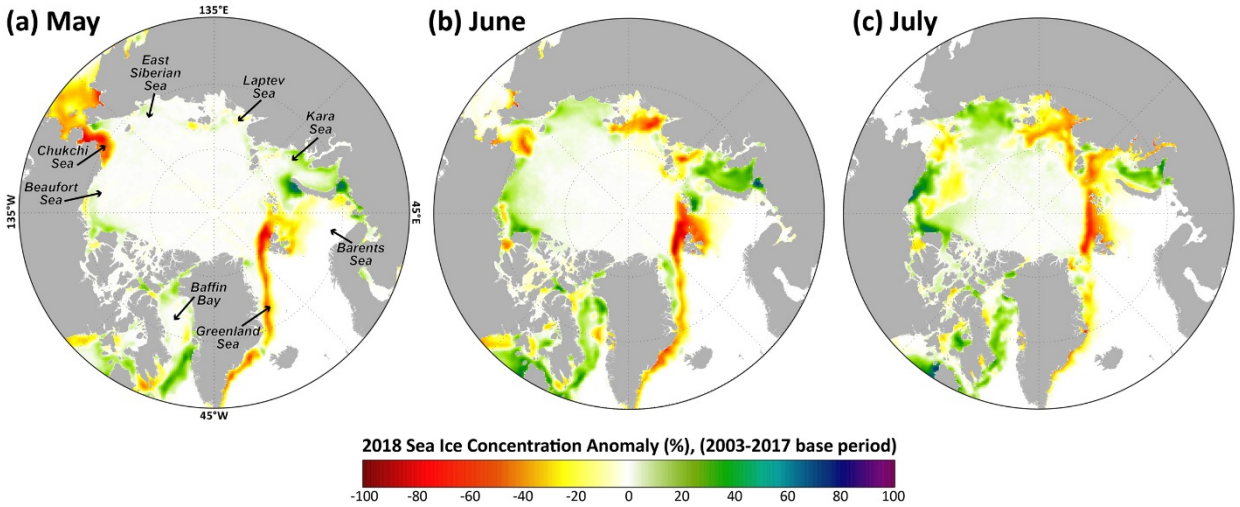

Fig. 2. Sea ice concentration anomalies (%) in 2018 (compared to a 2003-17 mean base period) for (a) May, (b) June, and (c) July. Satellite-based sea ice concentrations were derived from the Special Sensor Microwave/Imager (SSM/I) and Special Sensor Microwave Imager/Sounder (SSMIS) passive microwave instruments, calculated using the Goddard Bootstrap (SB2) algorithm (Comiso et al., 2017a, b).

As noted above, some of the largest positive anomalies in chlorophyll-*a* concentrations observed in 2018 occurred over the shelf region of the Bering Sea during June (**Fig. 3a**). Focusing in on the Pacific Arctic region, these positive anomalies are distributed across the Bering Sea shelf and range from ~400 to 500% of the 2003-17 average. This is in contrast to the negative anomalies in the Bering Sea south of the shelf break that average only ~20% of the 2003-17 average (**Fig. 3a**). In particular, focusing on the Distributed Biological Observatory Site 1 (DBO1; Moore and Grebmeier, 2018) in the St. Lawrence Island Polynya (SLIP) region, it is also apparent that the typical large blooms that occur in April and May did not occur in 2018; instead, we observe a redistribution of chlorophyll biomass in March (~275% increase over the 2003-17 average) and June (~500% increase over the 2003-17 average) (**Fig. 3b**).

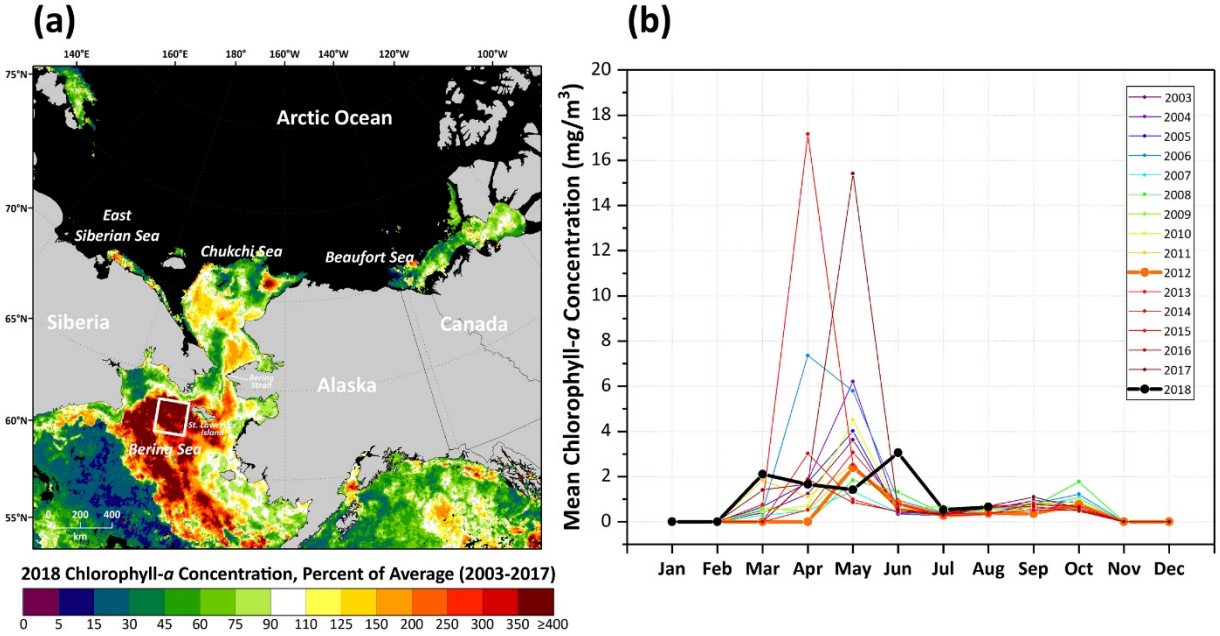

Fig. 3. (a) Mean chlorophyll-*a* concentrations in the Pacific Arctic region during June 2018, shown as a percent of the 2003-17 average. The white box denotes the Distributed Biological Observatory (DBO) Site 1, encompassing

the St. Lawrence Island Polynya (SLIP) region. (b) Mean chlorophyll-*a* concentrations for the DBO1/SLIP region from 2003-18, highlighting 2012 (one of the highest years of sea ice cover on record) and 2018 (the lowest year of sea ice cover on record).

This redistribution of the seasonal variability of chlorophyll biomass is of particular interest because this region experienced unprecedented declines in sea ice over the winter of 2018 (**Fig. 4**). For example, DBO1 on average (1981-2010) experiences ~149 days of sea ice cover per year, but in 2018 only had ~20 days of sea ice cover as a result of both later sea ice freeze-up and earlier sea ice break-up (**Fig. 4a, b**). Having knowledge of how regions experience changes in chlorophyll-*a* concentrations with such dramatic losses of sea ice cover will give insight into what to expect with future sea ice declines. In this particular instance, it is important to note that we do not observe simple overall increases in chlorophyll biomass with the unprecedented declines in Bering Sea ice in 2018, but rather a dampening of the large blooms typical of April-May and a redistribution of production in March and June. While many of these observed patterns are directly linked to sea ice variability (and therefore light availability), it is important to note that there are other dominant factors at play that add to the complexity of observed chlorophyll-*a* concentrations such as the distribution and availability of nutrients (e.g., Giesbrecht et al., 2018). Furthermore, more specific impacts of sea ice decline on water column phytoplankton (such as phytoplankton community composition and phytoplankton carbon biomass; Neeley et al., 2018) will be critical to continue to monitor.

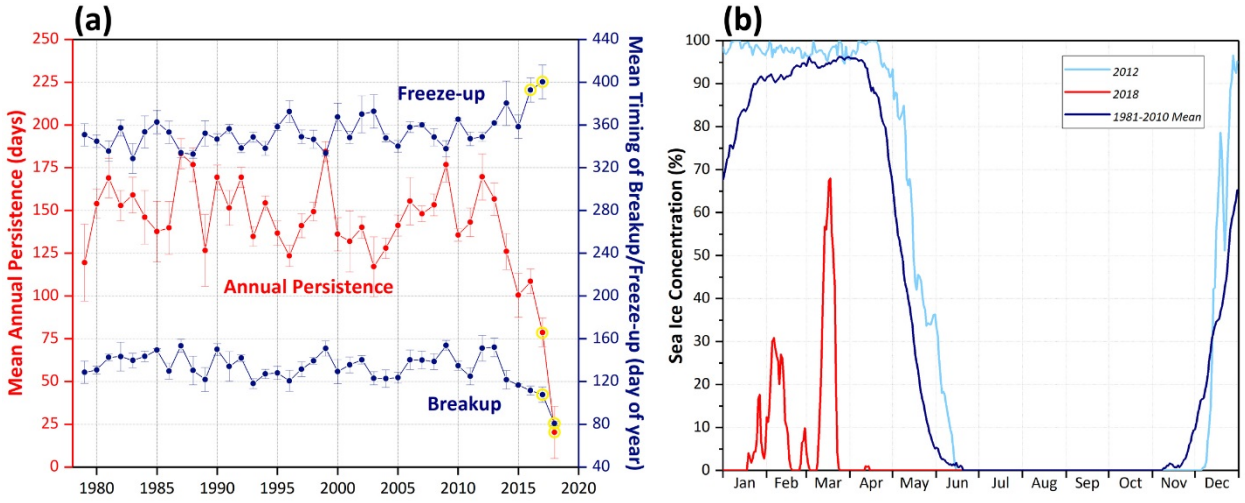

Fig. 4. (a) Sea ice variability (annual persistence and the timing of breakup/freeze-up) at the DBO1/SLIP region (see **Fig. 3** for location) from 1979 to 2018 (error bars as ±1 standard deviation depict spatial variability within the polygon) based on SMMR, SSM/I, and SSMIS data (Comiso et al., 2017a, b). See Frey et al. (2014, 2015) for further details of methodology. Circled in yellow are the outliers identified using a double Grubb's test ($p < 0.0001$). (b) Daily time series of sea ice concentration at the DBO1/SLIP region, highlighting the 1981-2010 mean, 2012 (one of the highest years of sea ice cover on record), and 2018 (the lowest year of sea ice cover on record).

Primary Production

Chlorophyll-*a* concentrations give an estimate of the standing stock of algal biomass. Rates of primary production (i.e., the production of organic carbon via photosynthesis) provide a different perspective, and can be estimated by combining remotely sensed chlorophyll-*a* concentrations with sea surface temperatures, incident solar irradiance, and mixed layer depths. Estimates of ocean primary productivity for nine regions (and the average of these nine regions) across the Arctic, relative to 2003-17 base

period, indicate above average primary productivity for 2018 in three regions and below average primary productivity in six regions as well as the overall Arctic region (**Fig. 5**, **Table 1**). Areas with the above average anomalies for 2018 include the Eurasian Arctic, the Bering Sea, and the Baffin Bay/Labrador Sea regions. In the longer term, positive trends in primary productivity occurred in all regions during the period 2003-18 (**Fig. 5**, **Table 1**). Statistically significant trends occurred in the Eurasian Arctic, Barents Sea, Greenland Sea, and North Atlantic, with the steepest trends found for the Barents Sea (12.85 g C/m^2/yr/dec, or a ~24.4% increase) and the Eurasian Arctic (12.74 g C/m^2/yr/dec, or a ~30.8% increase).

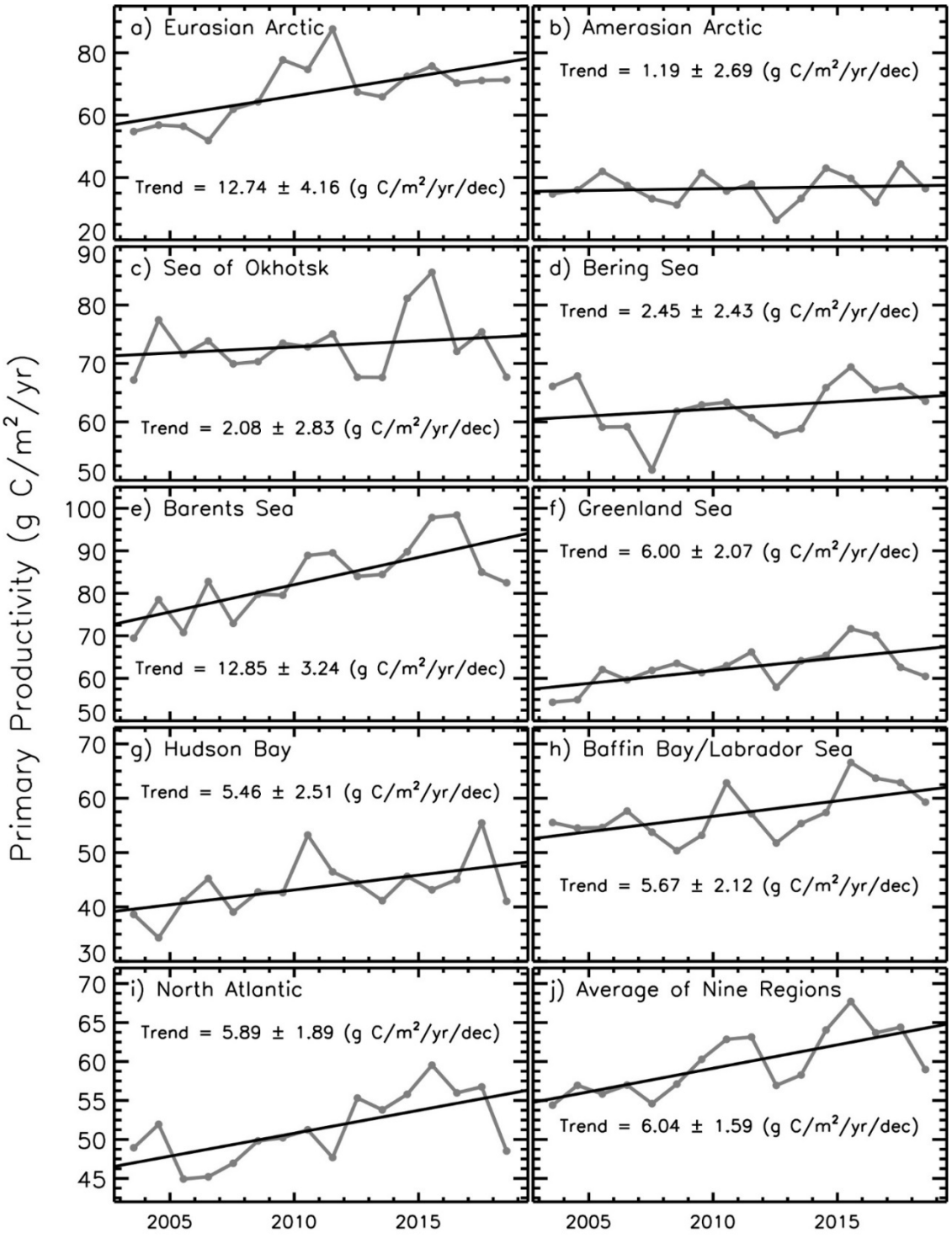

Fig. 5. Primary productivity (2003-18, March-September only) in nine different regions of the Northern Hemisphere (for a definition of the regions see Comiso (2015)), as well as the average of these nine regions, derived using chlorophyll-*a* concentrations from MODIS-Aqua data, the NOAA 1/4° daily Optimum Interpolation Sea Surface Temperature dataset (or daily OISST) that uses satellite sea surface temperatures from AVHRR, and additional parameters. Values are calculated based on the techniques described by Behrenfeld and Falkowski (1997) and represent net primary productivity (NPP). Additional information regarding these data can be found in **Table 1**.

Table 1. Linear trends, statistical significance, percent change, and primary productivity anomalies in 2018 (March-September) in the nine regions (and overall average) as shown in **Fig. 4**. Utilizing the Mann-Kendall test for trend, values in **bold** are significant at the 95% confidence level. The percent change was estimated from the linear regression of the 16-year time series.

Region	Trend, 2003-18 (g C/m^2/yr/decade)	Mann-Kendall *p* -value	% Change	2018 Anomaly (g C/m^2/yr) from a 2003-17 base period	2018 Primary Productivity (% of the 2003-17 average)
Eurasian Arctic	**12.74**	0.011	30.8	4.06	106.0
Amerasian Arctic	1.19	0.626	4.7	-0.10	99.7
Sea of Okhotsk	2.08	0.564	4.1	-5.75	92.2
Bering Sea	2.45	0.398	5.7	1.12	101.8
Barents Sea	**12.85**	0.001	24.4	-0.97	98.8
Greenland Sea	**6.00**	0.020	14.5	-2.11	96.6
Hudson Bay	5.46	0.064	19.3	-2.84	93.5
Baffin Bay/Labrador	5.67	0.064	15.0	2.13	103.7
North Atlantic	**5.89**	0.003	17.5	-3.08	94.0
Average of Nine	**6.04**	0.001	15.3	-0.84	98.6

While similar trends have been reported previously for these regions using both SeaWiFS and MODIS data (Comiso, 2015), satellite evidence does suggest that recent increases in cloudiness have dampened the increases in production that would have otherwise occurred as a function of sea ice decline alone (Bélanger et al., 2013). Further challenges remain with linking primary productivity, as well as depth-integrated chlorophyll biomass throughout the water column, to satellite-based surface chlorophyll-*a* values (Babin et al., 2015; Lee et al., 2015; Tremblay et al., 2015; Kahru, 2017). Satellite-based chlorophyll-*a* and primary productivity estimates continue to be confounded by issues such as river turbidity in coastal regions (e.g., Demidov et al., 2014; Chaves et al., 2015) and the presence of sea ice. Efforts to improve satellite retrieval algorithms based on in situ observations are thus critical to continue in all regions of the Arctic.

References

Ardyna, M., M. Babin, E. Devred, A. Forest, M. Gosselin, P. Raimbault, and J.-É. Tremblay, 2017: Shelf-basin gradients shape ecological phytoplankton niches and community composition in the coastal Arctic Ocean (Beaufort Sea). *Limnol. Oceanogr*., 62, 2113-2132, doi: 10.1002/lno.10554.

Babin, M., S. Bélanger, I. Ellinsten, A. Forest, V. Le Fouest, T. Lacour, M. Ardyna, and D. Slagstad, 2015: Estimation of primary production in the Arctic Ocean using ocean colour remote sensing and coupled physical-biological models: Strengths, limitations and how they compare. *Prog. Oceanogr.*, 139, 197-220, doi: 10.1016/j.pocean.2015.08.008.

Barber, D. G., H. Hop, C. J. Mundy, B. Else, I. A. Dmitrenko, J. -É. Tremblay, J. K. Ehn, P. Assmy, M. Daase, L. M. Candlish, and S. Rysgaard, 2015: Selected physical, biological and biogeochemical implications of a

rapidly changing Arctic Marginal Ice Zone. *Prog. Oceanogr.*, 139, 122-150, doi: 10.1016/j.pocean.2015.09.003.

Behrenfeld, M. J., and P. G. Falkowski, 1997: Photosynthetic rates derived from satellite-based chlorophyll concentration. *Limnol. Oceanogr.*, 42(1), 1-20.

Bélanger, S., M. Babin, and J. É. Tremblay, 2013: Increasing cloudiness in Arctic damps the increase in phytoplankton primary production due to sea ice receding. *Biogeosciences*, 10, 4087-4101, doi: 10.5194/bg-10-4087-2013.

Chaves, J., P. J. Werdell, C. W. Proctor, A. R. Neeley, S. A. Freeman, C. S. Thomas, and S. B. Hooker, 2015: Assessment of ocean color data records from MODIS-Aqua in the western Arctic Ocean. *Deep-Sea Res. Pt. II*, 118A, 32-43, doi: 10.1016/j.dsr2.2015.02.011.

Comiso, J. C., 2015: Variability and trends of the global sea ice covers and sea levels: Effects on physicochemical parameters, in *Climate and Fresh Water Toxin* s. L. M. Botana, M. C. Lauzao, and N. Vilarino, Eds., De Gruyter, Berlin, Germany.

Comiso, J. C., R. Gersten, L. Stock, J. Turner, G. Perez, and K. Cho, 2017a: Positive trends in the Antarctic sea ice cover and associated changes in surface temperature. *J. Clim.*, 30, 2251-2267, doi: 10.1175/JCLI-D-16-0408.1.

Comiso, J. C., W. N. Meier, and R. Gersten, 2017b: Variability and trends in the Arctic Sea ice cover: Results from different techniques. *J. Geophys. Res. Oceans*, 122, 6883-6900, doi: 10.1002/2017JC012768.

Demidov, A. B., S. A. Mosharov, and P. N. Makkaveev, 2014: Patterns of the Kara Sea primary production in autumn: Biotic and abiotic forcing of subsurface layer. *J. Marine Syst.*, 132, 130-149, doi: 10.1016/j.jmarsys.2014.01.014.

Frey, K. E., J. A. Maslanik, J. Clement Kinney, and W. Maslowski, 2014: Recent variability in sea ice cover, age, and thickness in the Pacific Arctic Region, in *The Pacific Arctic Region: Ecosystem status and trends in a rapidly changing environment*. J. M. Grebmeier, and W. Maslowski, Eds., Springer: Dordrecht, pp. 31-64.

Frey, K. E., G. W. K. Moore, L. W. Cooper, and J. M. Grebmeier, 2015: Divergent patterns of recent sea ice cover across the Bering, Chukchi and Beaufort seas of the Pacific Arctic Region. *Prog. Oceanogr.*, 136, 32-49, doi: 10.1016/j.pocean.2015.05.009.

Giesbrecht, K. E., D. E. Varela, D. E., J. Wiktor, J. M. Grebmeier, B. Kelly, and J.E. Long, 2018 (in press): A decade of summertime measurements of phytoplankton biomass, productivity and assemblage composition in the Pacific Arctic Region from 2006 to 2016. *Deep Sea Res. Pt. II–Top. Stud. Oceanogr.*, doi: 10.1016/j.dsr2.2018.06.010.

Hill, V., M. Ardyna, S. H. Lee, and D. E. Varela, 2018: Decadal trends in phytoplankton production in the Pacific Arctic Region from 1950 to 2012. *Deep-Sea Res. Pt. II*, 152, 82-94, doi: 10.1016/j.dsr2.2016.12.015.

Kahru, M., 2017: Ocean productivity from space: Commentary. *Global Biogeochem. Cycles*, 31, 214-216, doi: 10.1002/2016GB005582.

Lee, Y. J., et al., 2015: An assessment of phytoplankton primary productivity in the Arctic Ocean from satellite ocean color/in situ chlorophyll-*a* based models. *J. Geophys. Res. Oceans*, 120, 6508-6541, doi: 10.1002/2015JC011018.

Leu, E., C. J. Mundy, P. Assmy, K. Campbell, T. M. Gabrielsen, M. Gosselin, T. Juul-Pedersen, and R. Gradinger, 2015: Arctic spring awakening - Steering principles behind the phenology of vernal ice algal blooms. *Prog.Oceanogr.*, 139, 151-170, doi: 10.1016/j.pocean.2015.07.012.

Moore, S. E., and J. M. Grebmeier, 2018: The Distributed Biological Observatory: Linking physics to biology in the Pacific Arctic region. *Arctic*, 71 (Suppl. 1), 1-7; doi: 10.14430/arctic4606.

Müller-Karger, F. E., R. Varela, R. Thunell, R. Luerssen, C. Hu, and J. J. Walsh, 2005: The importance of continental margins in the global carbon cycle. *Geophys. Res. Lett.*, 32, L01602, doi: 10.1029/2004GL021346.

Neeley, A. R., L. A. Harris, and K. E. Frey, 2018: Unraveling phytoplankton community dynamics in the northern Chukchi and western Beaufort seas amid climate change. *Geophys. Res. Lett.*, 45, 7663-7671, doi: 10.1029/2018GL077684.

Tremblay J. -É., L. G. Anderson, P. Matrai, S. Bélanger, C. Michel, P. Coupel, and M. Reigstad, 2015: Global and regional drivers of nutrient supply, primary production and CO_2 drawdown in the changing Arctic Ocean. *Prog. Oceanogr.*, 139, 171-196, doi: 10.1016/j.pocean.2015.08.009.

November 19, 2018

Tundra Greenness

H. Epstein[1], U. Bhatt[2], M. Raynolds[3], D. Walker[3], B. Forbes[4], G. Phoenix[5], J. Bjerke[6], H. Tømmervik[6], S. -R. Karlsen[7], R. Myneni[8], T. Park[8], S. Goetz[9], G. Jia[10]

[1]Department of Environmental Sciences, University of Virginia, Charlottesville, VA, USA
[2]Geophysical Institute, University of Alaska Fairbanks, Fairbanks, AK, USA
[3]Institute of Arctic Biology, University of Alaska Fairbanks, AK, USA
[4]Arctic Centre, University of Lapland, Rovaniemi, Finland
[5]Department of Animal and Plant Sciences, University of Sheffield, Sheffield, UK
[6]Norwegian Institute for Nature Research, Tromsø, Norway
[7]Norut Northern Research Institute, Tromsø, Norway
[8]Department of Earth and Environment, Boston University, Boston, MA, USA
[9]School of Informatics, Computing, and Cyber Systems, Northern Arizona University, Flagstaff, AZ, USA
[10]Institute of Atmospheric Physics, Chinese Academy of Sciences, Beijing, China

Highlights

- The overall trend for the satellite record (1982-2017) is one of general greening; however, there are certain regions that exhibit browning, such as the Yukon-Kuskokwim Delta of western Alaska, the High Arctic of the Canadian Archipelago, and the northwestern and north-coastal Siberian tundra.
- Tundra greenness declined in 2017, relative to 2016, with a particularly sharp drop in the integrated growing-season value for Eurasia, which was coupled with a large decrease (24.6%) in Summer Warmth Index.
- Observations from the literature (field and other remote sensing data) across various spatial scales, from small plots to the circumpolar Arctic, continue to provide evidence for both greening and browning.

Arctic tundra vegetation has responded to dramatic environmental changes over the course of the last several decades. The overall tendency has been an increase in the above-ground quantity of live vegetation, commonly referred to as "greening." However, vegetation changes do vary spatially, in both direction and magnitude, throughout the circumpolar Arctic and are not necessarily changing in a consistent fashion over time (e.g., Bhatt et al., 2013; Reichle et al., 2018). This variability suggests that there are complex interactions among the vegetation, atmosphere, ground (soils and permafrost), and grazing animals of the Arctic system. Changes in tundra vegetation can have important effects on carbon cycling and soil-atmosphere energy exchange (e.g., Treharne et al., 2016; Frost et al., 2018, Lafleur and Humphreys, 2018). The latter has implications for active layer depth and permafrost stability, thereby impacting Arctic landscapes. Changes in tundra vegetation can also have important effects on wildlife habitats. For instance, bird and mammal species have been shown to respond favorably (e.g., greater range and larger populations) to Arctic greening, including shrub expansion (e.g., Wheeler et al., 2018). Continued evaluation of the current state and dynamics of the circumpolar Arctic vegetation improves our understanding of these complex interactions and their impacts on the Arctic system and beyond.

There are a number of controls on inter-annual dynamics of tundra productivity, with summer air temperature the most widely acknowledged factor responsible for increases (greening) in tundra

vegetation (Ackerman et al., 2018; Keenan and Riley, 2018; Myers-Smith and Hik, 2018; Weijers et al., 2018; Bjorkman et al., 2018). However, several reports have shown increased temperatures to have a detrimental (browning) or no effect on tundra vegetation (Lara et al., 2018; Maliniemi et al., 2018; Opala-Owczarek et al., 2018; Xu et al., 2018). Tundra browning has also been observed in response to extreme events, which include winter warming and snowmelt (followed by frost-drought), icing (e.g., rain-on-snow), mammalian herbivore population cycles (Olofsson et al., 2009), and insect outbreaks (Phoenix and Bjerke, 2016; Treharne et al., 2016). Precipitation and moisture availability are also important controls on tundra vegetation dynamics (Lara et al., 2018; Maliniemi et al., 2018; Opala-Owczarek et al., 2018; Wang et al., 2018; Bjorkman et al., 2018) and are linked to the effects of air temperature changes; increased temperatures may lead to reduced growing-season soil moisture and increased water stress in tundra plants (Ackerman et al., 2018; Keenan and Riley, 2018; Opala-Owczarek et al., 2018). Changes in the snow regime have been found to drive dynamics in tundra vegetation structure (e.g., height) and functioning (e.g., carbon cycling) (Christiansen et al., 2018; Maliniemi et al., 2018; Opala-Owczarek et al., 2018; Parmentier et al., 2018; Wang et al., 2018). Changes in the land cover also affect tundra greenness; reductions in cryogenic disturbances (e.g., frost circles) (Becher et al., 2018) and increased lake drainage (Lara et al., 2018) can both lead to greening.

Arctic tundra vegetation, specifically the Normalized Difference Vegetation Index (NDVI), has been monitored continuously since 1982 via Earth-observing satellites with sub-daily return intervals. The data reported here are from the Global Inventory Modeling and Mapping Studies (GIMMS) 3g V1 dataset (GIMMS, 2013) and are based largely on the Advanced Very High Resolution Radiometer (AVHRR) sensors aboard NOAA satellites (Pinzon and Tucker, 2014). At the time of writing, the GIMMS3g V1 dataset was only available through 2017. The GIMMS product (at 1/12° resolution for this report) is a bi-weekly, maximum-value composited dataset of the NDVI, calculated from Earth-surface reflectances in the Red and Near Infrared wavelengths. NDVI is highly correlated with the quantity of above-ground vegetation (e.g., Raynolds et al., 2012; Karlsen et al., 2018), or the "greenness," of the Arctic tundra. We use two metrics based on the NDVI: MaxNDVI and TI-NDVI. MaxNDVI is the peak NDVI value for the year (the peak of the growing season) and is related to yearly maximum above-ground vegetation biomass. TI (time-integrated) NDVI is the sum of the bi-weekly NDVI values for the growing season and is correlated with the total above-ground vegetation productivity. The mean NDVI values for Eurasian tundra are inherently substantially greater than those for the North American tundra. This is because most of the Eurasian tundra occurs at lower latitudes compared to the North American tundra and, hence, has greater NDVI.

Examining the overall trend in tundra greenness for the now 36-year record (1982-2017), it is apparent that the MaxNDVI and the TI-NDVI have increased throughout a majority of the geographic circumpolar Arctic tundra (**Fig. 1a, b**). Regions with the greatest increases in tundra greenness are the North Slope of Alaska, the Low Arctic (southern tundra subzones) of the Canadian tundra, and eastern Siberia. Tundra greenness has declined or shown "browning" on the Yukon-Kuskokwim Delta of western Alaska, the High Arctic of the Canadian Archipelago, and the northwestern and north-coastal Siberian tundra. Specific regions of greening and browning, measured by NDVI increases and decreases, respectively, tend to be consistent between MaxNDVI and TI-NDVI. However, decreases in TI-NDVI tend to be more spatially extensive than decreases in MaxNDVI.

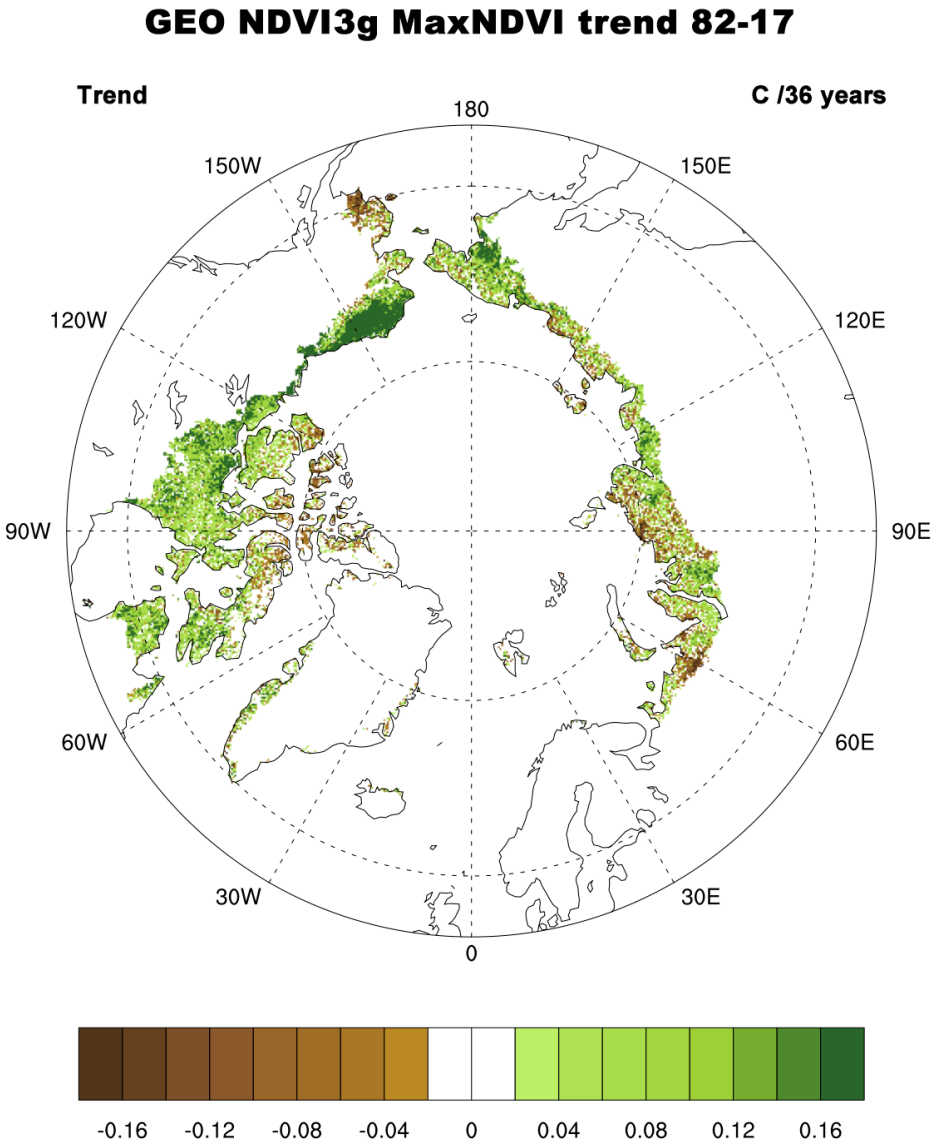

Fig. 1a. Magnitude of the overall trend in MaxNDVI (Maximum Normalized Difference Vegetation Index) for the period 1982-2017.

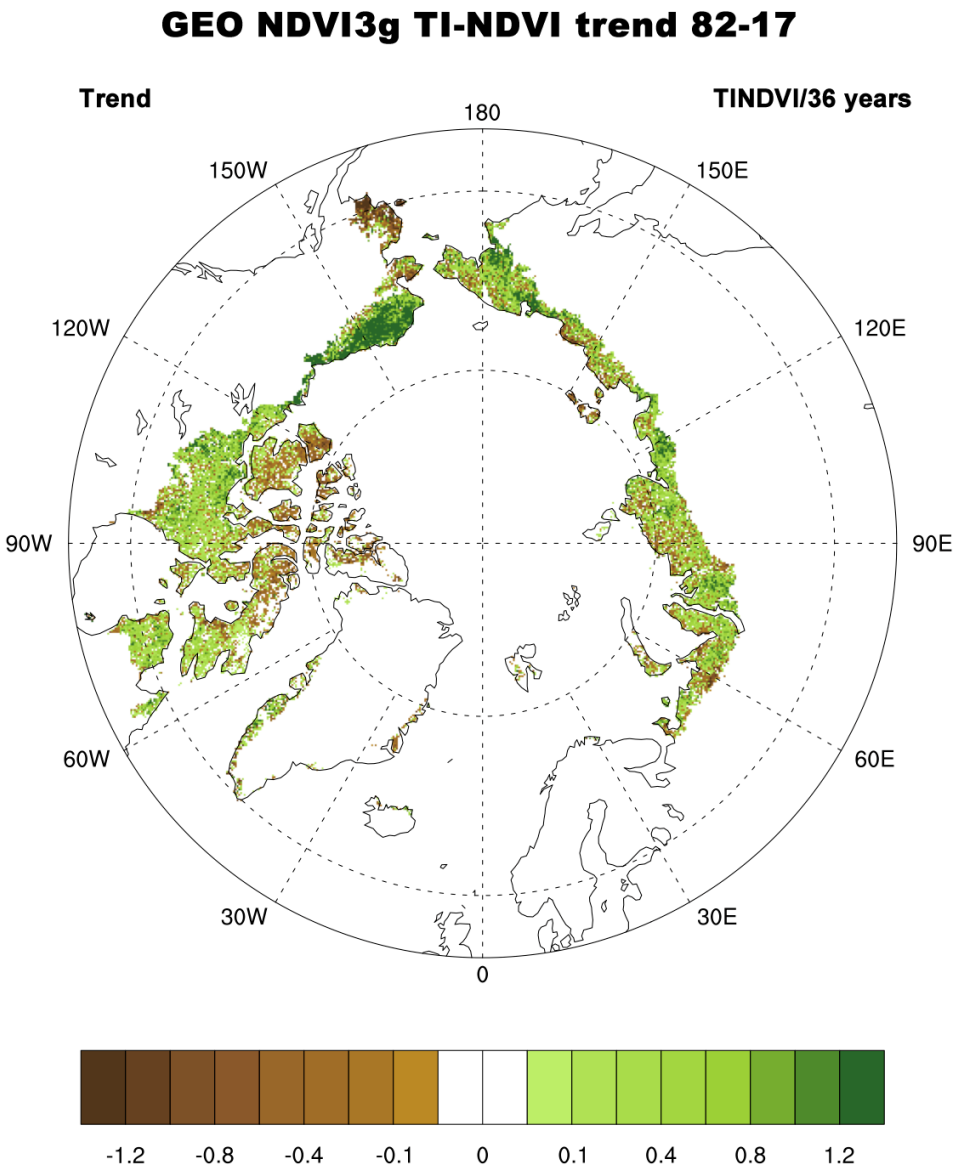

Fig. 1b. Magnitude of the overall trend in TI-NDVI (Time-integrated Normalized Difference Vegetation Index) for the period 1982 to 2017.

Considering variability on a year-to-year basis, NDVI declined in 2017 from the prior year for both indices over North America and Eurasia (**Fig. 2**). This decline follows two years of increases in the NDVI, with particularly high NDVI values observed in 2016. TI-NDVI in Eurasia declined substantially from 2016 to 2017 (9.7%—2nd largest single-year decline in the record), whereas it declined 3.9% for North America. MaxNDVI in Eurasia declined by 1.9% compared to 4.2% for North America.

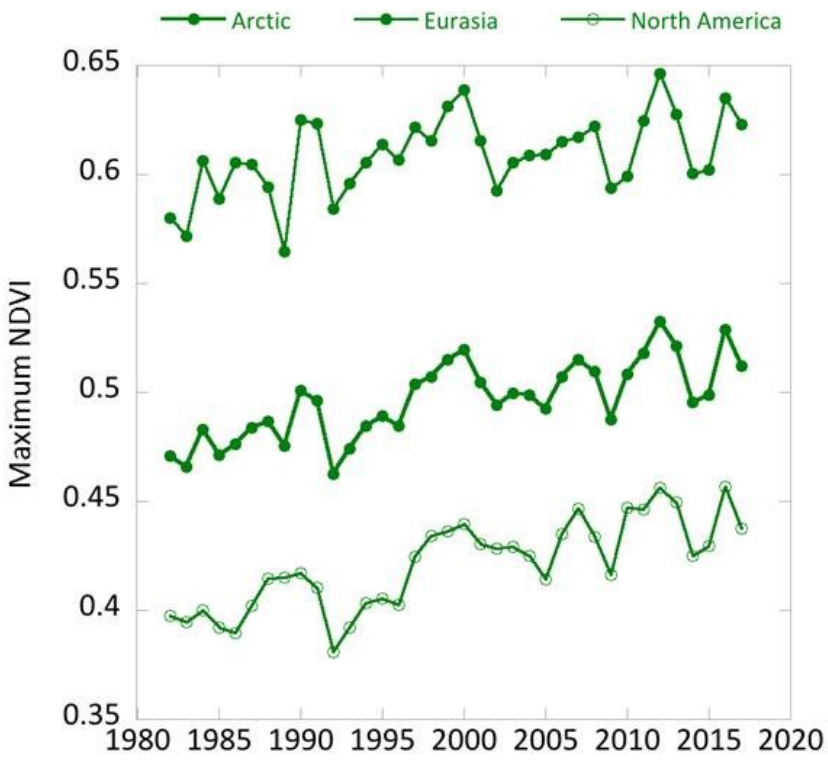

Fig. 2a. MaxNDVI from 1982 to 2017 for North America (bottom), Eurasia (top), and the Arctic as a whole (middle).

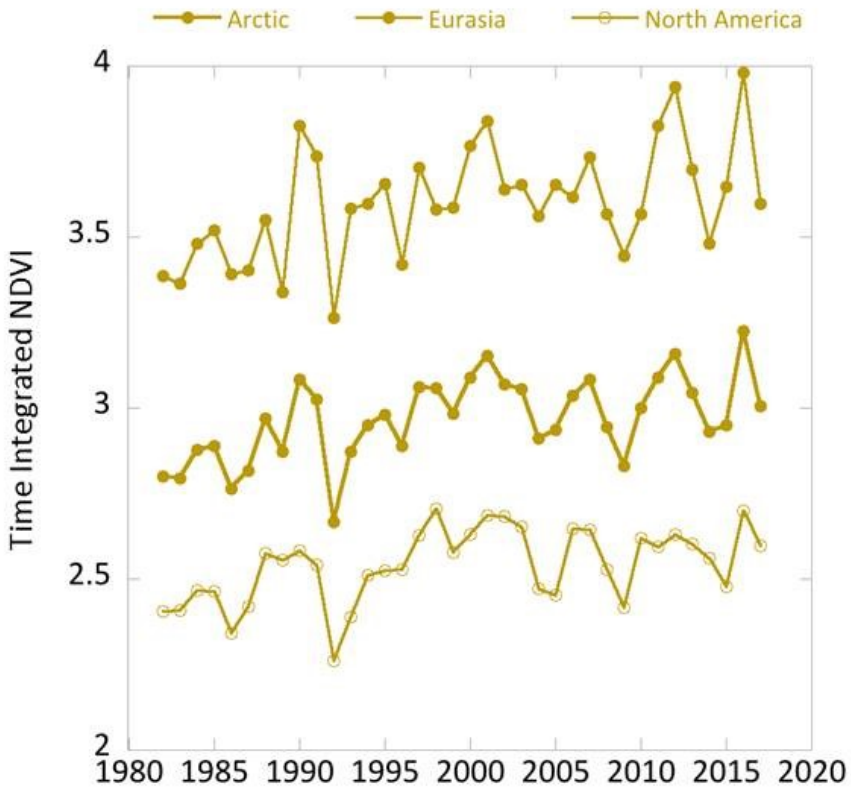

Fig. 2b. TI-NDVI from 1982 to 2017 for North America (bottom), Eurasia (top), and the Arctic as a whole (middle).

Despite the decline from 2016 to 2017, all of the NDVI values for 2017 were either equal to or greater than mean values for the 36-year record. MaxNDVI values for 2017 ranked 8th, 9th, and 8th for the Arctic, Eurasian Arctic, and North American Arctic, respectively. TI-NDVI values ranked 15th, 18th, and 13th for the Arctic, Eurasian Arctic, and North American Arctic, respectively. In order to compare NDVI changes with those of summer warmth (a key control of NDVI), we can use the remotely-sensed Land Surface Temperatures (LST), from the same sensors as those providing the NDVI values. The Summer Warmth Indices (SWI: sum of mean monthly temperatures >0° C) for the Arctic as a whole and for the North American Arctic were still relatively high, ranking 4th and 3rd, respectively, over the 36-year record. For the Eurasian Arctic, the SWI declined by 24.6% between 2016 and 2017, and the 2017 value was ranked 21st over the record.

References

Ackerman, D. E., D. Griffin, S. E. Hobbie, K. Popham, E. Jones, and J. C. Finlay, 2018: Uniform shrub growth response to June temperature on the North Slope of Alaska. *Environ. Res. Lett.*, 13, 044013.

Becher, M., J. Olofsson, L. Berglund, and J. Klaminder, 2018: Decreased cryogenic disturbance: one of the mechanisms behind the vegetation change in the Arctic. *Polar Biol.*, 41, 101-110.

Bhatt, U. S., D. A. Walker, M. K. Raynolds, P. A. Bieniek, H. E. Epstein, J. C. Comiso, J. E. Pinzon, C. J. Tucker, and I. V. Polyakov, 2013: Recent declines in warming and vegetation greening trends over pan-Arctic tundra. *Remote Sens.*, 4, 4229-4254.

Bjorkman, A. D., et al., 2018: Plant functional trait change across a warming tundra biome. *Nature*, 562, 57-62, doi: 10.1038/s41586-018-0563-7.

Christiansen, C. T., M. J. Lafreniere, G. H. R. Henry, and P. Grogan, 2018: Long-term deepened snow promotes tundra evergreen shrub growth and summertime ecosystem net CO_2 gain but reduces soil carbon and nutrient pools. *Global Change Biol.*, 24, 3508-3525.

Frost, G. V., H. E. Epstein, D. A. Walker, G. Matyshak, and K. Ermokhina, 2018: Seasonal and long-term changes in active-layer temperatures after tall shrubland expansion and succession in arctic tundra. *Ecosystems*, 21, 507-520.

Global Inventory Modeling and Mapping Studies (GIMMS), 2013: Available online: http://gcmd.nasa.gov/records/GCMD_GLCF_GIMMS.html

Karlsen, S. R., H. B. Anderson, R. van der Wal, and B. B. Hansen, 2018: A new NDVI measure that overcomes data sparsity in cloud-covered regions predicts annual variation in ground-based estimates of high arctic plant productivity. *Environ. Res. Lett.*, 13:025011.

Keenan, T. F., and W. J. Riley, 2018: Greening of the land surface in the world's cold regions consistent with recent warming. *Nature Clim. Chang* e, 8, 825-828, doi: 10.1038/s41558-018-0258-y.

Lafleur, P. M., and E. R. Humphreys, 2018: Tundra shrub effects on growing season energy and carbon dioxide exchange. *Environ. Res. Lett.*, 13, 055001.

Lara, M. J., I. Nitze, G. Grosse, P. Martin, and A. D. McGuire, 2018: Reduced arctic tundra productivity linked with landform and climate change interactions. *Sci. Rep.*, 8, 2345.

Maliniemi, T., J. Kapfer, P. Saccone, A. Skog, and R. Virtanen, 2018: Long-term vegetation changes of treeless heath communities in northern Fennoscandia: Links to climate change trends and reindeer grazing. *J. Veg. Sci.*, 29, 469-479.

Myers-Smith, I. H., and D. S. Hik, 2018: Climate warming as a driver of tundra shrubline advance. *J. Ecol.*, 106, 47-560.

Olofsson J., L. Oksanen, T. Callaghan, P. E. Hulme, T, Oksanen, and O. Suominen, 2009: Herbivores inhibit climate-driven shrub expansion on the tundra. *Global Change Biol.*, 15, 2681-2693.

Opala-Owczarek, M., E. Piroznikow, P. Owczarek, W. Szymanski, B. Luks, D. Kepski, M. Szymanowski, B. Wojtun, and K. Migala, 2018: The influence of abiotic factors on the growth of two vascular plant species (*Saxifraga oppositifolia* and *Salix polaris*) in the High Arctic. *Catena*, 163, 219-232.

Parmentier, F. -J., D. Rasse, M. Lund, J. W. Bjerke, B. G. Drake, S. Weldon, H. Tømmervik, and G. H. Hansen, 2018: Vulnerability and resilience of the carbon exchange of a subarctic peatland to an extreme winter event. *Environ. Res. Lett.*, 13, 065009.

Phoenix, G. K., and J. W. Bjerke, 2016: Arctic browning: Extreme events and trends reversing arctic greening. *Global Change Biol.*, 22, 2960-2962.

Pinzon, J., and C. Tucker, 2014: A non-stationary 1981-2014 AVHRR NDVI3g time series. *Remote Sens.*, 6, 6929-6960, doi: 10.3390/rs6086929.

Raynolds M. K., D. A. Walker, H. E. Epstein, J. E. Pinzon, and C. J. Tucker, 2012: A new estimate of tundra-biome phytomass from trans-Arctic field data and AVHRR NDVI. *Remote Sens. Lett.*, 3, 403-411.

Reichle, L. M., H. E. Epstein, U. S. Bhatt, M. K. Raynolds, and D. A. Walker, 2018: Spatial heterogeneity of the temporal dynamics of Arctic tundra vegetation. *Geophys. Res. Lett.*, 45, 9206-9215, doi: 10.1029/2018GL078820.

Treharne, R., J. W. Bjerke, L. D. Emberson, H. Tømmervik, and G. K. Phoenix, 2016: Arctic browning: Vegetation damage and implications for carbon balance. *Geophys. Res. Abstracts*, 18, EGU2016-8838.

Wang, X., T. Wang, H. Guo, D. Liu, Y. T. Zhao, T. T. Zhang, Q. Liu, and S. L. Piao, 2018: Disentangling the mechanisms behind winter snow impact on vegetation activity in northern ecosystems. *Global Change Biol.*, 24, 1651-1662.

Weijers, S., I. H. Myers-Smith, and J. Loeffler, 2018: A warmer and greener cold world: summer warming increases shrub growth in the alpine and high arctic tundra. *Erdkunde*, 72, 63-85.

Wheeler, H. C., T. T. Hoye, and J. -C. Svenning, 2018: Wildlife species benefitting from a greener Arctic are most sensitive to shrub cover at leading range edges. *Global Change Biol.*, 24, 212-223.

Xu, X., W. J. Riley, C. D. Koven, and G. S. Jia, 2018: Observed and simulated sensitivities of spring greenup to preseason climate in northern temperate and boreal regions. *J. Geophys. Res.–Biogeosci.*, 123, 60-78.

River Discharge

R. M. Holmes[1], A. I. Shiklomanov[2,3], A. Suslova[1], M. Tretiakov[3], J. W. McClelland[4], R. G. M. Spencer[5], S. E. Tank[6]

[1]Woods Hole Research Center, Falmouth, MA, USA
[2]University of New Hampshire, Durham, NH, USA
[3]Arctic and Antarctic Research Institute, St. Petersburg, Russia
[4]University of Texas at Austin, Marine Science Institute, Port Aransas, TX, USA
[5]Florida State University, Tallahassee, FL, USA
[6]University of Alberta, Edmonton, AB, Canada

Highlights

- In 2018, the combined daily discharge of the six largest Eurasian rivers peaked on June 4, five days earlier than the average over the 1980-89 reference period. The combined daily discharge of the Yukon and Mackenzie rivers peaked on May 29, four days earlier than the average during the reference period.
- In 2018, summer/autumn discharge (July 15-September 30) for the eight largest Arctic rivers was 20% greater than the 1980-89 reference period.
- Since last covered in the Arctic Report Card in 2015, Arctic river discharge has continued to increase, providing powerful evidence for the ongoing intensification of the Arctic hydrologic cycle.

The Arctic Ocean contains only about 1% of global ocean volume but receives greater than 10% of global river discharge (Aagaard and Carmack, 1989; McClelland et al., 2012). Consequently, terrestrial influences via river inputs are much stronger in the Arctic Ocean than in other ocean basins. Rapid change in the Arctic system is altering land-ocean linkages, impacting coastal and ocean physics, chemistry, and biology. Because rivers integrate processes occurring throughout watersheds, changes in the discharge and chemistry of large rivers can also signal widespread terrestrial change (Rawlins et al., 2010; Holmes et al., 2013).

Reported here are river discharge values for the eight largest Arctic rivers, updating the 2015 Arctic Report Card chapter (Holmes et al., 2015). Together, the watersheds of these eight rivers cover approximately two-thirds of pan-Arctic drainage area and account for over 60% of river water inputs to the Arctic Ocean (**Fig. 1**). Discharge measurements for the six Russian rivers began in 1936, whereas discharge measurements did not begin until 1973 for the Mackenzie River and 1976 for the Yukon River. Thus, we used 1980-89 as a reference period, the first decade with discharge measurements for all eight rivers.

Fig. 1. Map showing the watersheds of the eight rivers featured in this report. Together they cover two-thirds of the 16.8 x 10^6 km^2 pan-Arctic watershed. The red dots show the location of the discharge monitoring stations and the red line shows the boundary of the pan-Arctic watershed.

A long-term increase in Arctic river discharge has been well documented (Peterson et al., 2002; McClelland et al., 2006). There is still some uncertainty about what is driving this trend, but documented increases in cold seasons precipitation provide a particularly compelling explanation (Shiklomanov and Lammers, 2009; Overeem and Syvitski, 2010; Rawlins et al., 2010; Déry et al., 2016; Rood et al., 2017). The long-term increasing discharge trend has been greatest for rivers of the Eurasian Arctic and constitutes the strongest evidence of intensification of the Arctic freshwater cycle (Rawlins et al., 2010).

In 2018, the combined daily discharge of the six Eurasian Arctic rivers peaked on June 4, five days earlier than the 1980-89 average (**Fig. 2a**). For the first nine months of 2018 (January 1-September 30), Eurasian river discharge was 7% greater than the 1980-89 average for the same period (**Table 1**). Discharge was particularly high in the Eurasian rivers during summer and autumn 2018, with their combined discharge over the period July 15-September 30 being 25% greater than the 1980-89 average for that same period (**Fig. 2**).

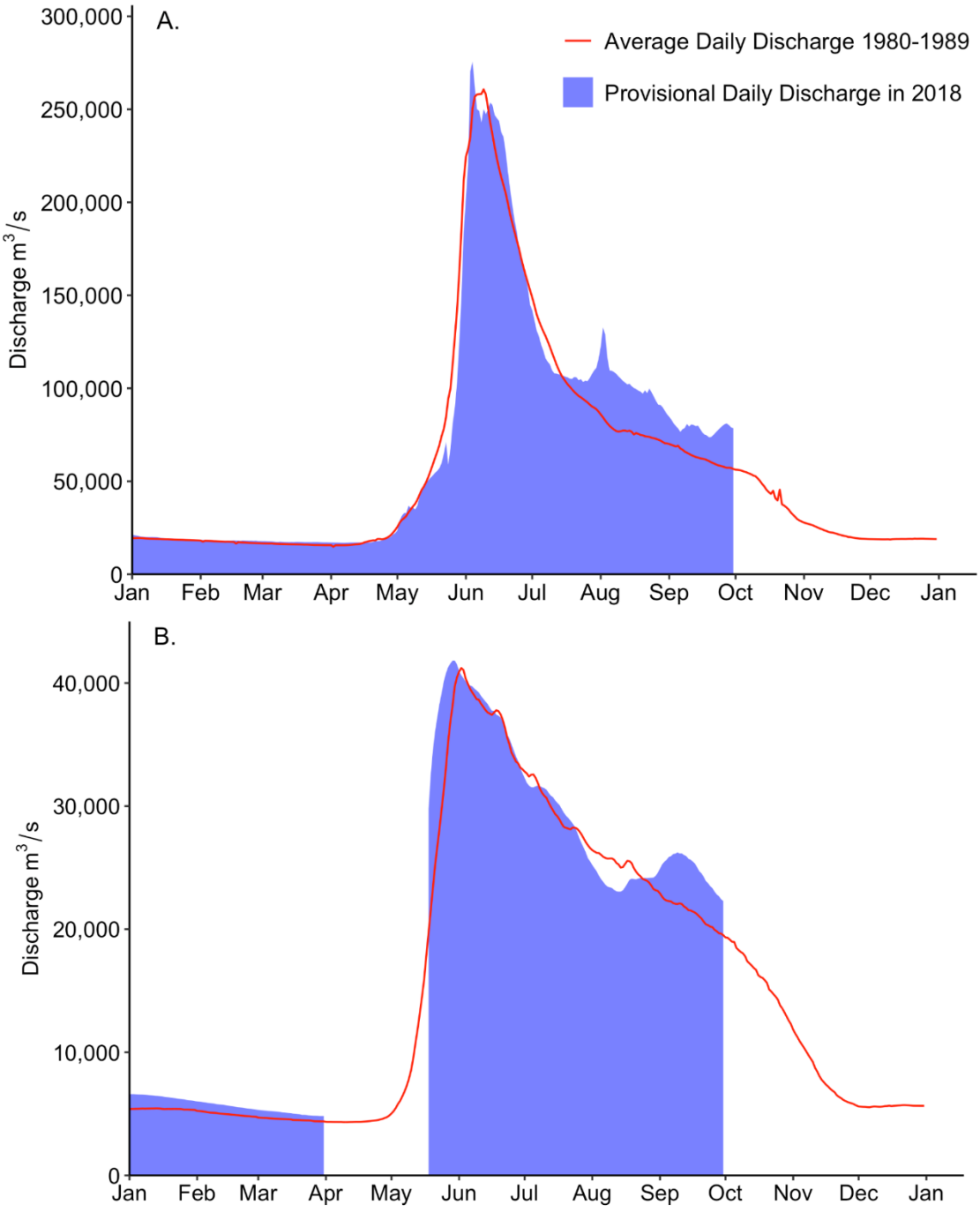

Fig. 2. Combined daily discharge (measured in cubic meters per second) for the first nine months of 2018 compared to the 1980-1989 average for the A) six Eurasian rivers, and B) two North American rivers. All 2018 data are provisional.

Table 1. Cumulative discharge for the first nine months of 2018 compared to the January-September average for 1980-89. Red values indicate provisional data and are subject to modification until official data are published. We

are not able to calculate Yukon River discharge for January-September 2018 because we are missing data for April 1-May 17.

	January - August Discharge (km^3)							
	Pechora	**S. Dvina**	**Ob'**	**Yenisey**	**Lena**	**Kolyma**	**Yukon**	**Mackenzie**
2018	82	94	353	502	571	91	NA	241
1980-89 Average	94	83	318	503	490	65	169	227

The combined daily discharge of the Yukon and Mackenzie rivers peaked on May 29, 2018, four days earlier than the 1980-89 average (**Fig. 2b**). Discharge for the North American rivers from July 15-September 30 was 4% greater than the average over the 1980-89 reference period. When the Eurasian and North American rivers are considered together, their combined discharge in 2018 over the July 15-September 30 period was 20% greater than the average over the 1980-89 reference period.

In 2017, Eurasian Arctic river discharge was 12% greater than the average for the 1980-89 reference period (**Table 2**). In 2016 and 2015, river discharge was 5% and 15% greater than the 1980-89 average, respectively. In fact, over the past 15 years, Eurasian Arctic river discharge exceeded the long-term average in all but two years, 2003 and 2012 (**Fig. 3**). Taken together, these results indicate a continuing long-term trend of increasing Eurasian Arctic river discharge.

Table 2. Annual discharge for the eight largest Arctic rivers since 2015, compared to long-term and decadal averages back to the start of observations. Red values indicate provisional data.

	Discharge (km^3/y)								
	Yukon	**Mackenzie**	**Pechora**	**S. Dvina**	**Ob'**	**Yenisey**	**Lena**	**Kolyma**	**Sum**
2017	192	290	109	127	446	608	590	108	2470
2016	242	281	87	97	431	530	652	66	2386
2015	213	265	137	80	527	649	585	64	2520
Average 2010-17	213	288	107	98	414	585	596	90	2391
Average 2000-09	206*	304	124	103	419	641	590	72	2459
Average 1990-99	216*	275*	117	111	405	613	532	68	2337
Average 1980-89	205	273	108	100	376	582	549	68	2261
Average 1970-79	183*	303*	108	94	441	591	529	65	2314
Average 1960-69	-	-	112	98	376	546	535	73	-
Average 1950-59	-	-	110	108	380	566	511	74	
Average 1940-49	-	-	102	100	424	578	498	72	-
Average for Period of Record	206	288	111	100	402	588	542	73	2310

*The first full year of Yukon discharge measurements at Pilot Station was 1976. Discharge measurements for the Yukon River at Pilot Station are missing for 1996-2001. The first full year of Mackenzie discharge measurements at

Arctic Red River was 1973. Discharge measurements for the Mackenzie River at Arctic Red River are missing for 1997 and 1998.

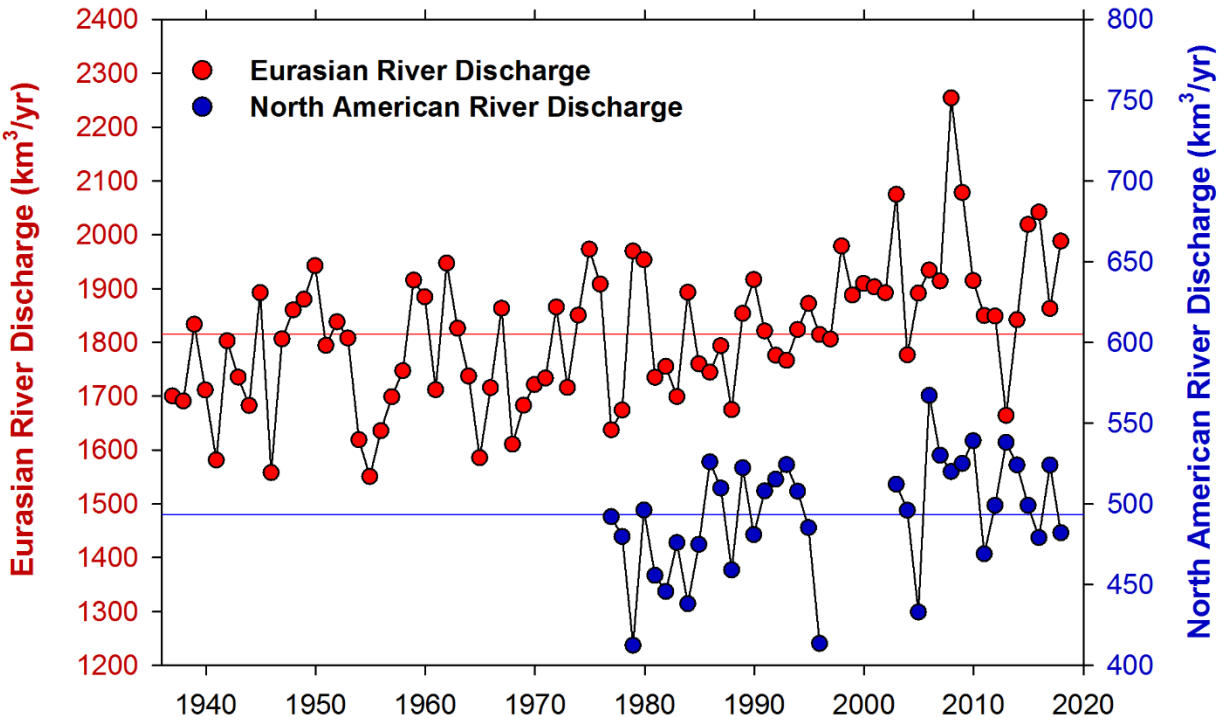

Fig. 3. Long-term trends in annual discharge for Eurasian (red) and North American (blue) Arctic rivers. Note the different scales for the Eurasian and North American river discharge; discharge from the former is 3-4 times greater than it is from the latter. Reference lines show long-term means for the Eurasian (1816 km^3/y, 1936-2017) and North American (493 km^3/y, 1976-2017) rivers.

In 2017, the combined discharge of the two largest North American Arctic rivers, the Yukon and Mackenzie, was 482 km^3, slightly above the 1980-89 reference period (**Table 2**). In 2016 the combined discharge of the Yukon and Mackenzie river was 9% greater than the 1980-89 reference period, whereas in 2015 the combined discharge of these two rivers was very similar to the reference period (**Table 2**). Since 1976, the increase in the combined river discharge has been 3.3±1.6% per decade for the Eurasian rivers and 2.0±1.8% per decade for the North American rivers (**Fig. 3**; Mann-Kendall trend analysis ±95% confidence interval).

Considering the eight Eurasian and North American Arctic rivers together, their combined discharge in 2017 (2470 km^3) was 9% greater than the average discharge for the period 1980-89 (**Table 2**). Values for 2016 (2387 km^3) and 2015 (2521 km^3) were 6% and 11% greater than the 1980-89 average, respectively. Overall these results indicate that Arctic river discharge continues to march upwards, providing powerful evidence for the intensification of the Arctic hydrologic cycle.

Acknowledgments

We thank the United States Geological Survey (Yukon), Water Survey of Canada (Mackenzie) and Roshydromet (Severnaya Dvina, Pechora, Ob', Yenisey, Lena, and Kolyma) for the discharge data used here. Most of these data are now available through the Arctic Great Rivers Observatory

(www.arcticgreatrivers.org). This work was supported by grants from the National Science Foundation in support of the Arctic Great Rivers Observatory (NSF 1602615, 1603149, 1602680, 1602879). The processing and analysis of near real time data for Russian Arctic rivers was supported in part by the Russian Foundation for Basic Research (grant 18-05-60192).

References

Aagaard, K., and E. C. Carmack, 1989: The role of sea ice and other fresh water in the Arctic circulation. *J. Geophys. Res.*, 94(C10): 14,485-14,498.

Déry, S. J., T. A. Stadnyk, M. K. MacDonald, and B. Gauli-Sharma, 2016: Recent trends and variability in river discharge across northern Canada. *Hydrol. Earth Syst. Sci.*, 20, 4801-4818, doi: 10.5194/hess-20-4801-2016.

Holmes, R. M., M. T. Coe, G. J. Fiske, T. Gurtovaya, J. W. McClelland, A. I. Shiklomanov, R. G. M. Spencer, S. E. Tank, and A. V. Zhulidov, 2013: Climate change impacts on the hydrology and biogeochemistry of Arctic Rivers, in *Global Impacts of Climate Change on Inland Waters*. C. R. Goldman, M. Kumagai, and R. D. Robarts, Eds., Wiley, pp. 3-26.

Holmes, R. M., A. I Shiklomanov, S. E. Tank, J. W. McCelland, and M. Tretiakov, 2015: River Discharge [in Arctic Report Card 2015], https://www.arctic.noaa.gov/Report-Card.

McClelland, J. W., S. J. Déry, B. J. Peterson, R. M. Holmes, and E. F. Wood, 2006: A pan-arctic evaluation of changes in river discharge during the latter half of the 20th century. *Geophys. Res. Lett.*, 33, L06715, doi: 06710.01029/02006GL025753.

McClelland, J. W., R. M. Holmes, K. H. Dunton, and R. Macdonald, 2012: The Arctic Ocean estuary. *Estuar. Coast.*, 35, 353-368, doi: 10.1007/s12237-010-9357-3.

Overeem, I., and J. P. M. Syvitski, 2010: Shifting discharge peaks in Arctic rivers, 1977-2007. *Geogr. Ann. A*, 92, 285-296.

Peterson, B. J., R. M. Holmes, J. W. McClelland, C. J. Vorosmarty, R. B. Lammers, A. I. Shiklomanov, I. A. Shiklomanov, and S. Rahmstorf, 2002: Increasing river discharge to the Arctic Ocean. *Science*, 298, 2171-2173.

Rawlins, M. A., et al., 2010: Analysis of the arctic system freshwater cycle intensification: Observations and expectations. *J. Clim.*, 23, 5715-5737, doi: 10.1175/2010JCLI3421.1.

Rood, S. B., S. Kaluthota, L. J. Philipsen, N. J. Rood, and K. P. Zanewich, 2017: Increasing discharge from the Mackenzie River system to the Arctic Ocean. *Hydrol. Process.*, 31, 150-160, doi: 10.1002/hyp.10986.

Shiklomanov A. I., and R. B. Lammers, 2009: Record Russian river discharge in 2007 and the limits of analysis. *Environ. Res. Lett.*, 4, 045015, doi: 10.1088/1748-9326/4/4/045015.

November 13, 2018

Lake Ice

C. Duguay[1], L. Brown[2]

[1]Department of Geography and Environmental Management, University of Waterloo, Canada
[2]Department of Geography, University of Toronto, Mississauga, Canada

Highlights

- Freeze-up during the 2017/18 ice season occurred within ±1-2 weeks of the 2004-17 mean for most regions of the Arctic. In striking contrast, Lakes Ladoga and Onega (Russia) and lakes within the southernmost part of Finland experienced later freeze-up, on the order of 4-5 weeks.
- With a few exceptions, break-up dates were within ±1 week from the 2004-17 mean across the Arctic.
- Ice cover duration anomalies largely mirrored those of freeze-up dates for much of the Arctic.

Lake ice is an important component of the cryosphere for several weeks to several months of the year in high-latitude regions. The presence (or absence) of ice cover on lakes during the winter months affects both regional weather and climate (e.g., thermal moderation and lake-induced snowfall) (Brown and Duguay, 2010; Baijnath-Rodino et al., 2018). Hence, monitoring of lake ice is critical to our skill at regional forecasting (Kheyrollah Pour et al., 2012; Eerola et al., 2014). Lake ice phenology, which encompasses freeze-up (ice-on) and break-up (ice-off) dates, and ice cover duration, is predominantly influenced by air temperature changes and, therefore, is a robust indicator of regional climate trends and variability. Lake ice cover has been identified as an Essential Climate Variable (ECVs) by the Global Climate Observing System (GCOS) (GCOS, 2016).

Analyses of records from ground-based observational networks have provided much of the evidence of long-term trends, variability and regime shifts in lake ice phenology. Satellite remote sensing has assumed a greater role in lake ice observing in recent years due to: 1) a dramatic reduction in ground-based observational recordings globally since the 1980s (IGOS, 2007; Jeffries et al., 2012; Duguay et al., 2015a) and 2) the availability of increasingly longer satellite datasets, particularly from 2000 onward (Duguay et al., 2015b). Recent analyses from satellite records (Šmejkalová et al., 2016; Surdu et al., 2016; Du et al., 2017) reveal that break-up continues to occur earlier in the 21st century for many lakes of the Arctic; a trend that continues to follow that documented from ground-based observations for the second half of the 20th century (Duguay et al., 2006).

For this report, lake ice phenology dates (freeze-up/ice-on and break-up/ice-off dates) and ice cover duration are derived from the NOAA Interactive Multisensor Snow and Ice Mapping System (IMS) 4-km resolution grid daily product for the 2017-18 ice season over the Arctic. These dates are compared to mean conditions for the length of the available satellite records, which begin in 2004. The IMS (Helfrich et al., 2007) incorporates a wide variety of satellite imagery (AVHRR, GOES, SSMI, etc.) as well as derived mapped products (USAF Snow/Ice Analysis, AMSU, etc.) and surface observations. Approximately 15,000 4-km pixels are identified as water in the region north of 58° N.

Freeze-up Period

Freeze-up (FU) in 2017/18 occurred earlier than the 2004-17 mean by ~1-3 weeks for most of Siberia, Norway, Sweden, and northern Finland. Ice in some valley lakes in the Scandinavian Mountains range began to form as early as mid-November, which is ~1 month earlier than the mean (**Fig. 1**). Lakes located in northeastern Canada and immediately to the west of Hudson Bay experienced FU close to the 2004-17 mean (±1 week earlier or later). West of the latter region, and in the Mackenzie Basin (e.g., Great Bear Lake) and the western coast of Alaska, FU occurred later than mean conditions by ~2 weeks, with some small sections of Great Bear Lake exceeding 3 weeks later. Despite the later FU on Great Bear Lake, when ice did begin to form, the lake froze over faster than the mean time needed to freeze, freezing over completely in 25 days (vs. 30 days mean). Located in the same region, Great Slave Lake froze over completely in 16 days (vs. 36 days mean). The most striking FU anomalies are noticeable in southern Finland and western Russia, where lake ice formed ~2-5 weeks later in 2017/18 compared to the mean period. Lakes Ladoga and Onega (western Russia) and lakes of smaller size in the southernmost part of Finland froze over in a period spanning mid-January to late February, later than any other region of the Arctic. FU anomalies of this magnitude were also observed for these lake regions during the 2013/14 ice season (Duguay et al., 2015a). When Lakes Ladoga and Onega did freeze over, a complete ice cover formed ~2 weeks faster than the mean freeze time for each lake. The mean freeze time is 54 days for Lake Ladoga and 40 days for Lake Oneida, for the 2004-07 period. Freeze time for 2017/18 was 36 and 24 days, respectively.

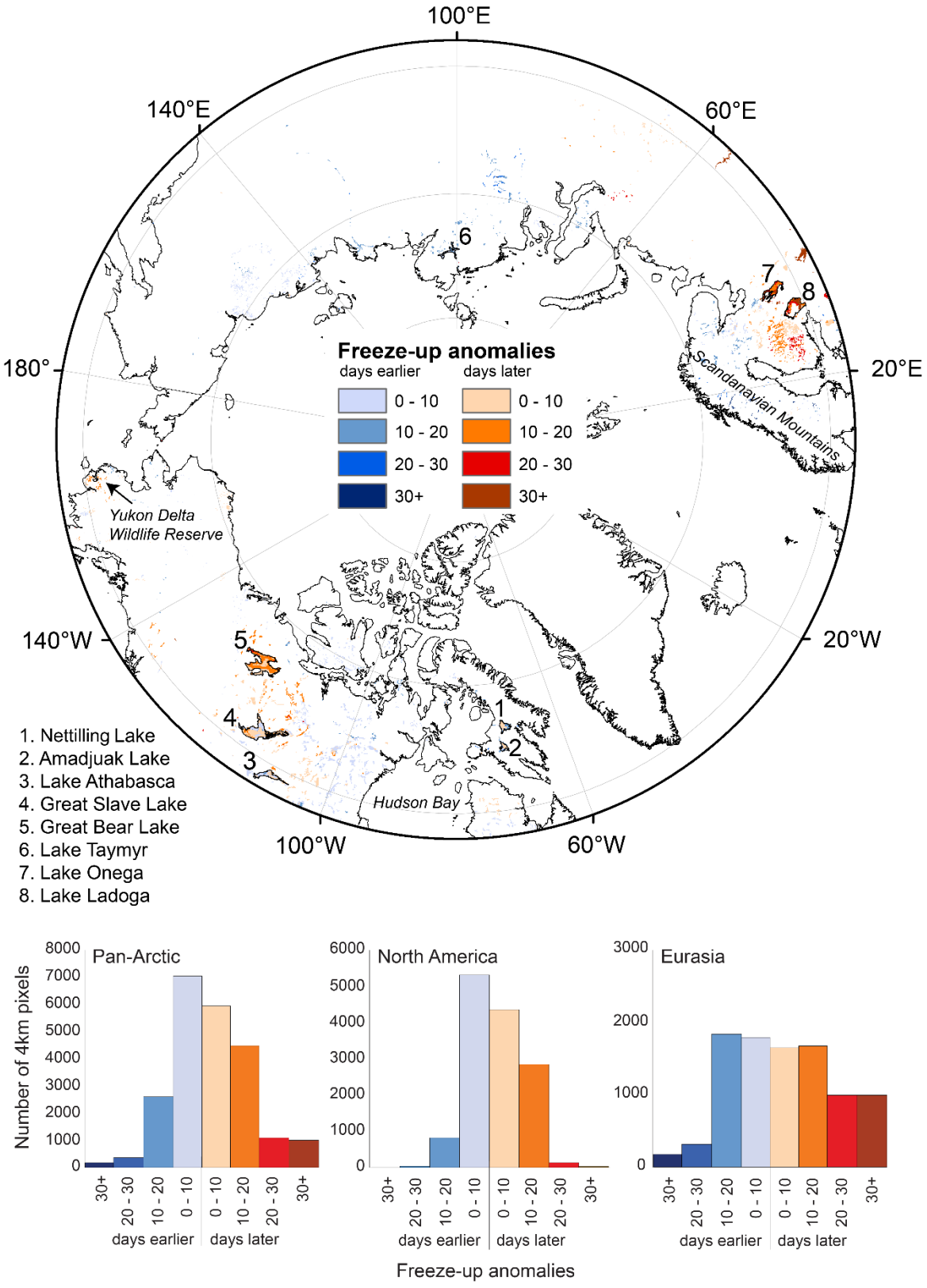

Fig. 1. Lake ice freeze-up anomalies in 2017/18 relative to the 2004-17 mean from the NOAA IMS 4-km product. Specific regions and lakes referred to in the text are highlighted.

Break-up Period

Break-up (BU) anomalies were relatively small for the 2017/18 ice season. BU dates occurred within ±1 week of the 2004-17 mean for most of the Arctic (**Fig. 2**). Some notable exceptions with earlier BU of ~2-3 weeks include Lake Taymyr (Siberia), and the lakes of southwestern Alaska (Yukon Delta Wildlife Refuge) and northern Scandinavia. At Lake Taymyr, the BU on most of the lake ranged from 10 to 16 days earlier, but with sections reaching as much as 1 month earlier and 1 week later. A few lakes with later BU anomalies of the same order of magnitude can be found in northeastern Canada (northern Quebec and Baffin Island, where ice persisted on Amadjuak Lake until 19 August) and Lake Ladoga (Russia), where ice cover persisted until late April (up to 23 days later than usual) and it took 28 days longer than normal for the lake to become ice free.

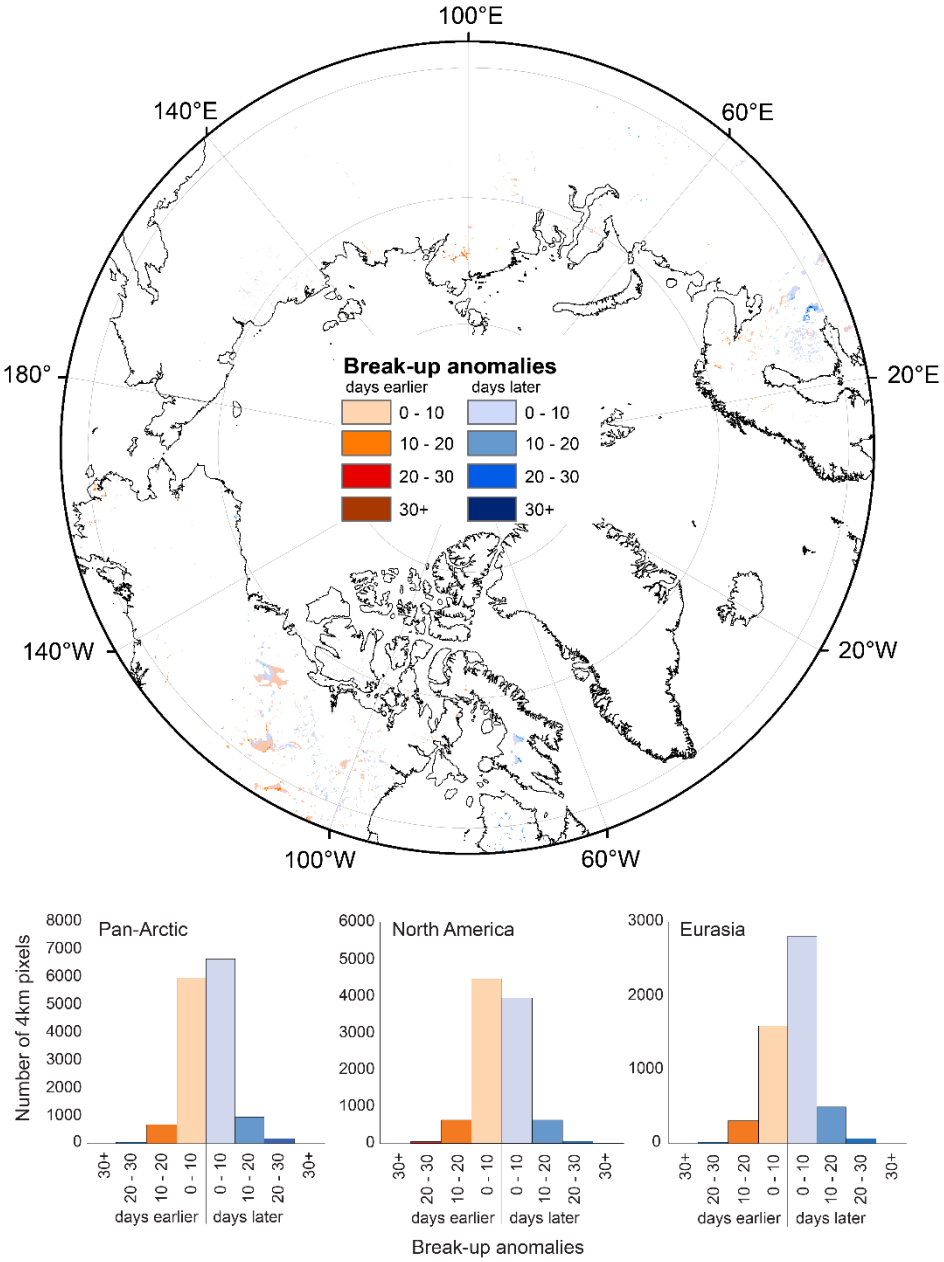

Fig. 2. Lake ice break-up anomalies in 2017/18 relative to the 2004-17 mean from the NOAA IMS 4-km product.

Ice Cover Duration

Since BU anomalies were relatively small, the spatial pattern of ice cover duration (ICD) anomalies followed closely that of FU anomalies. However, this is not always the case. For example, in the 2012/13 season, ICD followed the BU anomalies closely (Duguay et al., 2013) (**Fig. 3**). ICD for 2017/18 was shorter by up to ~1-4 weeks for Lakes Ladoga and Onega (western Russia) and 2-3 weeks shorter for lakes located in the southernmost part of Finland (ICDs as short as 98 days), northwestern Canada (Great Bear Lake and most of Great Slave and Athabasca lakes) and coastal southwestern Alaska. ICD was longer by ~1-2 weeks for most other regions of the Arctic. Exceptions are some lakes in the Scandinavian Mountains, where ICD was nearly 2 months longer, and Amadjuak and Nettilling lakes (the two largest lakes of Baffin Island). ICD was ~2-8 weeks longer in 2017/18 compared to 2004-17 mean for these lakes, with ice cover remaining on Amadjuak Lake for 311 days on the eastern side of the lake.

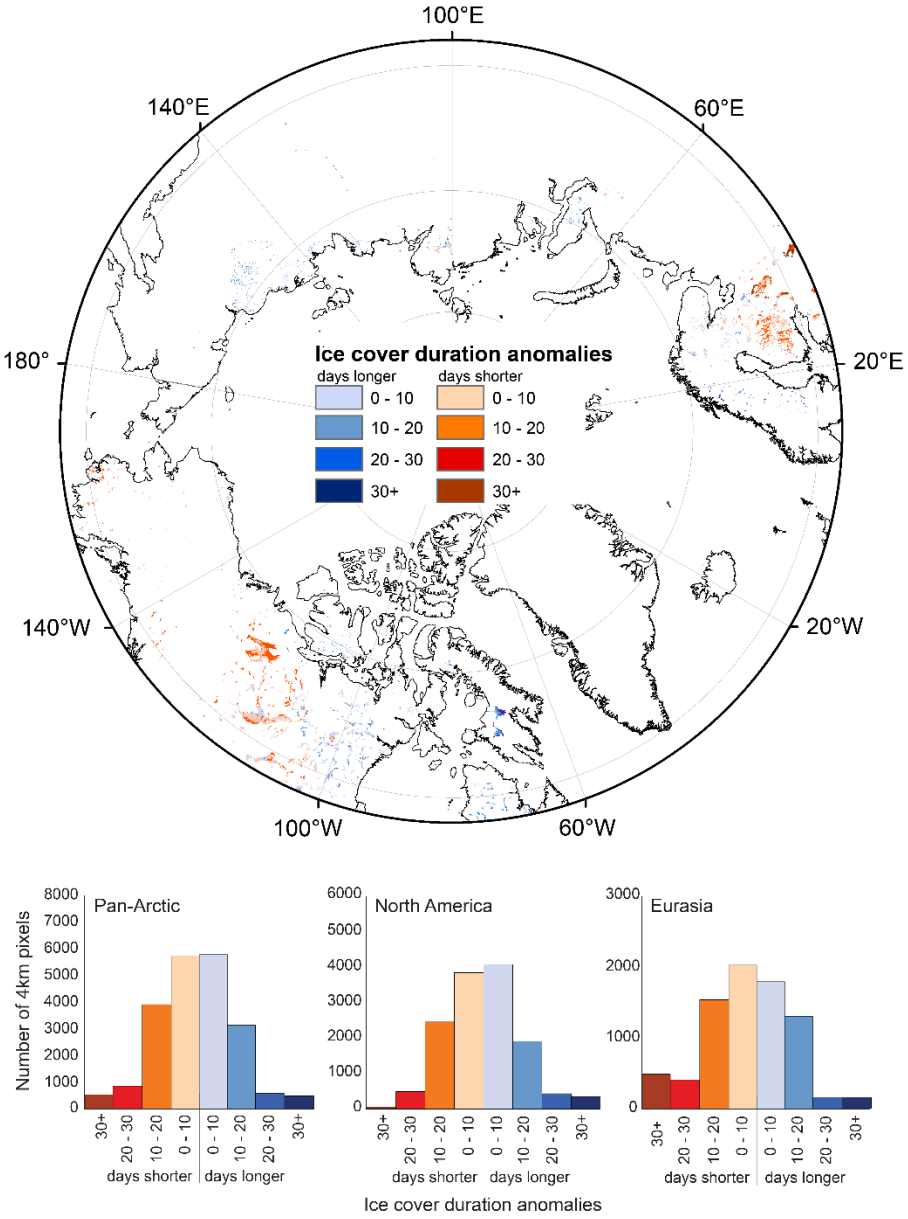

Fig. 3. Lake ice duration anomalies in 2017/18 relative to the 2004-17 mean from the NOAA IMS 4-km product.

Figure 4 provides lake-wide ice duration anomalies for selected large lakes in Canada and Russia for the 2004-18 period. Both Amadjuak and Nettilling lakes show a range of ICD from 11 days shorter to 15 and 18 days longer, respectively. These lakes have shown positive ICD anomalies for 7 of the last 14 ice seasons, with most of the longer ICD anomalies in the past six seasons. ICD on other large lakes, Great Bear and Great Slave lakes, and Lake Taymyr, show variations around the mean with ICD anomalies ranging from -18 to +26 days of ice compared to the mean of all seasons examined, with Great Slave and Great Bear lakes showing negative (shorter ICD) anomalies in 9 of past 14 seasons. Lakes Ladoga and Onega show the greatest variation in ICD anomalies over the full length of the IMS 4-km record (2004-18) with 59 days shorter to 57 days longer, respectively.

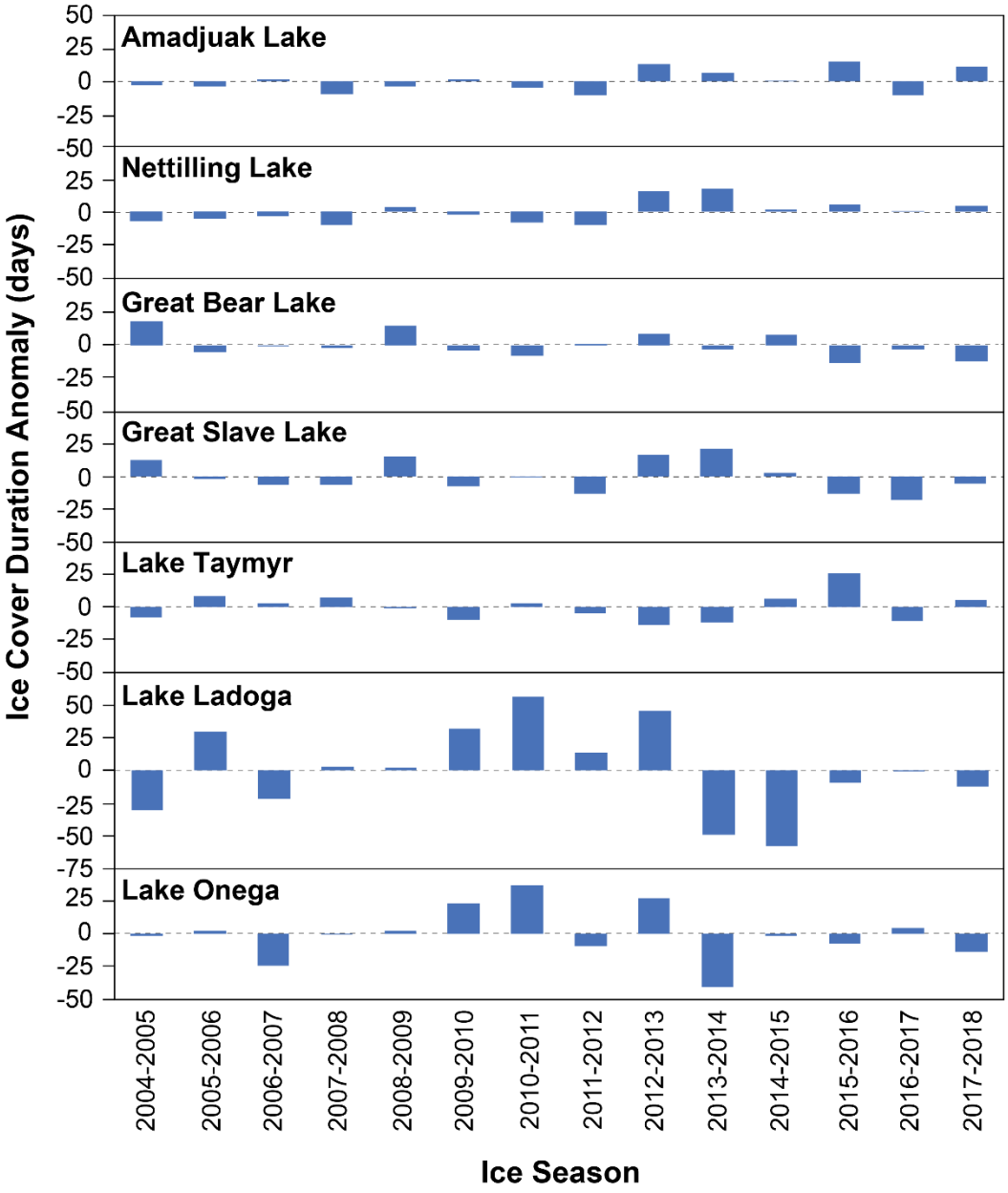

Fig. 4. Lake-wide ice duration anomalies for large lakes in Canada (Amadjuak, Nettilling, Great Bear, Great Slave) and Russia (Taymyr, Ladoga, Onega) derived from the full length of the NOAA IMS 4-km product (2004-18).

References

Baijnath-Rodino, J. A., C. R. Duguay, and E. F. LeDrew, 2018: Climatological trends of snowfall over the Laurentian Great Lakes Basin. *Int. J. Climatol.*, 38, 3942-3962.

Brown, L. C., and C. R. Duguay, 2010: The response and role of ice cover in lake-climate interactions. *Prog. Phys. Geogr.*, 34, 671-704.

Du, J., J. S. Kimball, C. R. Duguay, Y. Kim, and J. Watts, 2017: Satellite microwave assessment of Northern Hemisphere lake ice phenology from 2002 to 2015. *Cryosphere*, 11, 47-63.

Duguay, C., L. Brown, K. -K. Kang, and H. Kheyrollah Pour, 2015a: [The Arctic] Lake ice [in "State of the Climate in 2014"]. *Bull. Am. Meteorol. Soc.*, 96, S144-S145.

Duguay C. R., L. C. Brown, K. K. Kang, H. Kheyrollah Pour, 2013: Lake ice [in Arctic Report Card 2013], https://www.arctic.noaa.gov/Report-Card.

Duguay, C. R., M. Bernier, Y. Gauthier, and A. Kouraev, 2015b: Lake and river ice, in *Remote Sensing of the Cryosphere.* M. Tedesco, Ed., Wiley-Blackwell (Oxford, UK), pp. 273-306.

Duguay, C. R., T. D. Prowse, B. R. Bonsal, R. D. Brown, M. P. Lacroix, and P. Ménard, 2006: Recent trends in Canadian lake ice cover. *Hydrol. Process.*, 20, 781-801.

Eerola, K., L. Rontu, E. Kourzeneva, H. Kheyrollah Pour, and C. R. Duguay, 2014: Impact of partly ice-free Lake Ladoga on temperature and cloudiness in an anticyclonic winter situation—a case study using HIRLAM model. *Tellus A*, 66, 23929.

GCOS, 2016: *The Global Observing System for climate: Implementation needs*, GCOS-200. *GCOS 2016 Implementation Plan*. World Meteorological Organization, 315 pp.

Helfrich, S. R., D. McNamara, B. H. Ramsay, T. Baldwin, and T. Kasheta, 2007: Enhancements to, and forthcoming developments in the Interactive Multisensor Snow and Ice Mapping System (IMS). *Hydrol. Process.*, 21, 1576-1586.

IGOS, 2007: Integrated Global Observing Strategy Cryosphere Theme Report—For the Monitoring of our Environment from Space and from Earth. World Meteorological Organization, WMO/TD-No. 1405, 100 pp.

Jeffries, M. O., K. Morris, and C. R. Duguay, 2012: Floating ice: lake ice and river ice, in *Satellite Image Atlas of Glaciers of the World—State of the Earth's Cryosphere at the Beginning of the 21st Century: Glaciers, Global Snow Cover, Floating Ice, and Permafrost and Periglacial Environments*. R. S. Williams, Jr., and J. G. Ferrigno, Eds., U.S. Geological Survey Professional Paper 1386-A, A381-A424.

Kheyrollah Pour, H., C. R. Duguay, A. Martynov, and L. C. Brown, 2012: Simulation of surface temperature and ice cover of large northern lakes with 1-D models: A comparison with MODIS satellite data and in situ measurements. *Tellus A*, 64, 17614, doi: 10.3402/tellusa.v64i0.17614.

Šmejkalová, T., M. E. Edwards, and J. Dash, 2016: Arctic lakes show strong decadal trend in earlier spring ice-out. *Sci. Rep.*, 6, 38449.

Surdu, C. M., C. R. Duguay, and D. Fernández Prieto, 2016: Evidence of recent changes in the ice regime of high arctic lakes from spaceborne satellite observations. *Cryosphere*, 10, 941-960.

November 19, 2018

Migratory Tundra Caribou and Wild Reindeer

D. E. Russell[1], A. Gunn[2], S. Kutz[3]

[1]CircumArctic Rangifer Monitoring and Assessment (CARMA) Network, Yukon College, Whitehorse, YT, Canada
[2]CARMA, Salt Spring Island, BC, Canada
[3]Department of Ecosystem and Public Health, Faculty of Veterinary Medicine, University of Calgary, Calgary, AB, Canada

Highlights

- The abundance of migratory tundra caribou and wild reindeer has continued to drop since declines were detected in the mid-1990s.
- Of the 22 herds monitored, only two herds are at historic peak numbers and have not declined.
- Recent analyses link caribou productivity, particularly declining calf and adult survival, to changing climate conditions.
- Current low numbers of caribou and wild reindeer have imposed hardships for northern communities.

The abundance of migratory herds of caribou (North America and Greenland) and wild reindeer (Russia and Norway) in circum-arctic tundra regions (**Fig. 1**) has declined 56% (4.7 million to 2.1 million) over the last two decades. Five herds in particular, in the Alaska-Canada region, have declined more than 90% and show no sign of recovery (**Fig. 2**). It is normal for herd numbers to vary over decades (Fauchald et al., 2017), but currently some herds have all-time record low populations since reliable record keeping began. The extent and duration of the declines are a threat to the food security and culture of indigenous people who have depended on the herds. Caribou and wild reindeer are a key species in the arctic food web contributing to nutrient cycling between terrestrial and aquatic systems and the abundance of predators and scavengers.

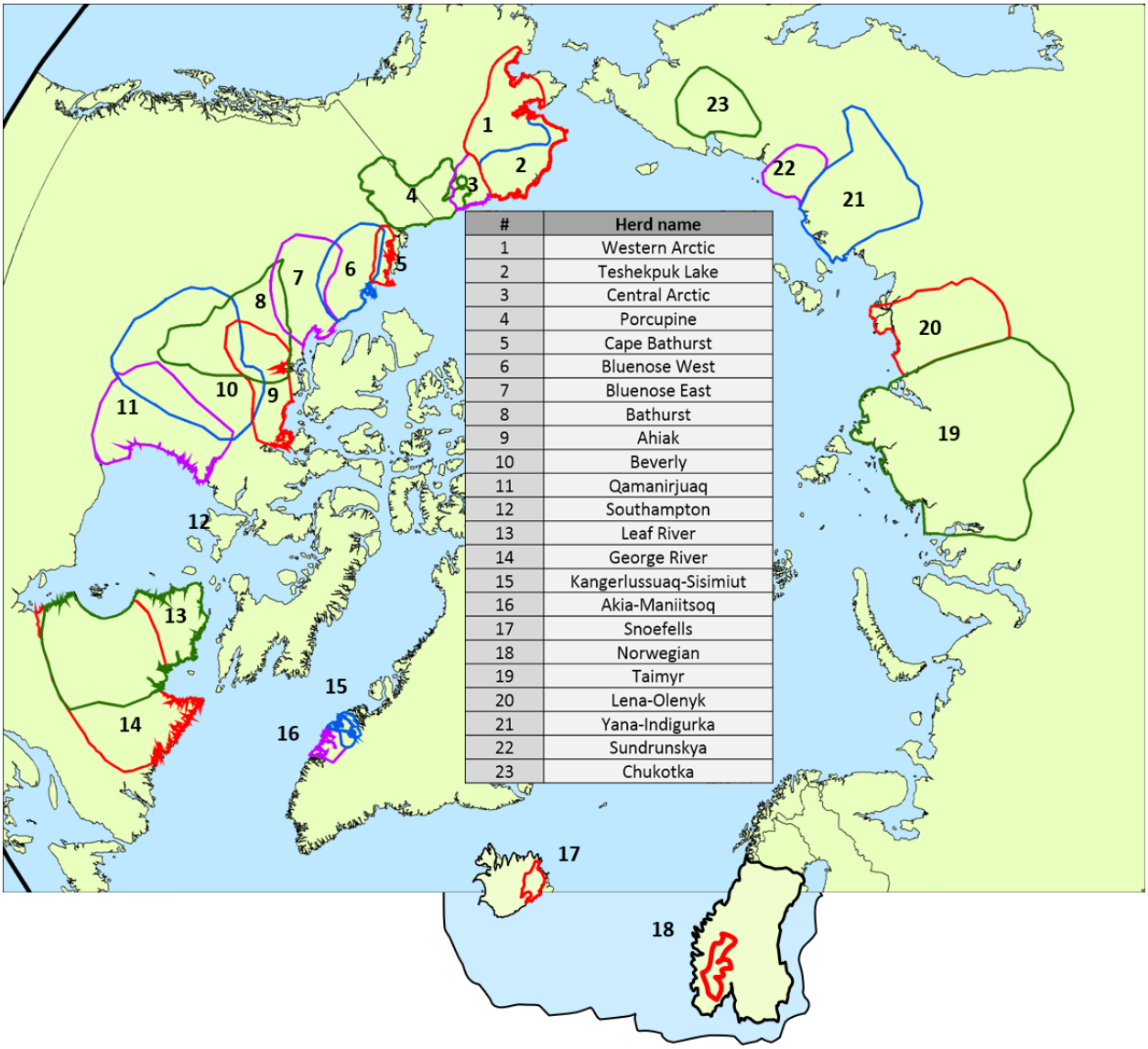

#	Herd name
1	Western Arctic
2	Teshekpuk Lake
3	Central Arctic
4	Porcupine
5	Cape Bathurst
6	Bluenose West
7	Bluenose East
8	Bathurst
9	Ahiak
10	Beverly
11	Qamanirjuaq
12	Southampton
13	Leaf River
14	George River
15	Kangerlussuaq-Sisimiut
16	Akia-Maniitsoq
17	Snoefells
18	Norwegian
19	Taimyr
20	Lena-Olenyk
21	Yana-Indigurka
22	Sundrunskya
23	Chukotka

Fig. 1. Migratory tundra caribou herds included in the CARMA Network. Different colors only used to easily separate overlapping ranges.

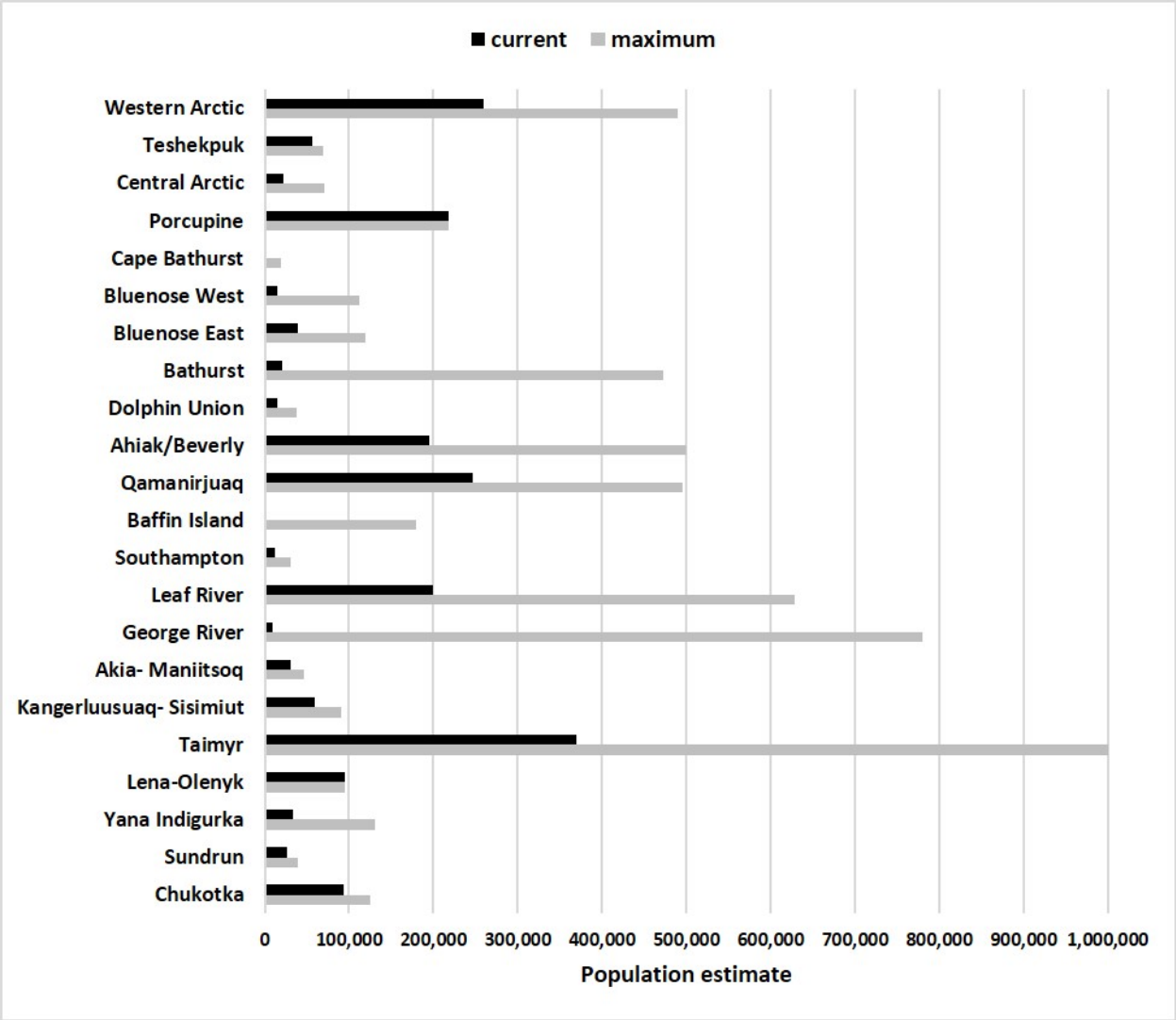

Fig. 2. The current and peak estimates for migratory tundra wild reindeer/caribou herds for the 22 herds with at least three censuses. Data from CARMA's population database and covers population estimates from 1970-2017. Herds are ordered from west to east, starting in western Alaska.

The status of the Arctic tundra caribou and wild reindeer herds (**Fig. 2**) is monitored by the CircumArctic Rangifer Monitoring and Assessment (CARMA) Network. CARMA relies on collaboration among scientists, wildlife management agencies, management boards, and Native organizations to share their data and information on caribou and wild reindeer herds. The CARMA Network maintains a relatively new, publicly accessible database of herd observations and descriptions (https://carma.caff.is/) collected via data sharing efforts, although accessible data archiving is still in its infancy. The CARMA database includes data for 23 herds (geographic sub-populations) with an average frequency of estimated herd size occurring every 5 years (0.47 Standard Error; range 2-10 years; **Fig. 1**).

Two aerial survey methods are used to estimate herd abundance. The first uses total counts based on photography of mid-summer aggregations as the caribou and wild reindeer gather to reduce their exposure to insect harassment (e.g., Klimstra, 2018, unpubl. comm.). The second method uses a sample count based on photography of calving grounds where the cows of a herd are known to come together

for calving. Calving ground sample counts are then extrapolated, using adult sex ratios, to estimate herd size (e.g., Adamczewski et al., 2017).

Regional variation in the extent and timing of the caribou declines is high. For example, of the five herds tracked in Alaska, three herds peaked between 2003 and 2010 before precipitously declining 53% by 2017, while during the same period, two Alaskan herds began to recover. Notably, one of the Alaska herds, the Porcupine (shared with Canada), is the only herd in the state to recently increase in population size (44% between 2001 and 2016).

Across the Canadian Arctic mainland, declines in nine herds have become severe enough that barren-ground caribou became nationally recognized as "Threatened" (as defined by COSEWIC) in 2016 (COSEWIC, 2016) and two herds of Eastern Migratory Caribou are now considered "Endangered" (COSEWIC, 2017). In Russia, where there is a high diversity of wild reindeer sub-species, recent declines are especially apparent for island, forest, and mountain reindeer. Of 19 herds assessed, 18 are rare, decreasing, or "Threatened" (I. Mizin, pers. comm., 2018).

In western Greenland, caribou inhabiting mountain (alpine) tundra, recently declined and harvesting is consunpuidered a leading factor (Cuyler et al., 2011). In south-central Norway, where mountain reindeer also live in alpine tundra, there are an estimated 6,000 wild reindeer that have maintained relatively stable populations since 2002 (Strand et al., 2012).

Causes of the caribou and wild reindeer population declines are complex and are related to a combination of factors that include forage availability, macro (worms and ectoparasites) and micro (viruses, bacteria, protozoa) parasites, predation (including hunting), and climate change (an overarching factor). To examine the influence of climate, a spatial climate dataset (Russell et al., 2013) was created for annual and seasonal ranges of circumpolar caribou and wild reindeer populations. In comparing herd vital rates in North American herds, climate indicators accounted for 54% of the variability in vital rates. This study also revealed "carry-over" effects reflecting the adaptability of caribou to buffer adverse weather. For example, a series of years with adverse conditions such as drought resulted in reduced pregnancy and calf survival.

Caribou and wild reindeer are adapted to the long Arctic winters, which is likely why herd vital rates did not negatively correlate with winter snow variables (snow depth on 31 March). The strongest and most consistent climate trends were the extent of October warming growing degree days and also increasing plant growing degree days in June and July temperatures. While these trends, and trends for earlier snow loss, are often beneficial to caribou, subsequent warmer summers also have adverse effects through increased drought, flies and parasites, and perhaps heat stress leading to increased susceptibility to pathogens and other stressors.

Trends observed between individual herd and climate variables are in good agreement with trends observed in regional climate observations. For example, Bhatt et al. (2017) reported summer warming trends for the North American Arctic that align with observations of Bathurst (Canada) caribou adult cow mortality. In this example, correlations emerged between warmer summer temperatures and reduced July rainfall, which increased the drought index. The 2-year running average of mean monthly July temperature and cumulative freezing rain from September to December explained 64% of the variation in adult cow survival which, in turn, is a determining factor in herd size (**Fig. 3**). The exact mechanism for the lower survival is uncertain but may be linked at least in part to heat stress and the

higher temperatures decreasing forage quality and reducing forage intake as digestive efficiency declines, while freezing rain reduces forage intake and increases movement rates.

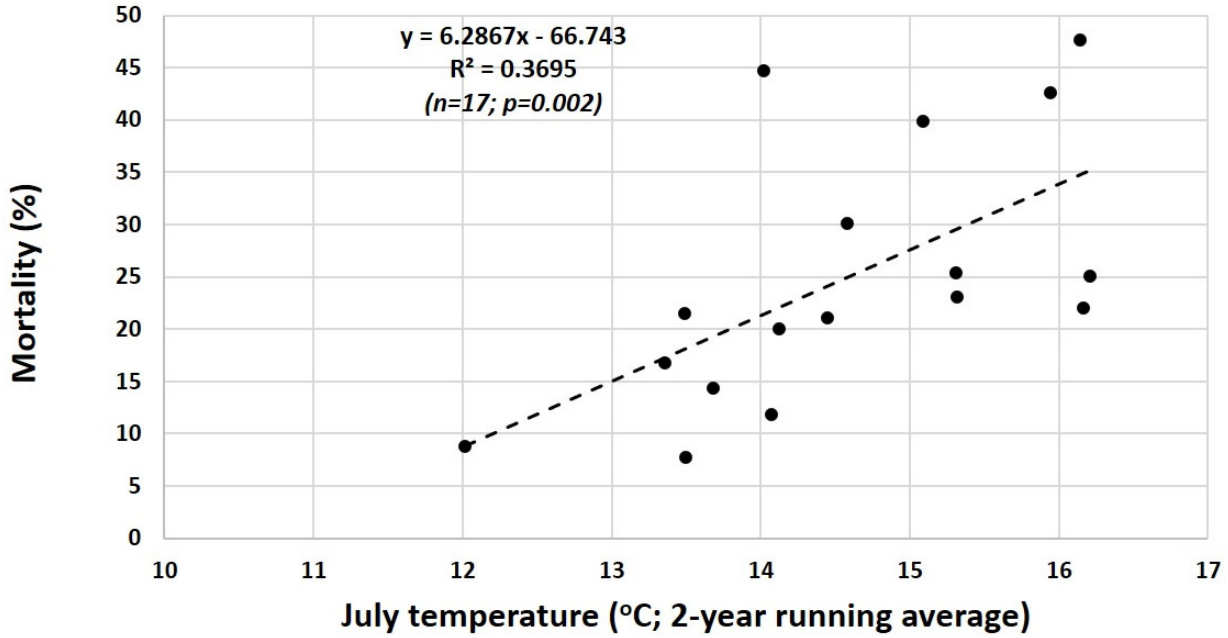

Fig. 3. Relationship between Bathurst caribou adult cow mortality and the 2-year running average of mean daily July temperature, 1997-2015. Climate data from CARMA climate database, mortality data courtesy of Government of Northwest Territories.

Warmer summer temperatures have also been linked to increased abundance and range expansion of Arctic pathogens (Kutz et al., 2013; Altizer et al., 2013; Kafle et al., 2018). Increasingly, we are understanding the role of these endemic pathogens in limiting wild ungulate populations (e.g., Tryland and Kutz, 2018); however, we also need to be aware of unanticipated effects of climate changes on infectious disease in wild populations. For example, spring and summer warming has the potential to trigger unexpected die-offs. This phenomenon was observed in an ecologically similar species when, in June 2015, an outbreak of *Pasteurella* in the gregariously calving saiga antelope (*Saiga tatarica*) killed more than 200,000 antelopes (Kock et al., 2018).

Disease outbreaks in muskoxen in the Canadian Arctic (Kutz et al., 2015) were only recognized when local ecological knowledge was collected (Tomaselli et al., 2018). Subsequent surveys demonstrate this same bacteria is also circulating across all North American caribou herds tested and that it can cause caribou deaths (K. J. Bondo et al., unpubl. report: "Health status of live-captured boreal caribou in Northeastern British Columbia during year of unusually high mortality"; S. J. Kutz et al., unpubl. data). While recent research ties climate variables to caribou and wild reindeer vital rates, the cascading and interacting effects of climate, nutrition, infectious and non-infectious disease, predation, and disturbance on caribou and wild reindeer require in depth and multi-disciplinary investigation to better understand their effects on population dynamics and future population trends.

Regional differences in climate and other landscape changes such as roads and industrial developments mean that herds are exposed to different cumulative effects and their consequent vulnerability varies among herds. With spatial climate trends, and monitoring herds, including systematic collection of local

ecological knowledge, we are increasingly better placed to assess herd vulnerability to promote adaptive capacity, which in turn will increase landscape resilience and support the adaptability of the arctic people.

References

Adamczewski, J., J. Boulanger, B. Croft, T. Davison, H. Sayine-Crawford, and B. Tracz, 2017: A comparison of calving and post-calving photo-surveys for the Bluenose-East herd of barren-ground caribou in northern Canada in 2010. *Can. Wildlife Biol. Manag.*, 6, 4-30.

Altizer, S., R. S. Ostfeld, P. T. Johnson, S. Kutz, and C. D. Harvell, 2013: Climate change and infectious diseases: From evidence to a predictive framework. *Science*, 341(6145), 514-519.

Bhatt, U. S., et al., 2017: Changing seasonality of panarctic tundra vegetation in relationship to climatic variables. *Environ. Res. Lett.*, 12, 055003, doi: 10.1088/1748-9326/aa6b0b.

COSEWIC, 2016: COSEWIC assessment and status report on the Caribou Rangifer tarandus, Barren-ground population in Canada. Committee on the Status of Endangered Wildlife in Canada (Ottawa), 136 pp.

COSEWIC, 2017: COSEWIC assessment and status report on the Caribou Rangifer tarandus, Eastern Migratory population and Torngat Mountains population, in Canada. Committee on the Status of Endangered Wildlife in Canada (Ottawa), 85 pp.

Cuyler, C., M. Rosing, H. Mølgaard, R. Heinrich, and K. Raundrup, 2011: Status of two West Greenland caribou populations 2010; 1) Kangerlussuaq-Sisimiut, 2) Akia-Maniitsoq, Part I. Pinngortitaleriffik - Greenland Institute of Natural Resources. Technical Report No. 78, 162 pp.

Fauchald, P., T. Park, H. Tommervik, R. Myneni, and V. H. Hausner, 2017: Arctic greening from warming promotes declines in caribou populations. *Sci. Adv.*, 3, e1601365, doi: 10.1126/sciadv.1601365.

Kafle, P., S. J. Peacock, S. Grond, K. Orsel, and S. Kutz, 2018: Temperature-dependent development and freezing survival of protostrongylid nematodes of Arctic ungulates: Implications for transmission. *Parasites Vectors*, 11, 400, doi: 10.1186/s13071-018-2946-x.

Klimstra, R, 2018: Summary of Teshekpuk Caribou Herd photocensus conducted July 14, 2017. Unpubl. memo, Alaska Department of Fish and Game, Division of Wildlife Conservation Northwest, Fairbanks, Alaska.

Kock, R. A., M. Orynbayev, S. Robinson, S. Zuther, and N. Singh, 2018: Saigas on the brink: Multidisciplinary analysis of the factors influencing mass mortality events. *Sci. Adv.*, 4, eaao2314.

Kutz, S. J., et al., 2013: Invasion, establishment, and range expansion of two parasitic nematodes in the Canadian Arctic. *Global Change Biol.*, 19(11), 3254-3262.

Kutz, S. J., et al., 2015: *Erysipelothrix rhusiopathiae* associated with recent widespread muskox mortalities in the Canadian Arctic. *Can. Vet. J.*, 56(6), 560-563.

Russell, D. E., P. H. Whitfield, J. Cai, A. Gunn, R.G. White, and K. Poole, 2013: CARMA's MERRA-based caribou climate database. *Rangifer*, 33(Special Issue 21), 145-152.

Strand, O., E. B. Nilsen, E. J. Solberg, and J. C. D. Linnell, 2012: Can management regulate the population size of wild reindeer (*Rangifer tarandus*) through harvest? *Can. J. Zool.*, 90, 163-171.

Tomaselli, M, S. Kutz, C. Gerlach, and S. Checkley, 2018: Local knowledge to enhance wildlife population health surveillance: Conserving muskoxen and caribou in the Canadian Arctic. *Biol. Conserv.*, 217, 337-348, doi: 10.1016/j.biocon.2017.11.010.

Tryland, M., and S. J. Kutz, 2018: *Reindeer and Caribou: Health and Disease*. CRC Press, 534 pp.

November 28, 2018

Clarity and Clouds: Progress in Understanding Arctic Influences on Mid-latitude Weather

J. A. Francis

Woods Hole Research Center, Falmouth, MA, USA

As we watch the ongoing rapid loss of Arctic sea ice, freshwater ice, permafrost, and spring snow cover, the corresponding amplified warming of the Arctic region (AAW) continues to increase (see essay on *Surface Air Temperature*). These disturbing changes to a key component of the Earth's climate system has spawned a blizzard of new studies that reveal influences of AAW on weather patterns within and beyond the Arctic. Media and public interest in the topic has also been keen, as the loss of Arctic sea ice is one of the most conspicuous symptoms of human-caused climate change (Notz and Stroeve, 2016) and unusual weather events often dominate headlines. A case in point: damage in the U.S.A. caused by extreme weather events in 2017 was the costliest in history at over 300 billion dollars (see https://www.climate.gov/news-features/blogs/beyond-data/2017-us-billion-dollar-weather-and-climate-disasters-historic-year). People are being affected directly by these events, and increasingly they're asking, "What's up with this? Is climate change playing a role?" Scientists can now answer a confident "yes" to that question, though the exact degree of influence is difficult to pin down.

It's clear that global warming is increasing the intensity of heatwaves and droughts, as well as the frequency of heavy precipitation events, but the lines of influence are fuzzier when it comes to the effects of AAW. Progress in understanding the connections, however, has been steady. In recent years, researchers have learned that it's not just one connection, but rather several that vary with season, region, and fluctuating natural states of the climate system (e.g., ocean temperature patterns like El Niño). The general hypothesis is that when the Arctic warms faster than lower latitude regions, the north-south temperature difference is reduced. Because that temperature difference provides the main fuel for the polar jet stream (a river of strong wind at levels where jet aircraft fly), the predominantly west winds of the jet stream weaken. A slower jet stream tends to favor a more meandering north-south path and to shift the mean jet latitude southward. A wavier pattern allows warm air to penetrate farther north and cold air to plunge farther south, compared to when the jet is strong and relatively straight (**Fig. 1**). Larger waves also tend to linger in one location, as do the surface weather systems they create, which results in persistent weather conditions that can turn into extreme events.

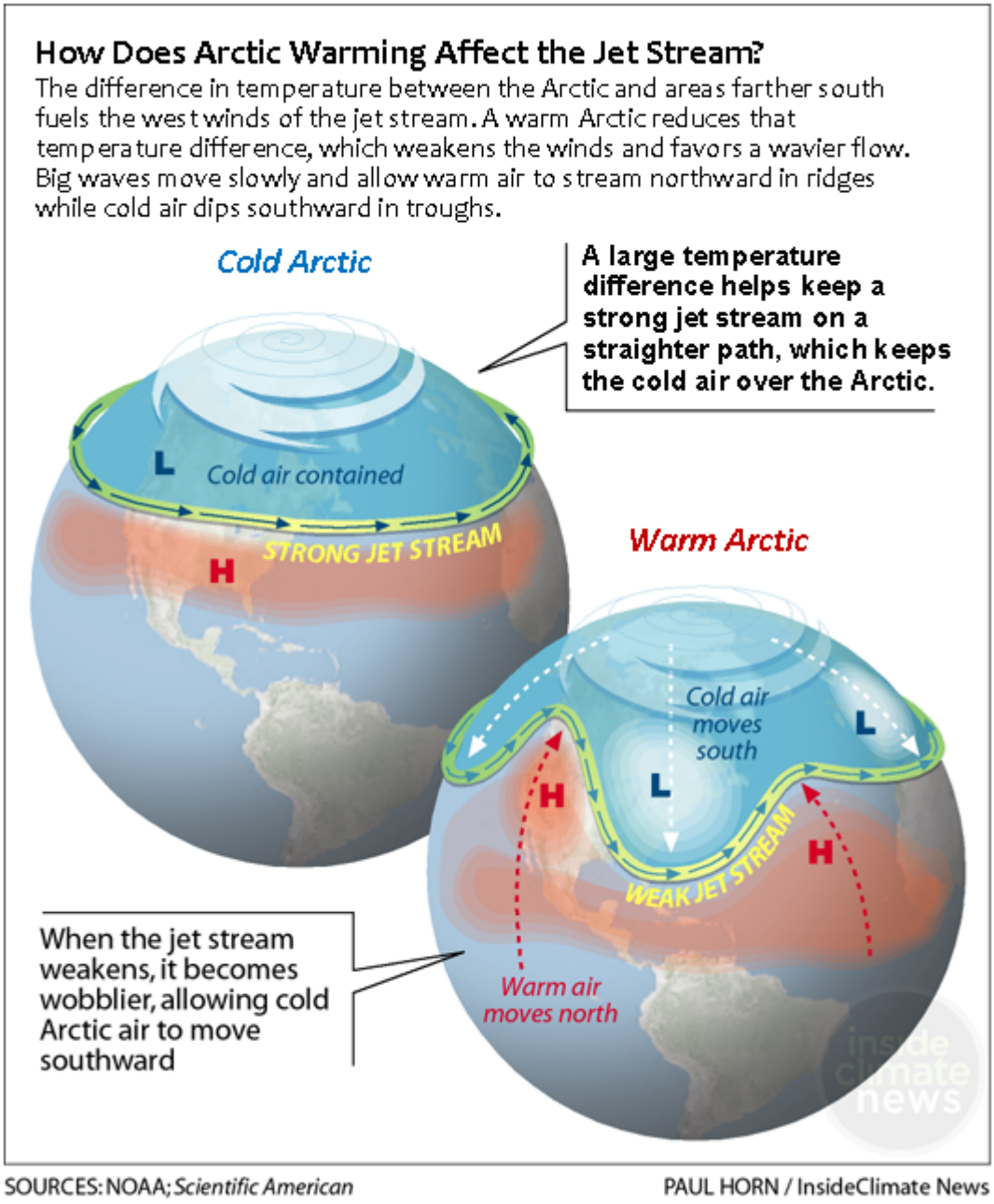

Fig. 1. Effects of Arctic temperature changes on the jet stream and mid-latitude weather. Adapted from the original sources: NOAA, Scientific American, and InsideClimate News.

In addition to AAW, we know that many changes in the climate system are happening simultaneously and are also affecting mid-latitude weather regimes. For example, most climate model simulations for the future indicate that another area of amplified warming will occur in the upper atmosphere over the tropics (though there's no sign of it yet in observations). This amplification will increase the north-south temperature difference between the tropics and mid-latitudes and oppose the influence of AAW (Peings et al., 2018; McCusker et al., 2017). The spectrum of change in the climate system, along with the inherently chaotic behavior of the atmospheric circulation, hinders efforts to assess the influence of any one factor on weather patterns (Vavrus, 2018).

Despite these obstacles, some aspects of the AAW's influence on the large-scale circulation have come into sharper focus in the past few years. Some recent investigations based on global climate models have convincingly demonstrated that including atmosphere-ocean interactions (Deser et al., 2016) and a well-resolved stratosphere (Zhang et al., 2018) are necessary to capture realistic atmospheric responses to sea-ice loss and AAW. However, many details of linkage mechanisms remain elusive (Sun et al., 2018). Progress in understanding three specific examples of Arctic/mid-latitude linkages is summarized here: west-east contrasts in North American weather, sea-ice loss and winter extremes over Eurasia, and stagnant conditions over continents during summer. For a more complete recent review, see Vavrus (2018).

North American warm/dry west–cold/wet east. Since late 2013, the predominant weather regime over North America has featured a strong and persistent jet-stream ridge aligned north/south in the eastern Pacific, which diverts storms away from California and sends abnormally warm winds into Alaska (**Fig. 1**). This so-called "ridiculously resilient ridge" (Swain et al., 2017) is perpetuating drought, heatwaves, and extensive wildfires across much of western North America. A strong jet-stream ridge is often accompanied by a downstream (eastward) trough, which allows cold Arctic air to plunge southward, bringing persistent icy conditions to the southeastern U.S.A. (Cohen et al., 2018) and can spawn a parade of destructive nor'easters along the eastern seaboard, as in winters of 2013-14 and 2017-18.

How might Arctic warming help promote this ridge/trough pattern? Recent studies reveal that a western ridge is more likely when ocean temperatures along the west coast of North America are warmer than normal (Swain et al., 2017). The strength of this ridge may then be bolstered by low sea-ice extent north of Alaska, where ocean temperatures are abnormally warm owing to extra solar heat absorbed during summer. This heat is then released back to the atmosphere when cold autumn air masses arrive, contributing to AAW in the region and augmenting the ridge's bulge in upper levels of the atmosphere. Strong ridges usually trigger a southward jet-stream dip to their east. Consequently, this persistent pattern is favored when a natural fluctuation in Pacific Ocean temperature anomalies combines with regional AAW in the Pacific sector of the Arctic (Francis et al., 2017), perhaps boosted by a tropical connection (Cvijanovic et al., 2017).

Cold Eurasian winters linked to sea-ice loss in the Barents and Kara seas. Similar to the North American situation, a strong and persistent ridge/trough pattern has occurred with increasing frequency in Eurasia in recent decades (**Fig. 2**). New studies have strengthened the evidence for a role played by sea-ice loss in the Barents and Kara seas (e.g., Ye et al., 2018; Zhang et al., 2018; Kretschmer et al., 2016; Yao et al., 2017), though other studies attribute it to random chance (e.g., McCusker et al., 2016). The story again begins with a climatological ridge (i.e., a long-term average pattern) that tends to form near the Ural Mountains, which acts as an obstacle to westerly jet-stream winds in western Russia. North of this ridge are the Barents and Kara seas in the Arctic Ocean, regions of rapid sea-ice loss and warming in recent years. As with the North American case, the existing ridge is intensified by the extra heat absorbed in and subsequently released from the ice-loss region. A stronger ridge creates a stronger surface high pressure system over central-eastern Asia and transports cold Arctic air over the continent, which depresses the jet stream southward into a deeper trough over Asia. Arctic air is then free to plunge southward, favoring persistent cold spells in eastern Asia and contributing to observed cooling trends in the region. Under the right conditions, this ridge/trough pattern can become so intense that the resulting wave energy in the jet stream is transferred upward into the stratosphere, disrupting the normally circular flow of the stratospheric polar vortex, causing it to bulge southward or perhaps even split into two circulation centers. When this occurs, large jet-stream waves often persist into late winter and even early spring, resulting in extended periods of unusual and sluggish weather patterns around

the Northern Hemisphere (Kretschmer et al., 2018). This mechanism clearly occurred in winter 2017-18, perpetuating large ridges and troughs around the Northern Hemisphere well into spring that were responsible for severe cold in East Asia, heatwaves at the North Pole, the "Beast from the East" in Europe, a swarm of nor'easters in New England, and a variety of other disruptive weather abnormalities.

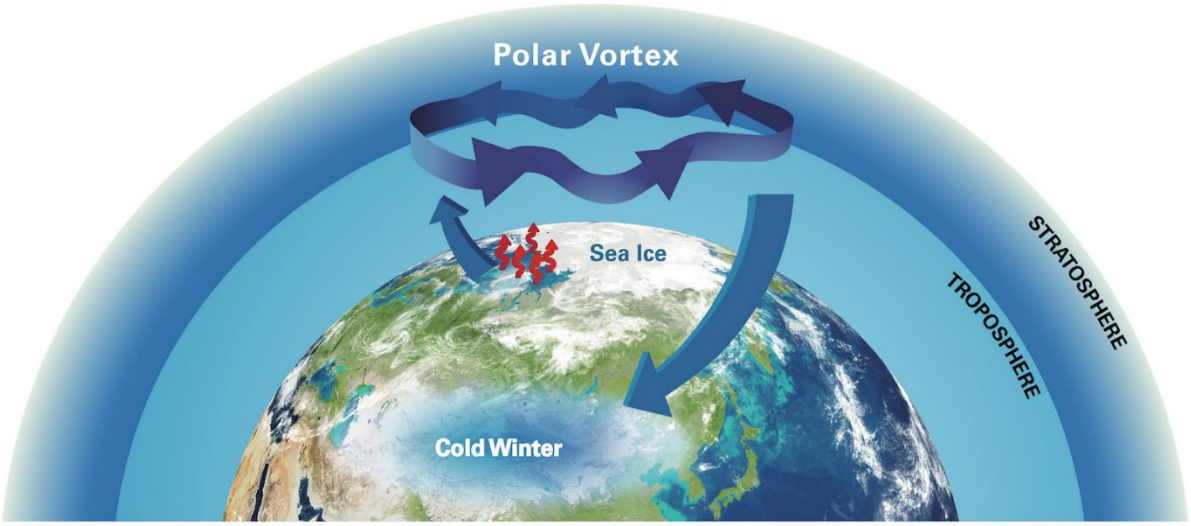

Fig. 2. Sea-ice loss in the Barents/Kara seas favors intensification of the climatological ridge located in the region, which strengthens the Siberian High pressure cell and transports cold Arctic air into east Asia. Wave energy from a more meandering jet stream disrupts the stratospheric jet stream and reinforces the pattern into late winter (Zhang et al., 2018). From https://usclivar.org/research-highlights/loss-arctic-sea-ice-impacts-cold-extreme-events.

Persistent summer weather patterns over continents. The Arctic meltdown may also be contributing to summer heatwaves, drought, wildfires, and flooding over Northern Hemisphere continents. New studies suggest that the disappearing spring snow cover focuses Arctic warming during late spring and early summer over the far-northern land areas (**Fig. 3** and Francis and Vavrus, 2012). This loss of snow during the season of most intense sunshine causes the soil to dry out and warm earlier, effectively giving summer heating a "jump start" (York et al., 2018). The zonal belt of warming that rings high-latitude continents also can create a double peak in the north-south temperature trend, which favors the formation of a split jet stream. Weather systems can become trapped between the jet branches, causing prolonged hot spells, drought, or rainy periods that can lead to extreme events (Mann et al., 2017). Recent deadly heatwaves (e.g., Europe in 2003 and 2018, Russia in 2010, Japan in 2018, and the U.S.A. in 2011 and 2018) and floods (e.g., Pakistan 2010 and Europe 2013) are consistent with this hypothesis. The general relationship between land-based AAW and summer extremes is also supported by model projections of the future analyzed by Vavrus et al. (2017). They found a belt of abnormally warm air temperatures overlying the snow-loss areas in North America, which created weakened upper-level westerly winds south of the belt and stronger winds to the north. The band of weak winds is associated with amplified jet-stream waviness measured as "sinuosity," which favors persistent drought and heat spells during summer in mid-latitude continental areas.

Fig. 3. Amplified Arctic warming in late spring and summer (yellow shading) tends to occur mainly over high-latitude continents. Through a mechanism called quasi-resonance, AAW favors the amplification of quasi-stationary jet-stream waves, leading to more persistent weather conditions and extreme events such as heatwaves, drought, floods in continental areas. (from Coumou et al., 2018).

The connections between climate change and extreme weather are a topic of intense scientific interest and of profound societal impact. Some of these effects are clear—more severe heatwaves, more frequent heavy precipitation events, and more intense droughts—but the understanding of other less direct influences is still partly to mostly cloudy. The role of a rapidly warming and melting Arctic is one of these factors that challenges present computer modeling capabilities and understanding of atmospheric dynamics. These limitations are now coming into better focus as changes in the real world either confirm or oppose expectations based on computer simulations, offering avenues to resolve disputes in our understanding of Arctic/mid-latitude linkages. Exactly how the northern meltdown will "play ball" with other changes and natural fluctuations in the system presents many questions that will keep scientists busy for years to come, but it's becoming ice-crystal-clear that change in the far north will increasingly affect us all.

References

Cohen, J., K. Pfeiffer, and J. A. Francis, 2018: Warm Arctic episodes linked with increased frequency of extreme winter weather in the United States. *Nat. Commun.*, 9, 869, doi: 10.1038/s41467-018-02992-9.

Coumou, D., G. Di Capua, S. Vavrus, L. Wang, and S. Wang, 2018: The influence of Arctic amplification on mid-latitude summer circulation. *Nat. Commun.*, 9, 2959, doi: 10.1038/s41467-018-05256-8.

Cvijanovic, I., B. D. Santer, C. Bonfils, D. D. Lucas, J. C. H. Chiang, and S. Zimmerman, 2017: Future loss of Arctic sea-ice cover could drive a substantial decrease in California's rainfall. *Nat. Commun.*, 8, 1947, doi: 10.1038/s41467-017-01907-4.

Deser, C., L. Sun, R. A. Tomas, and J. Screen, 2016: Does ocean coupling matter for the northern extratropical response to projected Arctic sea ice loss? *Geophys. Res. Lett.*, 43, 2149-2157, doi: 10.1002/2016GL067792.

Francis, J. A. and S. J. Vavrus, 2012: Evidence linking Arctic amplification to extreme weather in mid-latitudes. *Geophys. Res. Lett.*, 39, L06801, doi: 10.1029/2012GL051000.

Francis, J. A., S. J. Vavrus, and J. Cohen, 2017: Amplified Arctic warming and mid-latitude weather: New perspectives on emerging connections. *WIREs Clim. Change*, 8, e474, doi: 10.1002/wcc.474.

Kretschmer, M., D. Coumou, L. Agel, M. Barlow, E. Tziperman, and J. Cohen, 2018: More persistent weak stratospheric polar vortex states linked to cold extremes. *Bull. Am. Meteorol. Soc.*, 99, 49-60, doi: 10.1175/BAMS-D-16-0259.1.

Kretschmer, M., D. Coumou, J. F. Donges, and J. Runge, 2016: Using causal effect networks to analyze different Arctic drivers of midlatitude winter circulation. *J. Clim.*, 29, 4069-4081, doi: 10.1175/JCLI-D-15-0654.1.

Mann, M. E., S. Rahmstorf, K. Kornhuber, B. A. Steinman, S. K. Miller, and D. Coumou, 2017: Influence of anthropogenic climate change on planetary wave resonance and extreme weather events. *Sci. Rep.*, 7, 45242, doi: 10.1038/srep45242.

McCusker, K. E., J. C. Fyfe, and M. Sigmond, 2016: Twenty-five winters of unexpected Eurasian cooling unlikely due to Arctic sea ice loss. *Nat. Geosci.*, 9, 838-842, doi: 10.1038/NGEO2820.

McCusker, K. E., P. J. Kushner, J. C. Fyfe, M. Sigmond, V. V. Kharin, and C. M. Bitz, 2017: Remarkable separability of circulation response to Arctic sea ice loss and greenhouse gas forcing. *Geophys. Res. Lett.*, 44, 7955-7964, doi: 10.1002/2017GL074327.

Notz, D. and J. Stroeve, 2016: Observed Arctic sea-ice loss directly follows anthropogenic CO_2 emission. *Science*, 354(6313), 747-750, doi: 10.1126/science.aag2345.

Peings, Y., J. Cattiaux, S. J. Vavrus, and G. Magnusdottir, 2018: Projected squeezing of the wintertime North-Atlantic jet. *Environ. Res. Lett.*, 13, 074016, doi: 10.1088/1748-932/aacc79.

Sun, L., M. A. Alexander, and C. Deser, 2018: Evolution of the global coupled climate response to Arctic sea ice loss during 1990-2090 and its contribution to climate change. *J. Clim.*, 31, 7823-7843, doi: 10.1175/JCLI-D-18-0134.1.

Swain, D. L., D. Singh, D. E. Horton, J. S. Mankin, T. C. Ballard, and N. S. Diffenbaugh, 2017: Remote linkages to anomalous winter atmospheric ridging over the northeastern Pacific. *J. Geophys. Res. Atmos.*, 122, 12,194-12,209, doi: 10.1002/2017JD026575.

Vavrus, S. J., 2018: The influence of Arctic amplification on mid-latitude weather and climate. *Curr. Clim. Change Rep.*, 4, 238-249, doi: 10.1007/s40641-018-0105-2.

Vavrus, S. J., F. Wang, J. Martin, J. Francis, Y. Peings, and J. Cattiaux, 2017: Changes in North American atmospheric circulation and extreme weather: Influence of Arctic amplification and Northern Hemisphere snow cover. *J. Clim.*, 30, 4317-4333, doi: 10.1175/JCLI-D-16-0762.1.

Yao, Y., D. Luo, A. Dai, and I. Simmonds, 2017: Increased quasi stationarity and persistence of winter Ural blocking and Eurasian extreme cold events in response to Arctic warming. Part I: Insights from observational analyses. *J. Clim.*, 30, 4317-4333, doi: 10.1175/JCLI-D-16-0261.1.

Ye, K., T. Jung, and T. Semmler, 2018: The influences of the Arctic troposphere on the midlatitude climate variability and the recent Eurasian cooling. *J. Geophys. Res. Atmos.*, 123, 10,162-10,184, doi: 10.1029/2018JD028980.

York, A., U. Bhatt, R. Thoman, and R. Ziel, 2018: Wildland fire in boreal and arctic North America [in "State of the Climate in 2017"]. *Bull. Am. Meteorol. Soc*., 99(8), S167-S169, doi: 10.1175/2018BAMSStateoftheClimate.1.

Zhang, P., Y. Wu, I. R. Simpson, K. L. Smith, X. Zhang, B. De, and P. Callaghan, 2018: A stratospheric pathway linking a colder Siberia to Barents-Kara Sea sea ice loss. *Sci. Adv.*, 4, eaat6025, doi:10.1126/sciadv.aat6025.

November 13, 2018

Harmful Algal Blooms in the Arctic

D. M. Anderson[1], M. L. Richlen[1], K. A. Lefebvre[2]

[1]Woods Hole Oceanographic Institution, Biology Department, Woods Hole, MA, USA
[2]Environmental and Fisheries Science Division, Northwest Fisheries Science Center, National Marine Fisheries Service, NOAA, Seattle, WA, USA

Warming air temperatures and associated major reductions in the Arctic sea ice cover are driving increases in ocean temperature and changes to circulation patterns in the region. These changes are expected to impact the biogeographic boundaries of a range of marine species. For example, it is anticipated that many organisms may migrate northward or become more abundant as air and ocean temperatures continue to warm. However, few pose such significant threats to human and ecosystem health as harmful algal bloom (HAB) species. Data collected over the past decade clearly indicate that multiple toxic HAB species are present in the Arctic food web at dangerous levels, and it is very likely that this problem will persist and perhaps worsen in the future.

Harmful algal blooms, or HABs (commonly called "red tides"), are large accumulations of algae—both microscopic (phytoplankton) and macroscopic (seaweeds)—that affect human, wildlife, and ecosystem health, fisheries (shellfish and fish, both wild and cultured), tourism, and coastal aesthetics. Marine HAB phenomena affect virtually every coastal country, and take a variety of forms with multiple impacts. Some species produce potent neurotoxins, which can poison humans and wildlife when ingested, causing gastrointestinal distress, neurological problems and death in severe cases.

One major category of impact occurs when toxin-producing species (or microscopic animals that have eaten them) are filtered from the water as food by shellfish or fish, which then accumulate the algal-borne toxins to levels that can be lethal to both human and wildlife consumers. Poisonings are also possible from the consumption of other animals that have accumulated HAB toxins through the food chain. Toxic HABs can also cause mass mortalities of fish, shellfish, seabirds, and marine mammals, due to the production of neurotoxins or through the release of potentially lethal reactive compounds (Dorantes-Aranda et al., 2015). Together, these impacts have caused significant economic losses to fishing industries, ecotourism, and coastal aesthetics in countries around the world.

There have been reports of illness and even mortality from Paralytic Shellfish Poisoning (PSP) in Alaska going back decades, primarily from Southeast Alaska and the Aleutian Islands (Castrodale, 2015; Gessner and Middaugh, 1995). However, information on the present-day distribution and prevalence of PSP-causing species and other HAB taxa in Arctic waters is limited to a relatively small number of recent observations. Still, there is clear evidence that multiple taxa and at least five families of HAB toxins are present in the Arctic (saxitoxins, domoic acid, yessotoxins, spirolides, and dinophysistoxins/okadaic acid/pectenotoxins). Most data are for *Alexandrium catenella*, which produces neurotoxins called saxitoxins. Saxitoxins cause illness and mortalities via zooplankton, fish, birds, shellfish, and many other vectors relevant to subsistence harvesters in the Arctic. A second HAB group of growing concern includes domoic acid-producing *Pseudo-nitzschia* diatoms that poison humans or animals who eat shellfish or other contaminated marine organisms.

The frequency and geographic extent of HABs have expanded in recent decades, thereby increasing associated economic impacts on food, recreation, and commerce in the world's coastal zones

(Anderson, 1989; Hallegraeff, 1993; Anderson et al., 2012). Climate change, and specifically global ocean warming, have been implicated in the geographic expansion of certain HAB species distributions (Hallegraeff, 2010; Wells et al., 2015). Warming ocean temperatures, decreasing seasonal ice cover, and thinning sea ice will also serve to further expand the spatial and temporal windows for growth of endemic HAB species already present in Arctic waters (Moore et al., 2015). The northward shift of HABs means that the Arctic region is now vulnerable to species introductions and increasing bloom frequency in local communities and ecosystems that have little to no prior exposure to this phenomenon.

Harmful Algal Bloom Species in the Arctic

HABs are typically formed through the growth and accumulation of algal cells in the water column. However, some HABs species, like the dinoflagellate *A. catenella*, have the ability to form dormant resting cysts or spores. Cysts are highly resistant cells that typically form in large numbers as blooms terminate. These cysts then overwinter in bottom sediments until environmental conditions trigger them to germinate and initiate a bloom. *Alexandrium catenella* strains disperse readily and are highly adaptable to new regions due to this ability to form cysts and overwinter until conditions are suitable for germination and growth. This life stage represents one mechanism by which species might colonize Arctic waters via the advective transport of cysts from southern regions.

Alexandrium catenella. Collective observations over the last decade indicate that *A. catenella* cells and cysts are present in the Arctic north of Alaska and Canada, and within the Pacific and Atlantic inflows into the Arctic Ocean basin. More recent studies have expanded these observations considerably, particularly in the past five years (Gu et al., 2013; Natsuike et al., 2013; Vandersea et al., 2017). A recent significant observation is extremely high numbers of *A. catenella* cysts on the Chukchi shelf—among the highest densities ever reported for this species (**Fig. 1**). *Alexandrium catenella* were also found in the Chukchi Sea and northern Bering Sea shelves (Natsuike et al., 2017), with concentrations similar to those known to cause human poisonings and wildlife mortalities. Okolodkov (2005) published an early report of *A. catenella* cells near Utqiagvik (formerly Barrow), AK, and recent preliminary observations documented low concentrations of cells and cysts in the Beaufort Sea (D. M. Anderson, personal communication, 2018). In the Canadian/Greenland Arctic and subarctic, *Alexandrium* and PSP toxicity were first reported in Iceland in 2009 (Burrell et al., 2013) and in northwestern Greenland in 2012 (Baggesen et al., 2012). Along the Greenland coast, *A. catenella* cysts were present at low concentrations at nearly all stations sampled, extending as far as 76° N (Richlen et al., 2016; D. M. Anderson, unpub. data).

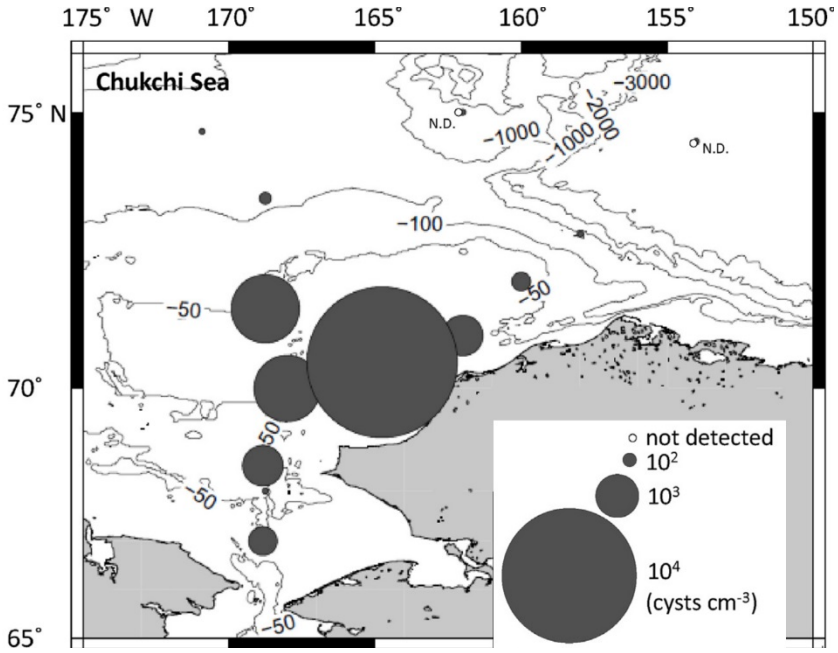

Fig. 1. Spatial distribution of *A. catenella* cyst abundances documented in the Chukchi Sea during surveys carried out in 2009. Adapted from Fig. 3, Natsuike et al. (2013).

Pseudo-nitzschia. *Pseudo-nitzschia* species are frequent inhabitants of Arctic marine waters, but less is known about their history, diversity, and toxicity than *A. catenella* in this region (see Booth and Horner, 1997; Percopo et al., 2016, and references therein). To date, up to eight *Pseudo-nitzschia* species have been identified in the Arctic (e.g., Poulin et al., 2011; Percopo et al., 2016), including toxigenic species (Poulin et al., 2011; Tammilehto et al., 2012, 2015; Harðardóttir et al., 2015), yet little is known of their biography or bloom dynamics.

Impacts of Harmful Algal Blooms in the Arctic

Impacts from toxins produced by *A. catenella* and *Pseudo-nitzschia* have been devastating to regions elsewhere in the world. Now, there is growing evidence of increasing HAB threats to human and wildlife health in the Arctic. Over the past several decades, PSP cases have increased in Alaska, which now has one of the highest incidences of PSP in the world. In addition to increasing numbers of human illness, there have also been recent and significant impacts to wildlife. On Kodiak Island, PSP toxins were implicated in the deaths of Kittlitz's Murrelet chicks during the 2011/12 breeding season (Shearn-Bochsler et al., 2014). High toxin levels were observed in nearly 90% of the nestling carcasses and thought to originate in planktivorous sand lance, a known vector for HAB toxins (Shumway et al., 2003). In August 2016, saxitoxins were also found in moderate to high levels in four animals sampled from a stranding event involving 39 walruses found dead in Bering Strait. This event prompted a public warning regarding consumption of contaminated fish and shellfish, including those taken directly from the guts of harvested walruses, which is traditional practice in some communities (Alaska Sea Grant, 2017).

In the Alaskan Arctic, recent surveys have found saxitoxins and/or domoic acid in many harvested or stranded marine mammals (**Fig 2**; Lefebvre et al., 2016). Notably, all species tested contained domoic acid, in spite of different foraging strategies, i.e., among seals (which may follow receding ice into the Chukchi Sea) and whales (which range between the southern Gulf of Alaska to the eastern Beaufort Sea). Some toxin levels were comparable to those found in dead or incapacitated marine mammals that

were diagnosed with domoic acid poisoning during severe *Pseudo-nitzschia* blooms along the US West Coast.

Fig. 2. Locations where HAB toxins were detected in stranded (s) and harvested (h) marine mammals. Red represents species positive for domoic acid and purple represents species positive for antitoxin. Marine mammal species are listed as follows: (A) humpback whales, (B) towhead whales, (C) beluga whales, (D) harbor porpoises, (E) northern fur seals, (F) Seller sea lions, (G) harbor seals, (H) ringed seals, (I) bearded seals, (J) spotted seals, (K) ribbon seals, (L) Pacific walruses and (M) northern sea otters. (Source: Lefebvre et al., 2016).

Summary

The warming Arctic Ocean may be experiencing an increase in the extent and magnitude of toxic HAB populations, posing considerable threats to human and ecosystem health. The impacts of this expansion will be significant in a region where traditional monitoring programs for toxins in shellfish or fish are not feasible due to remote and expansive coastlines. Management efforts going forward will be fostered by the recent creation of the Alaska Ocean Observing System's Alaska Harmful Algal Bloom (AHAB) Network, which was formed to coordinate among diverse coastal stakeholders for HAB awareness, monitoring, and response in Alaska. Warming ocean temperatures, decreasing seasonal ice cover, and thinning sea ice could further expand the spatial and temporal windows for *A. catenella* germination and growth in surface waters (Moore et al., 2015). These conditions will also likely support increased growth and expansion of toxic *Pseudo-nitzschia* species that exist within the Arctic. New observations and environmental monitoring are central to improving the understanding of the growing distribution, abundance, and impacts of HABs in the Arctic. Such observations will also serve to provide a baseline against which future climate change effects can be assessed and to guide management and mitigation strategies in this critically important system.

Acknowledgments

Support for DMA and MLR was provided by and by the National Science Foundation (Grants OCE-0850421 OCE-0430724, OCE-0911031, and OCE-1314642) and National Institutes of Health (NIEHS-1P50-ES021923-01) through the Woods Hole Center for Oceans and Human Health. Additional funding was provided from NOAA through the Cooperative Institute for the North Atlantic Region (CINAR) (NA14OAR4320158) and by the National Science Foundation Office of Polar Programs (OPP-1823002).

References

Alaska Sea Grant, "Bering Strait: Walruses and Saxitoxin-late summer/fall 2017," news release, November 15, 2017. https://seagrant.uaf.edu/news/2017/docs/Bering-Strait-Saxitoxin-2017-FINAL-Nov-15.pdf(accessed December 12, 2017).

Anderson, D. M. 1989: Toxic algal blooms and red tides: A global perspective, in *Red Tides: Biology, Environmental Science and Toxicology*. T. Okaichi, D. M. Anderson, and T. Nemoto, Eds., Elsevier, pp. 11-16.

Anderson, D. M., T. J. Alpermann, A. D. Cembella, Y. Collos, E. Masseret, and M. Montresor, 2012: The globally distributed genus *Alexandrium*: Multifaceted roles in marine ecosystems and impacts on human health. *Harmful Algae*, 14, 10-35.

Baggesen, C., Ø. Moestrup, N. Daugbjerg, B. Krock, A. D. Cembella, and S. Madsen, 2012: Molecular phylogeny and toxin profiles of *Alexandrium tamarense* (Lebour) Balech (Dinophyceae) from the west coast of Greenland. *Harmful Algae*, 19, 108-116.

Booth, B. C., and R. A. Horner, 1997: Microalgae on the Arctic Ocean Section, 1994: Species abundance and biomass. *Deep-Sea Res. Pt. II-Top. Stud. Oceanogr.*, 44(8), 1607-1622.

Burrell, S., T. Gunnarsson, K. Gunnarsson, D. Clarke, and A. D. Turner, 2013: First detection of paralytic shellfish poisoning (PSP) toxins in Icelandic mussels (*Mytilus edulis*): Links to causative phytoplankton species. *Food Control*, 31(2), 295-301.

Castrodale, L., 2015: Paralytic shellfish poisoning—Alaska, 1993-2014. *State of Alaska Epidemiology Bulletin*. Available at: http://epibulletins.dhss.alaska.gov/Document/Display?DocumentId=47

Dorantes-Aranda, J. J., A. Seger, J. I. Mardones, P. D. Nichols, and G. M. Hallegraeff, 2015: Progress in understanding algal bloom-mediated fish kills: The role of superoxide radicals, phycotoxins and fatty acids. *PLoS One*, 10(7), e0133549.

Gessner B. D., and J. P. Middaugh, 1995: Paralytic shellfish poisoning in Alaska: a 20-year retrospective analysis. *Am. J. Epidemiol.*, 141(6):766-70.

Gu, H., N. Zeng, Z. Xie, D. Wang, W. Wang, and W. Yang, 2013: Morphology, phylogeny, and toxicity of Atama complex (Dinophyceae) from the Chukchi Sea. *Polar Biol.*, 36, 427-436.

Hallegraeff, G. M., 1993: A review of harmful algal blooms and their apparent global increase. *Phycologia*, 32(2), 79-99.

Hallegraeff, G. M., 2010: Ocean climate change, phytoplankton community responses, and harmful algal blooms: A formidable predictive challenge. *J. Phycol.*, 46(2), 220-235.

Harðardóttir, S., M. Pančić, A. Tammilehto, B. Krock, E. F. Møller, T. G. Nielsen, and N. Lundholm, 2015: Dangerous relations in the Arctic marine food web: interactions between toxin producing *Pseudo-nitzschia* diatoms and *Calanus* copepodites. *Mar. Drugs*, 13(6), 3809-3835.

Lefebvre, K. A., et al., 2016: Prevalence of algal toxins in Alaskan marine mammals foraging in a changing arctic and subarctic environment. *Harmful Algae*, 55, 13-24.

Moore, S. K., B. D. Bill, L. R. Hay, J. Emenegger, K. C. Eldred, C. L. Greengrove, J. E. Masura, and D. M. Anderson, 2015: Factors regulating excystment of *Alexandrium* in Puget Sound, WA, USA. *Harmful Algae*, 43, 103-110.

Natsuike, M., S. Nagai, K. Matsuno, R. Saito, C. Tsukazaki, A. Yamaguchi, and I. Imai, 2013: Abundance and distribution of toxic *Alexandrium tamarense* resting cysts in the sediments of the Chukchi Sea and the eastern Bering Sea. *Harmful Algae*, 27, 52-59.

Natsuike, M., K. Matsuno, T. Hirawake, A. Yamaguchi, S. Nishino, and I. Imai, 2017: Possible spreading of toxic *Alexandrium tamarense* blooms on the Chukchi Sea shelf with the inflow of Pacific summer water due to climatic warming. *Harmful Algae*, 61, 80-86.

Okolodkov, Y. B. 2005: The global distributional patterns of toxic, bloom dinoflagellates recorded from the Eurasian Arctic. *Harmful Algae*, 4, 351-369.

Percopo, I., M. V. Ruggiero, S. Balzano, P. Gourvil, N. Lundholm, R. Siano, A. Tammilehto, D. Vaulot, and D. Sarno, 2016: *Pseudo-nitzschia arctica* sp. nov., a new cold-water cryptic *Pseudo-nitzschia* species within the *P. pseudodelicatissima* complex. *J. Phycol.*, 52(2), 184-199.

Poulin, M., N. Daugbjerg, R. Gradinger, L. Ilyash, T. Ratkova, and C. von Quillfeldt, 2011: The pan-Arctic biodiversity of marine pelagic and sea-ice unicellular eukaryotes: A first-attempt assessment. *Mar. Biodivers.*, 41(1), 13-28.

Richlen M. L., O. Zielinski, L. Holinde, U. Tillmann, A. Cembella, Y. Lyu, and D. M. Anderson, 2016: Distribution of *Alexandrium fundyense* (Dinophyceae) cysts in Greenland and Iceland, with an emphasis on viability and growth in the Arctic. *Mar. Ecol. Prog. Ser.*, 547, 33-46.

Shearn-Bochsler, V., E. W. Lance, R. Corcoran, J. Piatt, B. Bodenstein, E. Frame, and J. Lawonn, 2014: Fatal paralytic shellfish poisoning in Kittlitz's Murrelet (*Brachyramphus brevirostris*) nestlings, Alaska, USA. *J. Wildlife Dis.*, 50(4), 933-937.

Shumway, S. E., S. M. Allen, and P. D. Boersma, 2003: Marine birds and harmful algal blooms: Sporadic victims or under-reported events? *Harmful Algae*, 2(1), 1-17.

Tammilehto, A., T. G. Nielsen, B. Krock, E. F. Møller, and N. Lundholm, 2012: Calanus spp.—Vectors for the biotoxin, domoic acid, in the Arctic marine ecosystem? *Harmful Algae*, 20, 165-174.

Tammilehto, A., T. G. Nielsen, B. Krock, E. F. Møller, and N. Lundholm, 2015: Induction of domoic acid production in the toxic diatom *Pseudo-nitzschia seriata* by calanoid copepods. *Aquat. Toxicol.*, 159, 52-61.

Vandersea, M. W., et al., 2017: qPCR assays for *Alexandrium fundyense* and *A. ostenfeldii* (Dinophyceae) identified from Alaskan waters and a review of species-specific *Alexandrium* molecular assays. *Phycologia*, 56(3), 303-320.

Wells, M. L., V. L. Trainer, T. J. Smayda, B. S. Karlson, C. G. Trick, R. M. Kudela, A. Ishikawa, S. Bernard, A. Wulff, D. M. Anderson, and W. P. Cochlan, 2015: Harmful algal blooms and climate change: Learning from the past and present to forecast the future. *Harmful Algae*, 49, 68-93.

November 4, 2019

Microplastics in the Marine Realms of the Arctic with Special Emphasis on Sea Ice

I. Peeken, M. Bergmann, G. Gerdts, C. Katlein, T. Krumpen, S. Primpke, M. Tekman

Alfred Wegener Institute, Helmholtz Center for Polar and Marine Research, Bremerhaven, Germany

Marine plastic pollution is a major concern for the global oceans since an estimated 8 million tons of plastic are released from land into the ocean each year (Jambeck et al., 2015). A recent study reported more than a 20-fold increase in marine litter in the Arctic over the course of a decade at the northern station of the Hausgarten Observatory, east of Svalbard (Tekman et al., 2017). Once deposited in the ocean, plastic can be dispersed by both wind and ocean currents. For example, a recent study showed that the poleward branch of thermohaline circulation transfers floating debris from the North Atlantic into the Eurasian Arctic (Cózar et al., 2017). Plastic items are a major threat to marine life that can become entangled or ingest debris (Bergmann et al., 2017). In the subarctic and Arctic, there was early recognition that seabirds collected at the main colonies along the Alaskan coast were ingesting plastic particles (Robards et al., 1995). In fact, some seabird species (e.g., northern fulmars (*Fulmarus glacialis*)), have been used as sentinels for plastic pollution in the Arctic because of these early observations. During the first Arctic circumpolar study of microplastics in 2013, quantities of marine debris at the sea surface were relatively low in comparison to the other ocean basins, and particularly in comparison to the subtropical ocean gyres where much of the ocean's plastic debris accumulates (Cózar et al., 2017). However, the survey indicated particularly abundant plastic debris in the Greenland and Barents seas and estimated that 95% of the plastic load in the Arctic Ocean is found in the northeastern Atlantic sector of the Arctic Ocean. The nature of the particle shapes and sizes pointed to a distant source region confirming long-term model simulations that suggest that these microplastics were transported via the Atlantic branch of the thermohaline circulation (Cózar et al., 2017). A recent study on global patterns of marine micro-particles demonstrated that concentrations were higher in the Arctic Basin than all other ocean basins in the world (Barrows et al., 2018). Once reaching the Arctic plastic particles can be incorporated into sea ice, which acts as a sink and transport vehicle of microplastics in the Arctic (Peeken et al., 2018).

Despite public awareness of marine debris and specifically microplastics in the ocean and the growing number of studies and publications on the topic (Thompson, 2015), our knowledge of plastic pollution in the Arctic remains limited. Further, the lack of a global standard protocol for determining microplastic concentrations (Hidalgo-Ruz et al., 2012) often hampers quantitative comparison between studies. Thus, the overview presented here is based on average values from limited recent publications and sampling efforts in order to give first insight about the knowledge and understanding of marine microplastic pollution in the Arctic Ocean.

Increasing Marine Microplastics Impacts on Arctic Ecosystems

Plastic debris in the ocean are broken down and degraded into small fragments by sunlight, fluctuating temperature, mechanical abrasion and wave action (Andrady, 2015). By definition, particles < 5 mm are called microplastics. Microplastics are a major concern because these micro-sized particles can easily be

consumed by organisms that are food sources at lower levels of the food web, causing great accumulation in higher-level consumer organisms. This relationship has great potential health effects on both marine life and a range of trophic levels and humans, which consume contaminated food sources (Galloway, 2015; Lusher, 2015). Microplastics found globally (Kershaw and Rochman, 2016; Thompson, 2015; www.litterbase.org), have also been observed within Arctic sea ice in concentrations that are several orders of magnitude higher than the average concentrations found in global ocean waters (Obbard et al., 2014). Given the marked reduction in age, thickness, and extent of the sea ice cover in recent decades (Polyakov et al., 2012; Stroeve et al., 2012; see *Sea Ice* essay), it is likely that microplastics temporarily stored in sea ice will be increasingly released into the pelagic Arctic system.

While studies of microplastics in the Arctic have increased over the past few years, considerable geographic regions, namely the Siberian and Amerasian Arctic, are greatly understudied (**Fig. 1**). Existing Arctic studies have reported microplastics in a range of different habitats including sea ice, the water column and deep-sea sediments (**Table 1**). A synthesis of current microplastic concentration data (**Fig. 1**) reveals relatively high contamination levels in the northeastern Atlantic Arctic sector and even in remote central regions of the Arctic. The highest Arctic sea-surface concentrations of microplastics (average 33 N/L) were reported in the Arctic with particular high concentrations in the Beaufort Sea (Barrows et al., 2018). There appears to be an increasing trend in concentrations over the last approximately 10 years in certain regions of the Arctic where repeated studies were carried out. For example, microplastic concentrations in the Greenland Sea have doubled between 2004 and 2015 (Amélineau et al., 2016).

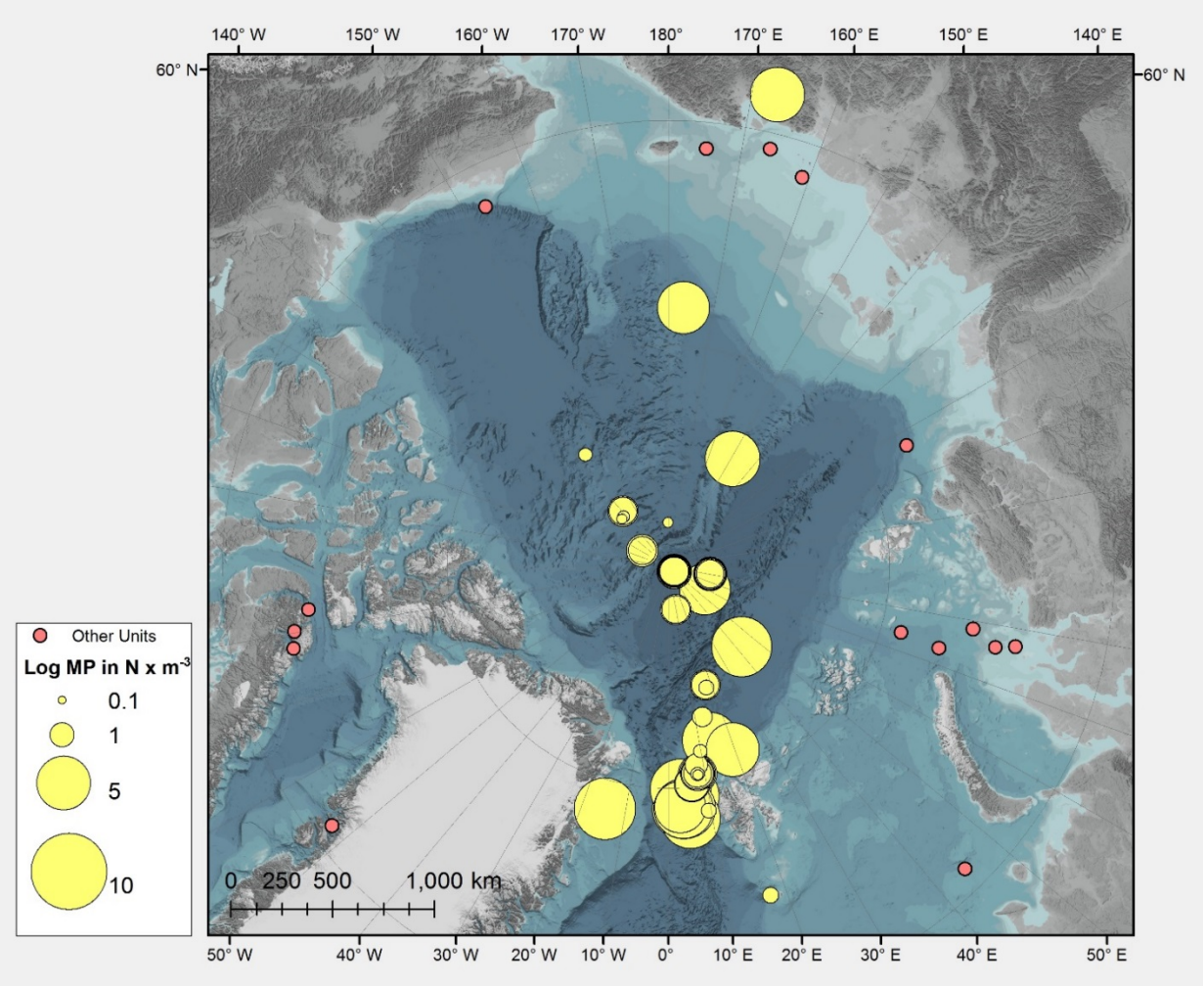

Fig. 1. Map of current archived MP sampling (until 06/2018) in the Central Arctic, showing concentrations levels. Source: AWI LITTERBASE

Table 1. Average concentrations of microplastic particles in various marine habitats of the Arctic Ocean.

Habitat	Sampling area	Sampling year	Average MP concentration (N L^{-1})	Reference
Sea ice	Central Arctic	2005/2010	108	Obbard et al., 2014
	Central Arctic	2014/2015	4500	Peeken et al., 2018
Water	Southwest Svalbard	2014	0.0013	Lusher et al., 2015
	Greenland Sea	2005	0.0009	Amélineau et al., 2016
	Greenland Sea	2014	0.0162	Amélineau et al., 2016
	Arctic	2013-2017	31.3	Barrows et al., 2018
	NE Greenland	2015	0.0024	Morgana et al., 2018
	Central Arctic	2016	0.165*	Kanhai et al., 2018 * AVG maximum Table 1
Sediment	Southwest Svalbard	2001	268 #	Woodal et al., 2014 #upscaled from 50ml
	Fram Strait	2015	2264	Bergmann et al., 2017

Compared to the water column, sea ice and deep-sea sediments have microplastic concentrations that are several orders of magnitude higher (**Table 1**). It is well known that particles such as sediments become concentrated in sea ice during ice formation (Nurnberg et al., 1994), but the phenomenon for microplastic incorporation and concentration into sea ice remains to be investigated. A study found that microplastic concentrations in deep-sea sediments in the Fram Strait were considerably higher than sediments collected elsewhere within the Arctic (Woodall et al., 2014). The high volumes of sea ice transported from the Arctic Ocean via the Fram Strait are a potential source for these relatively high sediment microplastic accumulations and imply that the sea floor might be the final destination of anthropogenic pollution.

Microplastic concentrations in Arctic seabirds have been relatively well-studied since the 1980s (**Table 2**). Early studies of northern fulmars documented ingestion of plastic as early as the 1980. The increasing trend of microplastic particles observed in sea water has interestingly not been evident in Arctic seabirds. For instance, the repeated study between 2004 and 2015 in the Greenland Sea found no difference in the amount of plastic found in the pouches of little auks (*Alle alle*) despite a doubling of microplastic concentrations measured in seawater (Amélineau et al., 2016). Regional variations in seabird ingestion of microplastics are clear, with much higher contamination levels observed in the Eurasian Arctic relative to the Canadian Arctic. Limited recent studies indicate that microplastics have found their way into other elements of the Arctic food web, including polar cod (*Boreogadus saida*) around Svalbard and the Central Arctic (Kühn et al., 2018) and bigeye sculpin (*Triglops nybelini*) around Svalbard (Morgana et al., 2018). A recent report revealed microplastics in 11 species of benthic invertebrates, with concentrations between 0.04 and 1.67 N per individual (**Table 2**; Fang et al., 2018), which are at the lower end of contamination found for this organisms in the world. Plastic has also been found to have even been consumed by Greenland shark (*Somniosus microcephalus*) off Svalbard and Greenland (Leclerc et al., 2012; Nielsen et al., 2014).

Table 2. Examples of plastic ingestions of small particles, mainly MP, by marine birds, fish, and megafauna from the Arctic.

Species	Year of collection	N	Percentage with plastic (%)	Mean number of particles per individual	Region	Reference
Northern fulmars (*Fulmarus glacialis*)	1980 ff	79	92	11.9	Netherland and Arctic colonies	van Franeker, 1985
Northern fulmars (*Fulmarus glacialis*)	2002	15	36	3.6	Davis Strait, Canadian Arctic	Mallory et al., 2006
Thick-billed murre (*Uria lomvia*)	2007/2008	186	11	0.2	Canadian Arctic	Provencher et al., 2010
Little auks (*Alle alle*)	2005	44	100	9.9	East Greenland	Amélineau et al., 2016
Little auks (*Alle alle*)	2014	44	100	8.9	East Greenland	Amélineau et al., 2016
Northern fulmars (*Fulmarus glacialis*)	2014/2015	70	79	11.6	Labrador Sea	Avery-Gomm et al., 2018
Northern fulmars (*Fulmarus glacialis*)	2008	10	80	2.5	Canadian Arctic	Poon et al., 2017
Northern fulmars (*Fulmarus glacialis*)	2013	9	89	3.4	Canadian Arctic	Poon et al., 2017
Black-legged kittiwakes (*Rissa tridactyla*)	2013	11	9	0.18	Canadian Arctic	Poon et al., 2017
Big eye sculpin (*Triglops nybelini*)	2015	71	34	1	Northeast Greenland	Morgana et al., 2018
Polar cod (*Boreogadus saida*)	2015	85	18	1.1	Northeast Greenland	Morgana et al., 2018
Polar cod (*Boreogadus saida*)	2012-2015	72	2.8	1	Eurasian Basin, Svalbard	Kühn et al., 2018 only non-fibrous plastic
Eleven benthic species (e.g., *A. rubens*, *P. borealis*, *C. opilio*, *L. Polaris*, and *E. nana*...)	2017	417	100	0.04-1.67	Bering/Chukchi Sea	Fang et al., 2018

Arctic Sea Ice: An Important Vector of Microplastics

The identification of the various polymer types of microplastic allow the opportunity to draw some conclusion about the main sources of the marine litter which have been disposed (Kershaw, 2015). For example, cellulose acetate is primarily used in the manufacture of cigarette filters and reflects their deposition footprint even in several samples of the Arctic (**Table 3**). A recent study of sea ice cores revealed strong differences in the polymer composition between sea ice cores (**Fig. 2** and **Table 3**; Peeken et al., 2018) as well as within individual horizons studied from a single core (e.g., Fig. 5, in Peeken et al., 2018). Particular ice floes, that are driven in the Pacific water masses of the Canadian Basin or connected to the Atlantic inflow (**Fig. 3**) contained high concentrations of polyethylene and polypropylene particles, which are above all used in packaging material and bottle caps and suggest a long-range transport in this region. In contrast, paint particles from ship's paint (varnish, CE-Alkylated, **Fig. 3**) were mainly found in ice from the shallow marginal seas of Siberia. Overall shipping activities have increased between 2009 and 2014 in the Arctic (Ellis and Brigham, 2009; Miller and Ruiz, 2014) and fisheries account for a major share of the increasing ship traffic in the Arctic Ocean (Eguíluz et al., 2016; Ellis and Brigham, 2009). Polyamide, also called nylon, is a typical polymer associated with the waste of fishing gear, which was present in most studies conducted in the Arctic (**Table 3**). These findings suggest that both the expanding shipping and fishing activities in the Arctic also point to local pollution in the Arctic. Since large fractions of the sea ice are melting at the outflow gateways of the Fram Strait and the Canadian Arctic Archipelago, sea ice can only be a temporally sink for microplastic. Given the ongoing decline in sea ice (Arctic Report Card 2017, Sea Ice Essay), the release of microplastic might accelerate in the future. Whether these potentially released marine plastic particles are sedentary or remain and accumulate in Arctic waters or are transported to lower latitudes still needs to be studied.

Table 3. Most common identified composition of MP particles (average) in various marine habitats of the Arctic Ocean. To evaluate how much these common polymer types contribute to all studied polymers in each study, the % of identified plastic particles is listed in the second column. Polyethylene (PE), polyester (PES), polyethylene terephthalate (PET), polyamide (PA), polypropylene (PP), polyvinyl chloride (PVC), polystyrene (PS), cellulose acetate (CA). Data were extracted from the various publications, taken from text, tables, or figures.

Habitat / Animals	% of all identified particles	PE	PES / PET	PA	PP	Acrylic / Varnish	PVC	PS	CA	Reference
ice	46	2	21	16	3	2		2		Obbard et al., 2014
	89	48.3	3.0	6.5	1.7	27.2	0.1	0.3	5.4	Peeken et al., 2018
water	50	5	15	15		10	5			Lusher et al., 2015
	100	23.3	53.3	3.3	10		3.3	0	6.7	Amélineau et al., 2016
	72	3.8	44.6	9.2	6.3	6.6	1.2			Barrows et al., 2018 AVG coastal, open water
	94	41.2		<6	23.5	<6	11.8	<6		Morgana et al., 2018
	82		77	2.7			2.7			Kanhai et al., 2018
sediment	49	3.53	2.62	20	20	1.27	1.39			Bergmann et al., 2017
bird	100	30	7.5				60		2.5	Amélineau et al., 2016
fish	96	17	34	21		24				Morgana et al., 2018
benthic fauna	87	23	18	46						Fang et al., 2018

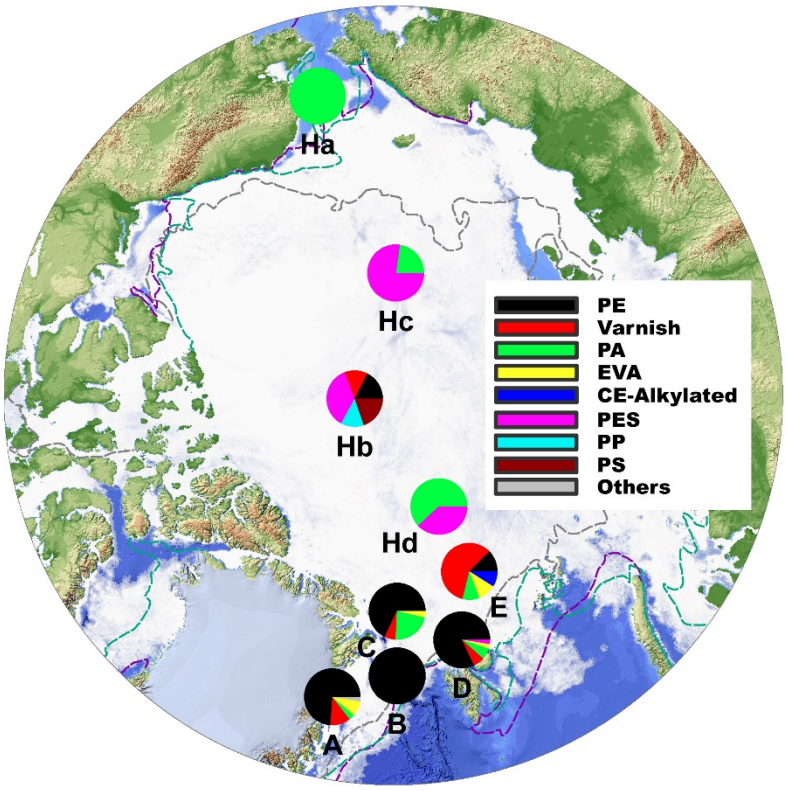

Fig. 2. Sampling position and polymer composition of sea ice cores (A-E) obtained during three RV Polarstern expeditions. For comparison, previously sampled sea ice cores by Obbard et al. (2014) are indicated (Ha-Hd). The average % composition of polymers from the entire core (this study) and digitized data of figure two from Obbard et al. (2014)*, acrylic equals varnish. Polyethylene (PE), polyamide (PA), ethylene-vinyl-acetate (EVA), chemical modified cellulose (CE-Alkylated), polyester (PES), polypropylene (PP), and Others (acrylonitrile butadiene, chlorinated polyethylene, nitrile rubber, polycaprolactone, polycarbonate, polylactic acid, polyimide, polystyrene, polyvinyl chloride, and rubber) were found. The map was created using ArcGIS 10.3 and based on the General Bathymetric Chart of the Oceans (GEBCO)-08 grid, version 20100927, https://www.gebco.net, with permission from the British Oceanographic Data Centre (BODC). *The polymer rayon was excluded. (Figure modified after Peeken et al., 2018.)

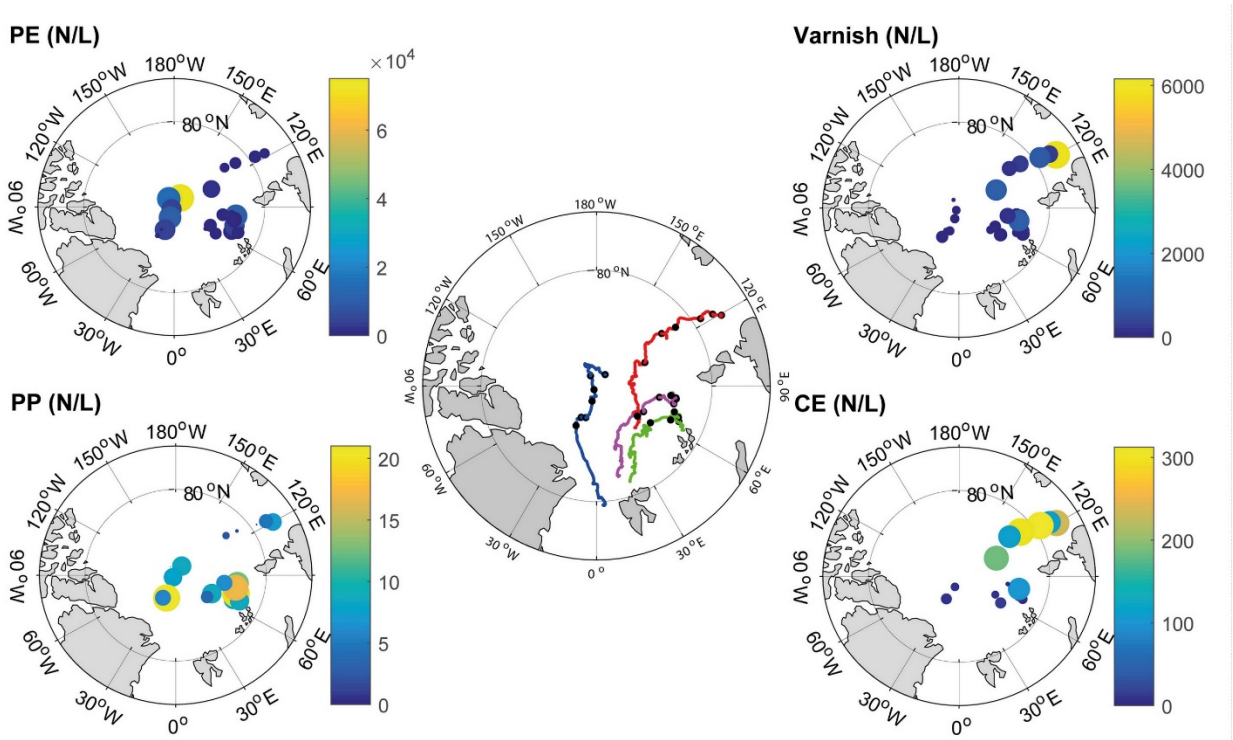

Fig. 3. Back trajectories of the modelled ice cores with black dots representing the mean locations where the ice of the respective vertically resolved samples was formed (center). Based on this derived regional distribution of polyethylene (PE), polypropylene (PP), varnish, and CE-Alkylated (CE) concentration are given in particles x L^{-1} in all georeferenced ice samples. Colors represent the MP concentration on a linear color bar and the circle diameters are proportional to MP concentration depicted on a logarithmic scale for a better visibility. (Figure modified after Peeken et al., 2018.)

Plastic pollution is present throughout the various Arctic realms from the water column to deep sea fauna. In the Arctic, it is clear that sea ice is a particular transport vector, but currently very little is known about the effect of microplastic on the sympagic (or sea ice dwelling) biota, which are an important food source for the Arctic ecosystem. Future studies are needed to evaluate which negative influence these pollutants have on the performance of this currently productive ecosystem.

References

Amélineau, F., D. Bonnet, O. Heitz, V. Mortreux, A. M. A. Harding, N. Karnovsky, W. Walkusz, J. Fort, and D. Grémillet, 2016: Microplastic pollution in the Greenland Sea: Background levels and selective contamination of planktivorous diving seabirds. *Environ. Pollut.*, 219, 1131-1139, doi: 10.1016/j.envpol.2016.09.017.

Andrady, A. L., 2015: Persistence of plastic litter in the oceans, in *Marine Anthropogenic Litter*. M. Bergmann, L. Gutow, and M. Klages, Eds., Springer, pp. 57-72.

Avery-Gomm, S., J. F. Provencher, M. Liboiron, F. E. Poon, and P. A. Smith, 2018: Plastic pollution in the Labrador Sea: An assessment using the seabird northern fulmar Fulmarus glacialis as a biological monitoring species. *Mar. Pollut. Bull.*, 127, 817-822.

Barrows, A. P. W., S. E. Cathey, and C. W. Petersen, 2018: Marine environment microfiber contamination: Global patterns and the diversity of microparticle origins. *Environ. Pollut.*, 237, 275-284.

Bergmann, M., M. B. Tekman, and L. Gutow, 2017: Marine litter: Sea change for plastic pollution. *Nature*, 544, 297, doi: 10.1038/544297a.

Cózar, A., et al., 2017: The Arctic Ocean as a dead end for floating plastics in the North Atlantic branch of the Thermohaline Circulation. *Sci. Adv.*, 3, e1600582, doi: 10.1126/sciadv.1600582.

Eguíluz, V. M., J. Fernández-Gracia, X. Irigoien, and C. M. Duarte, 2016: A quantitative assessment of Arctic shipping in 2010-2014. *Sci. Rep.*, 6, 30682, doi: 10.1038/srep30682.

Ellis, B., and L. Brigham, 2009: Arctic Marine Shipping Assessment 2009 Report. Arctic Council, Tromsø, Norway. http://hdl.handle.net/11374/54.

Fang, C., et al., 2018: Microplastic contamination in benthic organisms from the Arctic and sub-Arctic regions. *Chemosphere*, 209, 298-306, doi: 10.1016/j.chemosphere.2018.06.101.

Galloway, T. S., 2015: Micro- and nano-plastics and human health, in *Marine Anthropogenic Litter*. M. Bergmann, L. Gutow, and M. Klages, Eds., Springer, pp. 343-366.

Hidalgo-Ruz, V., L. Gutow, R. C. Thompson, and M. Thiel, 2012: Microplastics in the marine environment: A review of the methods used for identification and quantification. *Environ. Sci. Technol.*, 46, 3060-3075.

Jambeck, J. R., R. Geyer, C. Wilcox, T. R. Siegler, M. Perryman, A. Andrady, R. Narayan, and K. L. Law, 2015: Plastic waste inputs from land into the ocean. *Science*, 347, 768-771.

Kanhai, L. D., K. K. Gårdfeldt, O. Lyashevska, M. Hassellöv, R. C. Thompson, and I. O'Connor, 2018: Microplastics in sub-surface waters of the Arctic Central Basin. *Mar. Pollut. Bull.*, 130, 8-18.

Kershaw, P. J., Ed., 2015: Sources, fate and effects of microplastics in the marine environment: A global assessment. *Rep. Stud. GESAMP 90*. IMO/FAO/UNESCO-IOC/UNIDO/WMO/IAEA/UN/UNEP/UNDP Joint Group of Experts on the Scientific Aspects of Marine Environmental Protection, 96 pp.

Kershaw, P., and C. M. Rochman, 2016: Sources, fate and effects of microplastics in the marine environment: Part two of a global assessment. *Rep. Stud. GESAMP 93*. IMO/FAO/UNESCO-IOC/UNIDO/WMO/IAEA/UN/UNEP/UNDP Joint Group of Experts on the Scientific Aspects of Marine Environmental Protection, 220 pp.

Kühn, S., F. L. Schaafsma, B. van Werven, H. Flores, M. Bergmann, M. Egelkraut-Holtus, M. B. Tekman, and J. A. van Franeker, 2018: Plastic ingestion by juvenile polar cod (*Boreogadus saida*) in the Arctic Ocean. *Polar Biol.*, 41, 1269-1278.

Leclerc, L. -M. E., C. Lydersen, T. Haug, L. Bachmann, A. T. Fisk, and K. M. Kovacs, 2012: A missing piece in the Arctic food web puzzle? Stomach contents of Greenland sharks sampled in Svalbard, Norway. *Polar Biol.*, 35, 1197-1208.

Lusher, A. L., 2015: Microplastics in the marine environment: Distribution, interactions and effects, p. 245-307, in *Marine Anthropogenic Litter*. M. Bergmann, L. Gutow, and M. Klages, Eds., Springer, pp. 245-307.

Lusher, A. L., V. Tirelli, I. O'Connor, and R. Officer, 2015: Microplastics in Arctic polar waters: The first reported values of particles in surface and sub-surface samples. *Sci. Rep.*, 5, 14947, doi: 10.1038/srep14947.

Mallory, M. L., G. J. Roberston, and A. Moenting, 2006: Marine plastic debris in northern fulmars from Davis Strait, Nunavut, Canada. *Mar. Pollut. Bull.*, 52, 813-815.

Miller, A. W., and G. M. Ruiz, 2014: Arctic shipping and marine invaders. *Nat. Clim. Change*, 4, 413-416.

Morgana, S., L. Ghigliotti, N. Estévez-Calvar, R. Stifanese, A. Wieckzorek, T. Doyle, J. S. Christiansen, M. Faimali, and F. Garaventa, 2018: Microplastics in the Arctic: A case study with sub-surface water and fish samples off Northeast Greenland. *Environ Pollut. B*, 242, 1078-1086, doi: 10.1016/j.envpol.2018.08.001.

Nielsen, J., R. B. Hedeholm, M. Simon, and J. F. Steffensen, 2014: Distribution and feeding ecology of the Greenland shark (*Somniosus microcephalus*) in Greenland waters. *Polar Biol.*, 37, 37-46.

Nurnberg, D., I. Wollenburg, D. Dethleff, H. Eicken, H. Kassens, T. Letzig, E. Reimnitz, and J. Thiede, 1994: Sediments in Arctic sea ice: Implications for entrainment, transport and release. *Mar. Geol.*, 119, 185-214.

Obbard, R. W., S. Sadri, Y. Q. Wong, A. A. Khitun, I. Baker, and R. C. Thompson, 2014: Global warming releases microplastic legacy frozen in Arctic Sea ice. *Earth's Future*, 2, 315-320.

Peeken, I., S. Primpke, B. Beyer, J. Gütermann, C. Katlein, T. Krumpen, M. Bergmann, L. Hehemann, and G. Gerdts, 2018: Arctic sea ice is an important temporal sink and means of transport for microplastic. *Nat. Commun.*, 9, 1505, doi: 10.1038/s41467-018-03825-5.

Polyakov, I. V., J. E. Walsh, and R. Kwok, 2012: Recent changes of Arctic multiyear sea ice coverage and the likely causes. *Bull. Am. Meteorol. Soc.*, 93, 145-151.

Poon, F. E., J. F. Provencher, M. L. Mallory, B. M. Braune, and P. A. Smith, 2017: Levels of ingested debris vary across species in Canadian Arctic seabirds. *Mar. Pollut. Bull.*, 116, 517-520.

Provencher, J. F., A. J. Gaston, M. L. Mallory, P. D. O'Hara, and H. G. Gilchrist, 2010: Ingested plastic in a diving seabird, the thick-billed murre (*Uria lomvia*), in the eastern Canadian Arctic. *Mar. Pollut. Bull.*, 60, 1406-1411.

Robards, M. D., J. F. Piatt, and K. D. Wohl, 1995: Increasing frequency of plastic particles ingested by seabirds in the sub-Arctic North Pacific. *Mar. Pollut. Bull.*, 30, 151-157.

Stroeve, J. C., M. C. Serreze, M. M. Holland, J. E. Kay, J. Malanik, and A. P. Barrett, 2012: The Arctic's rapidly shrinking sea ice cover: A research synthesis. *Clim. Change*, 110, 1005-1027.

Tekman, M. B., T. Krumpen, and M. Bergmann, 2017: Marine litter on deep Arctic seafloor continues to increase and spreads to the North at the HAUSGARTEN observatory. *Deep-Sea Res. Pt. I*, 120, 88-99.

Thompson, R. C. 2015: Microplastics in the marine environment: sources, consequences and solutions, in *Marine Anthropogenic Litter*. M. Bergmann, L. Gutow, and M. Klages, Eds., Springer, pp. 185-200.

van Franeker, J. A., 1985: Plastic ingestion in the North Atlantic fulmar. *Mar. Pollut. Bull.*, 16, 367-369.

Woodall, L. C., et al., 2014: The deep sea is a major sink for microplastic debris. *Roy. Soc. Open Sci.*, 1, 140317, doi: 10.1098/rsos.140317.

November 19, 2018

Landfast Sea Ice in a Changing Arctic

A. R. Mahoney

Geophysical Institute, University of Alaska Fairbanks, Fairbanks, AK, USA

Landfast ice is an essential component of the coastal sea ice system. Acting as a floating extension of the land (**Fig. 1**), landfast ice is the most accessible form of sea ice and the one most often encountered by people. Members of Arctic coastal communities travel across landfast ice (**Fig. 2**) and hunt marine mammals and birds that are commonly found at its seaward edge (George et al., 2004; Laidre et al., 2015; Lovvorn et al., 2018). Ringed seals, in particular, are an important prey species for polar bears and subsistence hunters. These seals are uniquely adapted to maintain breathing holes in landfast ice (Smith and Hammill, 1981), which otherwise lacks the openings (e.g., cracks and leads) used by marine mammals in the drifting ice pack. Additionally, landfast ice serves as a platform for the oil and gas industry, which relies on ice roads across landfast ice to access nearshore production and exploration facilities (Potter et al., 1981; Masterson, 2009). Landfast ice also plays an important role in the sediment dynamics of coastal waters (Eicken et al., 2005a) and can buffer the coast against the erosive action of waves (Lantuit and Pollard, 2008). By isolating the underlying ocean from wind mixing, landfast ice allows river plumes to extend farther than they would under open water or pack ice (Ingram, 1987; Granskog et al., 2005; Kasper and Weingartner, 2015). In some cases, the hydrographic influence of landfast extends well beyond the coastal zone (Itkin et al., 2015), affecting the locations of upwelling in locations such as the Beaufort Sea (Pickart et al., 2009) and deep convection on the Eurasian Arctic shelf (Dmitrenko et al., 2005).

Fig. 1. Landfast ice is distinguished from the drifting pack ice by its attachment to the land. A flaw lead of open water is sometimes present at the seaward edge of the landfast ice. When the pack ice pushes against the landfast ice edge, ice deformation often occurs and creates ridges within and along the boundary of the landfast ice.

Fig. 2. Two community members returning by snowmobile from a flaw lead at the seaward edge of the landfast ice near Utqiaġvik, Alaska.

What distinguishes landfast ice from drifting pack ice and allows it to fulfill all its roles in the Earth system is its attachment to the coast and, hence, the immobility this provides. Depending on the coastal setting, there are two principal ways in which sea ice can become attached to the land (**Fig. 1**). In lagoons, fjords, channels, and other enclosed waters, sea ice can become landlocked, typically shortly after freeze-up is complete (Galley et al., 2012; Hata and Tremblay, 2015a, 2015b). Isolated from dynamic forces, the landlocked ice remains largely undeformed and level. In contrast, landfast ice along open coasts frequently interacts with drifting pack ice at its seaward edge. This interaction often leads to the creation of large pressure ridges, which form when ice converges and piles up both above and below the waterline. Sometimes known as stamukhi (Barnes et al., 1978), these ridges anchor the landfast ice in place when they become grounded on the seafloor (Mahoney et al., 2007; Jones et al., 2016). These ridges can become grounded either during their formation process or they may form offshore and drift into shallow water (Reimnitz et al., 1978; Mahoney et al., 2007; Jones et al., 2016). As a result of these processes, landfast ice formed along open coastlines invariably has a rough surface (**Fig. 2**). Also, in sufficiently shallow waters (typically $\lesssim$ 1.5 m), sea ice may freeze to the seafloor and become bottomfast (Reimnitz and Barnes, 1974; Dammann et al., 2018a).

Geographic Extent

Landfast ice is found along coastlines wherever sea ice occurs. In the Arctic, it typically reaches an average annual maximum extent of 1.8 million km^2 (Yu et al., 2013), or approximately 12% of the total Northern Hemisphere wintertime sea ice cover (**Fig. 3**). Over one third of landfast ice (660,000 km^2) is found in the Kara, Laptev, and East Siberian seas (Yu et al., 2013), where it can extend up to 300 km from the Eurasian shore (Divine et al., 2004). The channels and straits of the Canadian Arctic Archipelago, which can be up to 160 km wide, account for almost another third of total Arctic landfast extent (540,000 km^2) (Yu et al., 2013). The remaining third is spread more thinly along the coasts of the other Arctic and sub-Arctic seas, typically extending less than 50 km from the coast (e.g., Mahoney et al., 2014). The distribution of landfast ice extent in the Arctic can be largely explained by regional variations in the depth and slope of the inner continental shelf. Except in landlocked regions, the extent of landfast ice is largely limited by local bathymetry and the depth to which the keels of pressure ridges in the region extend below the water. As a result, despite the large differences in overall distance from shore, the seaward edge of landfast ice in most regions of the Arctic is usually found in 15-30 m of water (Granskog et al., 2006; Mahoney et al., 2014; Selyuzhenok et al., 2015). In some cases, grounded icebergs may allow landfast ice to extend into waters deeper than 100 m along the coasts of Greenland, northern Canada, Severnaya Zemlya, and Svalbard (Jacobs et al., 1975; Divine et al., 2004).

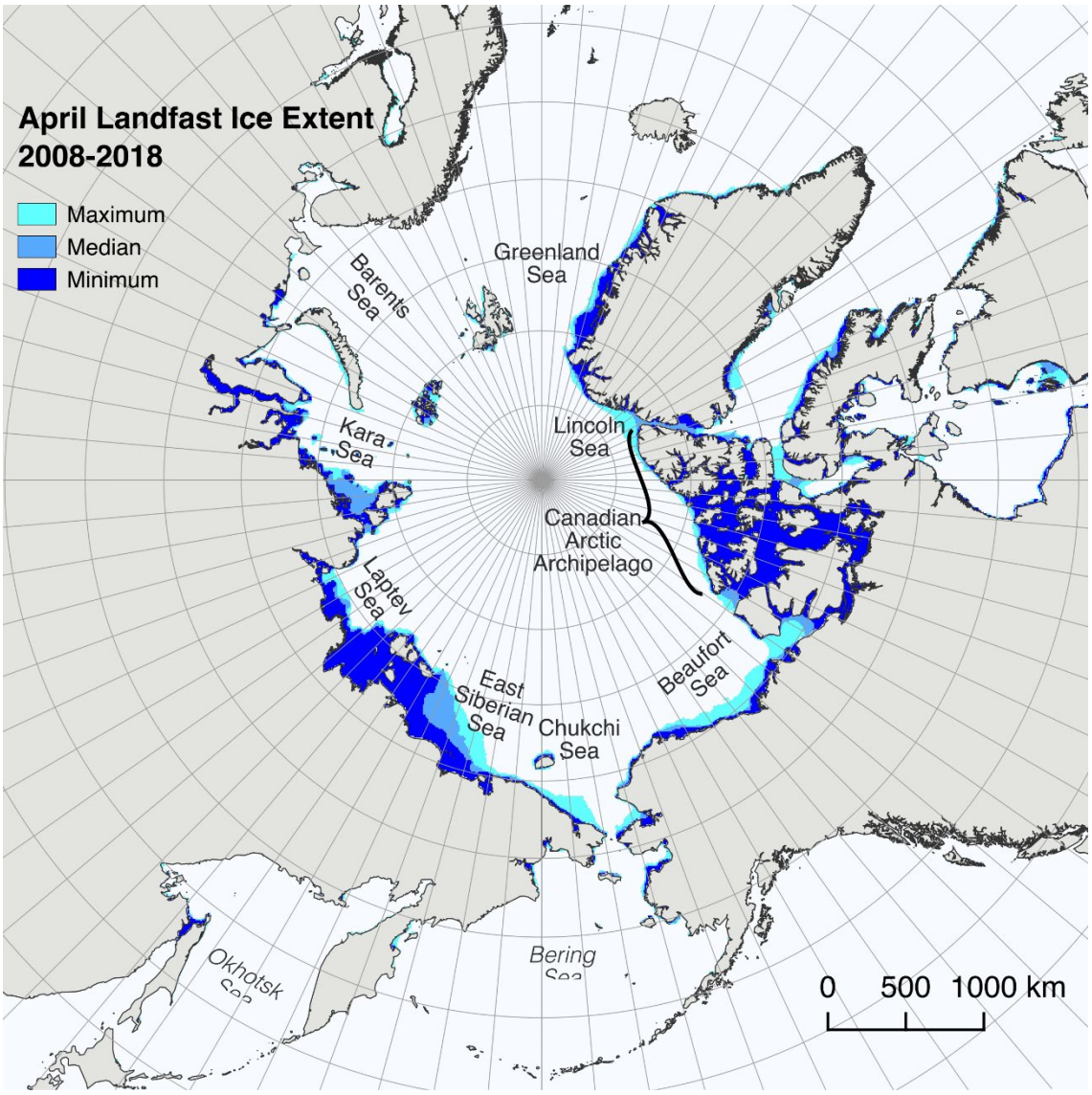

Fig. 3. Minimum, median, and maximum Arctic landfast ice extent derived from NIC ice charts for the period 2008-18.

Annual Cycle

Landfast ice is typically a seasonal phenomenon, forming each fall and breaking up the following spring. However, landfast ice persists through the summer melt season in a number of locations in the Canadian Arctic Archipelago (Alt et al., 2006; Galley et al., 2012; Pope et al., 2012) and is sometimes found in the Taymyr Peninsula region of Siberia (Reimnitz et al., 1995). The typical annual cycle begins in early winter with the first attachment of ice to the shoreline, which usually happens sometime after the first appearance of drifting sea ice in coastal waters. Landfast ice formation occurs earliest in sheltered locations such as the lagoons (Mahoney et al., 2014), shallow waters around deltas (Divine et al., 2004; Selyuzhenok et al., 2015), and the channels and sounds of the Canadian Arctic Archipelago (Galley et al., 2012). In such areas, the ice cover becomes landfast as the pack ice gradually loses mobility as it thickens and extends between shorelines (Selyuzhenok et al., 2017). By comparison, landfast ice along open coastlines largely forms through an accretionary process, whereby ice formed elsewhere is

transported into the coastal region and becomes attached to the shoreline or seaward edge of existing landfast ice (Reimnitz et al., 1978; Mahoney et al., 2007). This process may be interrupted or reversed by breakout events (Mahoney et al., 2007; Jones et al., 2016; Selyuzhenok et al., 2017), but by the end of most winters the landfast ice on open coastlines will reach a maximum extent limited by local bathymetry, as described above.

Break-up of landfast ice is the result of both dynamic and thermodynamic processes. In the most general case, the ice cover is weakened by warming and thinning until it is detached from the coast or other landfast ice by winds, currents, or waves. In landlocked areas, breakup is a predominantly thermodynamic process (Melling, 2002) and in the Canadian Arctic Archipelago this results in a relatively consistent break-up date each year (Galley et al., 2012). Similarly, if landfast ice on open coastlines is not heavily grounded, break-up date correlates well with the cumulative amount of solar energy reaching the Earth's surface (Petrich et al., 2012). However, if the landfast ice cover along these open coastal regions is more firmly anchored, the timing of breakup is more likely to be controlled by the occurrence of strong winds and currents or changes in local sea level (Divine et al., 2004; Mahoney et al., 2007; Jones et al., 2016). Near major rivers, the break-up of landfast ice can be triggered by spring discharge (Bareiss et al., 1999; Divine et al., 2003). The fate of landfast sea ice after break-up is not well understood, but fragments of former landfast ice may represent an important refuge for walrus and other ice-dependent pinnipeds, while also representing a potential hazard for coastal shipping.

Interannual Variability and Decadal Trends

Due to its accessibility, the longest records of sea ice thickness anywhere in the Arctic come from measurements made in landfast ice, dating back to the 1930s in the Russian Arctic (Polyakov et al., 2003) and the 1950s in the Canadian Arctic Archipelago (Brown and Cote, 1992; Howell et al., 2016). Recent analyses suggest there has been a reduction in annual maximum ice thickness of around 25 cm (approximately 10%) at most locations in the Canadian Arctic Archipelago (Howell et al., 2016). Similarly, landfast ice at Hopen on the Barents Sea coast was found to be thinning by approximately 1 cm per year between 1966 and 2007 (Gerland et al., 2008). A 16-year record of landfast ice thickness near Utqiaġvik (Eicken et al., 2012) indicates the annual maximum ice thickness has decreased by around 30 cm since 2000 (Eicken et al., 2012).

Weekly charts from the U.S. National Ice Service (NIC) indicate that overall landfast ice extent in the Arctic decreased by approximately 12,300 $km^2\ yr^{-1}$ (0.7% yr^{-1}) between 1976 and 2007 (Yu et al., 2013). It should be noted that the NIC results represent changes in the seasonal average extent from January to May, rather than the full maximum extent at the end of the growth season. In the Chukchi Sea, the annual maximum width of landfast ice reduced by an average of 13 km (~50%) between the periods 1973-76 (Stringer, 1978) and 1996-2008 (Mahoney et al., 2014), while the maximum extent of landfast ice in the Beaufort Sea changed little during this time. Also, charts from the Arctic and Antarctic Research Institute (AARI) in Russia show no consistent trend in maximum landfast ice extent in the Laptev Sea between 1999 and 2013 (Selyuzhenok et al., 2015).

The declining seasonal average extent of Arctic landfast ice is in part caused by a later date of formation and earlier break-up. Over the period 1976-2007, NIC ice charts indicate that the duration of landfast ice is decreasing by approximately 0.8 d/yr on average across the Northern Hemisphere, with the fastest changes occurring mostly in the Russian Arctic (Yu et al., 2013). AARI ice charts show a declining trend in Laptev Sea landfast ice duration of almost 3 d/yr (Selyuzhenok et al., 2015) while Canadian Ice Service charts show similar trends in the Alaska Beaufort Sea and Mackenzie Delta area, and a shorter landfast

ice season throughout the Canadian Arctic Archipelago (Galley et al., 2012). A comparison between results from studies covering the periods 1973-77 (Barry et al., 1979) and 1996-2008 shows a shortening of the landfast season of approximately 53 days (~2 d/yr) in the western Beaufort Sea and 38 days (~1.4 d/yr) in the Chukchi Sea (Mahoney et al., 2014). The reduced length of the landfast ice season is also likely a strong driver of the reduced end-of-winter thickness of landfast ice described above.

Landfast Ice as a Potential Arctic Indicator

Throughout the Arctic, landfast ice is shrinking in all dimensions, albeit with significant regional variability. Due to a later start to formation and an earlier break-up, it is occupying the coastline for a shorter period of time each year and it is not growing as thick as it used to. In some areas, its maximum winter extent is also decreasing. These changes are having direct impacts on residents of coastal communities. These communities are needing to adapt to increasingly unsafe and unpredictable ice conditions (Ford et al., 2008; Laidler et al., 2009; Druckenmiller et al., 2010), which exacerbate impacts from other climatic and socio-economic changes (Ford et al., 2009). Improved observations of landfast ice will allow communities to better identify vulnerabilities and develop adaption plans (Furgal and Seguin, 2006). Such observations are also expected to be of value to the operators of nearshore oil and gas platforms in the Arctic (Dammann et al., 2018c). Additionally, since it occupies the intersection between the terrestrial, marine, and atmospheric domains, improved observations of landfast ice will lead to a better understanding of how these systems interact in a changing Arctic. Recent developments in modeling of landfast ice have relied on observations of its seasonal development for validation (Lemieux et al., 2015; Olason, 2016).

As a rapidly changing and interconnected component of the Arctic system directly impacting local residents, it would seem that landfast ice is well suited for inclusion as an 'Indicator' essay in the Arctic Report Card. However, we currently lack a clear understanding of changes in the last few years and an observing strategy to meet future needs. Such an observing strategy will need to be capable of measuring the extent and thickness of landfast ice and resolving its annual cycle. There is growing awareness of the value of community partnerships in Arctic science, and this is particularly true for landfast sea ice research. Not only does community-based monitoring offer a means of collecting high quality in situ observations of the thickness and annual cycle of coastal ice (Mahoney et al., 2009; Eicken et al., 2014), but co-production of knowledge (Behe and Daniel, 2018) at early stages of research design can help ensure a sound observing strategy that will generate information of value for all stakeholders.

Satellite data also have a key role to play in monitoring landfast ice as an indicator of Arctic change. However, there is currently no standardized or automated approach for measuring landfast ice extent. Our longest continuous records come from satellite-derived operational ice charts, which were not intended to be long-term records of sea ice variability. With the recent and imminent launch of several new satellites, interferometric SAR (InSAR) currently holds great promise for automated classification and mapping of landfast ice (Meyer et al., 2011). Although computationally intensive, InSAR is able to detect small-scale ice motion and has proven capable of mapping bottomfast ice (Dammann et al., 2018a; Tibbles et al., 2018) and other zones of variable stability within the landfast ice cover (Dammann et al., 2018b). Bottomfast ice extent may be particularly valuable as an indicator of change due to its sensitivity to ice thickness and importance for underlying permafrost (Eicken et al., 2005b).

References

Alt, B., K. Wilson, and T. Carrières, 2006: A case study of old-ice import and export through Peary and Sverdrup Channels in the Canadian Arctic Archipelago: 1998-2005. *Ann. Glaciol.*, 44, 329-338.

Bareiss, J., H. Eicken, A. Helbig, and T. Martin, 1999: Impact of river discharge and regional climatology on the decay of sea ice in the Laptev Sea during spring and early summer. *Arct. Antarct. Alp. Res.*, 31, 214-229.

Barnes, P. W., E. Reimnitz, and L. J. Toimil, 1978: Stamukhi zone processes: Implications for developing the Arctic offshore area. *J. Petrol. Technol.*, 30, 982-986.

Barry, R. G., R. E. Moritz, and J. C. Rogers, 1979: The fast ice regimes of the Beaufort and Chukchi Sea coasts, Alaska. *Cold Reg. Sci. Technol.*, 1, 129-152.

Behe, C., and R. Daniel, 2018: Indigenous knowledge and the coproduction of knowledge process: Creating a holistic understanding of arctic change [in "State of the Climate in 2017"]. *Bull. Am. Meteorol. Soc.*, 99, S160-S161.

Brown, R. D., and P. Cote, 1992: Interannual variability of landfast ice thickness in the Canadian High Arctic, 1950-89. *Arctic*, 45, 273-284.

Dammann, D., L. Eriksson, A. Mahoney, C. Stevens, J. van der Sanden, H. Eicken, F. Meyer, and C. Tweedie, 2018a: Mapping Arctic bottomfast sea ice using SAR interferometry. *Remote Sens.*, 10, 720.

Dammann, D. O., L. E. B. Eriksson, A. R. Mahoney, H. Eicken, and F. J. Meyer, 2018b: Landfast sea ice stability - mapping pan-Arctic ice regimes with implications for ice use, subsea permafrost and marine habitats. *Cryosphere Discuss.*, doi: 10.5194/tc-2018-129.

Dammann, D. O., H. Eicken, A. R. Mahoney, F. J. Meyer, J. T. Freymueller, and A. M. Kaufman, 2018c: Evaluating landfast sea ice stress and fracture in support of operations on sea ice using SAR interferometry. *Cold Reg. Sci. Technol.*, 149, 51-64, doi: 10.1016/j.coldregions.2018.02.001.

Divine, D., R. Korsnes, and A. Makshtas, 2003: Variability and climate sensitivity of fast ice extent in the north-eastern Kara Sea. *Polar Res.*, 22, 27-34.

Divine, D. V., R. Korsnes, and A. P. Makshtas, 2004: Temporal and spatial variation of shore-fast ice in the Kara Sea. *Cont. Shelf Res.*, 24, 1717-1736.

Dmitrenko, I. A., K. N. Tyshko, V. N. Churun, J. A. Hoelemann, H. Eicken, H. Kassens, and S. A. Kirillov, 2005: Impact of flaw polynyas on the hydrography of the Laptev Sea. *Global Planet. Change*, 48, 9-27.

Druckenmiller, M. L., H. Eicken, J. C. George, and L. Brower, 2010: Assessing the shorefast ice: Iñupiat whaling trails off Barrow, Alaska, in *SIKU: Knowing Our Ice*, I. Krupnik, C. Aporta, S. Gearheard, G. J. J. Laidler, and L. K. Kielsen Holm, Eds., Springer Netherlands, pp. 203-228.

Eicken, H., R. Gradinger, A. Graves, A. Mahoney, I. Rigor, and H. Melling, 2005a: Sediment transport by sea ice in the Chukchi and Beaufort Seas: Increasing importance due to changing ice conditions? *Deep-Sea Res. II*, 52, 3281-3302.

Eicken, H., I. Dmitrenko, K. Tyshko, A. Darovskikh, W. Dierking, U. Blahak, J. Groves, and H. Kassens, 2005b: Zonation of the Laptev Sea landfast ice cover and its importance in a frozen estuary. *Global Planet. Change*, 48, 55-83.

Eicken, H., R. Gradinger, T. Heinrichs, M. A. Johnson, A. L. Lovecraft, and M. Kaufman, 2012: Automated ice mass balance site data (SIZONET).NSF Arctic Data Center. https://arcticdata.io/catalog/#view/doi:10.18739/A2BM0G

Eicken, H., M. Kaufman, I. Krupnik, P. Pulsifer, L. Apangalook, P. Apangalook, W. Weyapuk, and J. Leavitt, 2014: A framework and database for community sea ice observations in a changing Arctic: an Alaskan prototype for multiple users. *Polar Geogr.*, 37, 5-27.

Ford, J. D., T. Pearce, J. Gilligan, B. Smit, and J. Oakes, 2008: Climate change and hazards associated with ice use in Northern Canada. *Arct. Antarct. Alp. Res.*, 40, 647-659.

Ford, J. D., W. A. Gough, G. J. Laidler, J. MacDonald, C. Irngaut, and K. Qrunnut, 2009: Sea ice, climate change, and community vulnerability in northern Foxe Basin, Canada. *Clim. Res.*, 38, 137-154.

Furgal, C., and J. Seguin, 2006: Climate change, health, and vulnerability in Canadian northern Aboriginal communities. *Environ. Health Perspect.*, 114, 1964-1970.

Galley, R. J., B. G. T. Else, S. E. L. Howell, J. V. Lukovich, and D. G. Barber, 2012: Landfast sea ice conditions in the Canadian Arctic: 1983-2009. *Arctic*, 65, 133-144.

George, J. C., H. P. Huntington, K. Brewster, H. Eicken, D. W. Norton, and R. Glenn, 2004: Observations on shorefast ice dynamics in Arctic Alaska and the responses of the Iñupiat hunting community. *Arctic*, 57, 363-374.

Gerland, S., A. H. H. Renner, F. Godtliebsen, D. Divine, and T. B. Løyning, 2008: Decrease of sea ice thickness at Hopen, Barents Sea, during 1966-2007. *Geophys. Res. Lett.*, 35, L06501, doi: 10.1029/2007GL032716.

Granskog, M. A., J. Ehn, and M. Niemelä, 2005: Characteristics and potential impacts of under-ice river plumes in the seasonally ice-covered Bothnian Bay (Baltic Sea). *J. Mar. Sys.*, 53, 187-196.

Granskog, M., H. Kaartokallio, H. Kuosa, D. N. Thomas, and J. Vainio, 2006: Sea ice in the Baltic Sea - A review. *Estuar., Coast. Shelf Sci.*, 70, 145-160.

Hata, Y., and L. B. Tremblay, 2015a: A 1.5-D anisotropic sigma-coordinate thermal stress model of landlocked sea ice in the Canadian Arctic Archipelago. *J. Geophys. Res.-Oceans*, 120, 8251-8269, doi: 10.1002/2015JC010820.

Hata, Y., and L. B. Tremblay, 2015b: Anisotropic internal thermal stress in sea ice from the Canadian Arctic Archipelago. *J. Geophys. Res.-Oceans*, 120, 5457-5472, doi: 10.1002/2015JC010819.

Howell, S. E. L., F. Laliberté, R. Kwok, C. Derksen, and J. King, 2016: Landfast ice thickness in the Canadian Arctic Archipelago from observations and models. *Cryosphere*, 10, 1463-1475.

Ingram, G., 1987: Under-ice characteristics of La Grande Riviere Plume. *Atmos. Ocean*, 25, 242-250.

Itkin, P., M. Losch, and R. Gerdes, 2015: Landfast ice affects the stability of the Arctic halocline: Evidence from a numerical model. *J. Geophys. Res.-Oceans*, 120, 2622-2635.

Jacobs, J. D., R. G. Barry, and R. L. Weaver, 1975: Fast ice characteristics, with special reference to the eastern Canadian Arctic. *Polar Rec.*, 110, 521-536.

Jones, J., H. Eicken, A. Mahoney, M. Rohith, C. Kambhamettu, Y. Fukamachi, K. I. Ohshima, and J. C. George, 2016: Landfast sea ice breakouts: Stabilizing ice features, oceanic and atmospheric forcing at Barrow, Alaska. *Cont. Shelf Res.*, 126, 50-63.

Kasper, J. L., and T. J. Weingartner, 2015: The spreading of a buoyant plume beneath a landfast ice cover. *J. Phys. Oceanogr.*, 45, 478-494.

Laidler, G. J., J. D. Ford, W. A. Gough, T. Ikummaq, A. S. Gagnon, S. Kowal, K. Qrunnut, and C. Irngaut, 2009: Travelling and hunting in a changing Arctic: Assessing Inuit vulnerability to sea ice change in Igloolik, Nunavut. *Clim. Change*, 94, 363-397.

Laidre, K. L., H. Stern, K. M. Kovacs, L. Lowry, S. E. Moore, E. V. Regehr, S. H. Ferguson, Ø. Wiig, P. Boveng, R. P. Angliss, E. W. Born, D. Litovka, L. Quakenbush, C. Lydersen, D. Vongraven, and F. Ugarte, 2015: Arctic marine mammal population status, sea ice habitat loss, and conservation recommendations for the 21st century. *Conserv. Biol.*, 29, 724-737.

Lantuit, H., and W. H. Pollard, 2008: Fifty years of coastal erosion and retrogressive thaw slump activity on Herschel Island, southern Beaufort Sea, Yukon Territory, Canada. *Geomorphology*, 95, 84-102.

Lemieux, J. -F., L. B. Tremblay, F. Dupont, M. Plante, G. C. Smith, and D. Dumont, 2015: A basal stress parameterization for modeling landfast ice. *J. Geophys. Res.-Oceans*, 120, 3157-3173.

Lovvorn, J. R., A. R. Rocha, A. H. Mahoney, and S. C. Jewett, 2018: Sustaining ecological and subsistence functions in conservation areas: eider habitat and access by Native hunters along landfast ice. *Environ. Conserv.*, 45, 361-369, doi: 10.1017/S0376892918000103.

Mahoney, A. R., H. Eicken, and L. Shapiro, 2007: How fast is landfast sea ice? A study of the attachment and detachment of nearshore ice at Barrow, Alaska. *Cold Reg. Sci. Technol.*, 47, 233-255.

Mahoney, A., S. Gearheard, T. Oshima, and T. Qillaq, 2009: Sea ice thickness measurements from a community-based observing network. *Bull. Am. Meteorol. Soc.*, 90, 370-377.

Mahoney, A. R., H. Eicken, A. G. Gaylord, and R. Gens, 2014: Landfast sea ice extent in the Chukchi and Beaufort Seas: The annual cycle and decadal variability. *Cold Reg. Sci. Technol.*, 103, 41-56.

Masterson, D. M., 2009: State of the art of ice bearing capacity and ice construction. *Cold Reg. Sci. Technol.*, 58, 99-112.

Melling, H., 2002: Sea ice of the northern Canadian Arctic Archipelago. *J. Geophys. Res.*, 107, 3181, doi: 10.1029/2001JC001102.

Meyer, F. J., A. R. Mahoney, H. Eicken, C. L. Denny, H. C. Druckenmiller, and S. Hendricks, 2011: Mapping arctic landfast ice extent using L-band synthetic aperture radar interferometry. *Remote Sens. Environ.*, 115, 3029-3043.

Olason, E., 2016: A dynamical model of Kara Sea land-fast ice. *J. Geophys. Res.-Oceans*, 121, 3141-3158.

Petrich, C., H. Eicken, J. Zhang, J. Krieger, Y. Fukamachi, and K. I. Ohshima, 2012: Coastal landfast sea ice decay and breakup in northern Alaska: Key processes and seasonal prediction. *J. Geophys. Res.-Oceans*, 117, C02003, doi: 10.1029/2011JC007339.

Pickart, R. S., G. W. K. Moore, D. J. Torres, P. S. Fratantoni, R. A. Goldsmith, and J. Y. Yang, 2009: Upwelling on the continental slope of the Alaskan Beaufort Sea: Storms, ice, and oceanographic response. *J. Geophys. Res.-Oceans*, 114, C00A13, doi: 10.1029/2008JC005009.

Polyakov, I., G. V. Alekseev, R. V. Bekryaev, U. S. Bhatt, R. L. Colony, M. A. Johnson, V. P. Karklin, D. Walsh, and A. V. Yulin, 2003: Long-term ice variability in Arctic marginal seas. *J. Clim.*, 16, 2078-2085.

Pope, S., L. Copland, and D. Mueller, 2012: Loss of multiyear landfast sea ice from Yelverton Bay, Ellesmere Island, Nunavut, Canada. *Arct. Antarct. Alp. Res.*, 44, 210-221.

Potter, R. E., J. T. Walden, and R. A. Haspel, 1981: Design and construction of sea ice roads in the Alaskan Beaufort Sea. OTC-4080-MS. *Offshore Technology Conference*, 135-140, doi: 10.4043/4080-MS.

Reimnitz, E., and P. Barnes, 1974: Sea ice as a geologic agent on the Beaufort Sea shelf of Alaska in *The coast and shelf of the Beaufort Sea.* J. C. Reed, and J. E. Sater, Eds., Arctic Institute of North America, pp. 301-353.

Reimnitz, E., L. Toimil, and P. Barnes, 1978: Arctic continental shelf morphology related to sea-ice zonation, Beaufort Sea, Alaska. *Mar. Geol.*, 28, 179-210.

Reimnitz, E., H. Eicken, and T. Martin, 1995: Multi-year fast ice along the Taymyr Peninsula, Siberia. *Arctic*, 48, 359-367.

Selyuzhenok, V., T. Krumpen, A. Mahoney, M. Janout, and R. Gerdes, 2015: Seasonal and interannual variability of fast ice extent in the southeastern Laptev Sea between 1999 and 2013. *J. Geophys. Res.-Oceans*, 120, 7791-7806.

Selyuzhenok, V., A. Mahoney, T. Krumpen, G. Castellani, and R. Gerdes, 2017: Mechanisms of fast-ice development in the south-eastern Laptev Sea: a case study for winter of 2007/08 and 2009/10. *Polar Res.*, 36, 1411140, doi: 10.1080/17518369.2017.1411140.

Smith, T. G., and M. O. Hammill, 1981: Ecology of the ringed seal, Phoca hispida, in its fast ice breeding habitat. *Can. J. Zool.*, 59, 966-981.

Stringer, W. J., 1978: Morphology of Beaufort, Chukchi and Bering Seas near shore ice conditions by means of satellite and aerial remote sensing. *Environmental assessment of the Alaskan continental shelf. Principal investigators' annual reports for the year ending March 1978*. Vol.X: Transport, Outer Continental Shelf Environmental Assessment Program, 1-220.

Tibbles, M., J. A. Falke, A. R. Mahoney, M. D. Robards, and A. C. Seitz, 2018: An InSAR habitat suitability model to identify overwinter conditions for coregonine whitefishes in Arctic lagoons. *Trans. Am. Fish. Soc*., 147, 1167-1178, doi: 10.1002/tafs.10111.

Yu, Y., H. Stern, C. Fowler, F. Fetterer, and J. Maslanik, 2013: Interannual variability of Arctic landfast ice between 1976 and 2007. *J. Clim.*, 27, 227-243.

November 13, 2018

Authors and Affiliations

J. K. Andersen, Geological Survey of Denmark and Greenland, Copenhagen, Denmark

D. M. Anderson, Woods Hole Oceanographic Institution, Biology Department, Woods Hole, MA, USA

M. Bergmann, Alfred Wegener Institute, Helmholtz Center for Polar and Marine Research, Bremerhaven, Germany

U. S. Bhatt, Geophysical Institute, University of Alaska Fairbanks, Fairbanks, AK, USA

J. Bjerke, Norwegian Institute for Nature Research, Tromsø, Norway

J. E. Box, Geological Survey of Denmark and Greenland, Copenhagen, Denmark

L. Brown, Department of Geography, University of Toronto, Mississauga, Canada

R. Brown, Climate Research Division, Environment and Climate Change Canada, Canada

J. Cappelen, Danish Meteorological Institute, Copenhagen, Denmark

J. C. Comiso, Cryospheric Sciences Laboratory, NASA Goddard Space Flight Center, Greenbelt, MD, USA

L. W. Cooper, Chesapeake Biological Laboratory, University of Maryland Center for Environmental Science, Solomons, MD, USA

B. Decharme, Centre National de Recherches Météorologiques, France

C. Derksen, Climate Research Division, Environment and Climate Change Canada, Canada

C. Duguay, Department of Geography and Environmental Management, University of Waterloo, Canada

H. Epstein, Department of Environmental Sciences, University of Virginia, Charlottesville, VA, USA

S. Farrell, NOAA Earth System Science Interdisciplinary Center, University of Maryland, College Park, MD, USA

R. S. Fausto, Geological Survey of Denmark and Greenland, Copenhagen, Denmark

X. Fettweis, University of Liege, Liege, Belgium

B. Forbes, Arctic Centre, University of Lapland, Rovaniemi, Finland

J. A. Francis, Woods Hole Research Center, Falmouth, MA, USA

K. E. Frey, Graduate School of Geography, Clark University, Worcester, MA, USA

G. Gerdts, Alfred Wegener Institute, Helmholtz Center for Polar and Marine Research, Bremerhaven, Germany

S. Gerland, Norwegian Polar Institute, Fram Centre, Tromsø, Norway

S. Goetz, School of Informatics, Computing, and Cyber Systems, Northern Arizona University, Flagstaff, AZ, USA

J. M. Grebmeier, Chesapeake Biological Laboratory, University of Maryland Center for Environmental Science, Solomons, MD, USA

A. Gunn, CARMA, Salt Spring Island, BC, Canada

C. Haas, Alfred Wegener Institute, Helmholtz Centre for Polar and Marine Research, Bremerhaven, Germany

E. Hanna, School of Geography and Lincoln Centre for Water and Planetary Health, University of Lincoln, Lincoln, UK

I. Hanssen-Bauer, Norwegian Meteorological Institute, Blindern, Oslo, Norway

S. Helfrich, NOAA/NESDIS Center for Satellite Applications and Research, USA

S. Hendricks, Alfred Wegener Institute, Helmholtz Centre for Polar and Marine Research, Bremerhaven, Germany

R. M. Holmes, Woods Hole Research Center, Falmouth, MA, USA

M. Jeffries, Cold Regions Research and Engineering Laboratory of the Engineer Research and Development Center, U.S. Army Corps of Engineers, Hanover, NH, USA

G. Jia, Institute of Atmospheric Physics, Chinese Academy of Sciences, Beijing, China

S. -R. Karlsen, Norut Northern Research Institute, Tromsø, Norway

C. Katlein, Alfred Wegener Institute, Helmholtz Center for Polar and Marine Research, Bremerhaven, Germany

S. -J. Kim, Korea Polar Research Institute, Incheon, Republic of Korea

T. Krumpen, Alfred Wegener Institute, Helmholtz Centre for Polar and Marine Research, Bremerhaven, Germany

S. Kutz, Department of Ecosystem and Public Health, Faculty of Veterinary Medicine, University of Calgary, Calgary, AB, Canada

C. Ladd, Pacific Marine Environmental Laboratory, NOAA, Seattle, WA, USA

K. A. Lefebvre, Environmental and Fisheries Science Division, Northwest Fisheries Science Center, National Marine Fisheries Service, NOAA, Seattle, WA, USA

K. Luojus, Arctic Research Centre, Finnish Meteorological Institute, Finland

A. R. Mahoney, Geophysical Institute, University of Alaska Fairbanks, Fairbanks, AK, USA

J. W. McClelland, University of Texas at Austin, Marine Science Institute, Port Aransas, TX, USA

W. Meier, National Snow and Ice Data Center, Boulder CO, USA

T. Mote, Department of Geography, University of Georgia, Athens, GA, USA

L. Mudryk, Climate Research Division, Environment and Climate Change Canada, Canada

R. Myneni, Department of Earth and Environment, Boston University, Boston, MA, USA

E. Osborne, National Oceanic and Atmospheric Administration, Arctic Research Program, Silver Spring, MD, USA

J. E. Overland, NOAA/Pacific Marine Environmental Laboratory, Seattle, WA, USA

T. Park, Department of Earth and Environment, Boston University, Boston, MA, USA

I. Peeken, Alfred Wegener Institute, Helmholtz Center for Polar and Marine Research, Bremerhaven, Germany

D. Perovich, Thayer School of Engineering, Dartmouth College, Hanover, NH, USA

G. Phoenix, Department of Animal and Plant Sciences, University of Sheffield, Sheffield, UK

C. Polashenski, Thayer School of Engineering, Dartmouth College, Hanover, NH, USA; ERDC - CRREL, 72 Lyme Road, Hanover, NH, USA

S. Primpke, Alfred Wegener Institute, Helmholtz Center for Polar and Marine Research, Bremerhaven, Germany

M. Raynolds, Institute of Arctic Biology, University of Alaska Fairbanks, AK, USA

M. L. Richlen, Woods Hole Oceanographic Institution, Biology Department, Woods Hole, MA, USA

J. Richter-Menge, University of Alaska Fairbanks, Institute of Northern Engineering, Fairbanks, AK, USA

R. Ricker, Alfred Wegener Institute, Helmholtz Centre for Polar and Marine Research, Bremerhaven, Germany

D. E. Russell, CircumArctic Rangifer Monitoring and Assessment (CARMA) Network, Yukon College, Whitehorse, YT, Canada

A. I. Shiklomanov, University of New Hampshire, Durham, NH, USA; Arctic and Antarctic Research Institute, St. Petersburg, Russia

C. J. P. P. Smeets, Institute for Marine and Atmospheric Research Utrecht, Utrecht University, Utrecht, The Netherlands

R. G. M. Spencer, Florida State University, Tallahassee, FL, USA

L. V. Stock, Cryospheric Sciences Laboratory, NASA Goddard Space Flight Center, Greenbelt, MD, USA

A. Suslova, Woods Hole Research Center, Falmouth, MA, USA

S. E. Tank, University of Alberta, Edmonton, AB, Canada

M. Tedesco, Lamont Doherty Earth Observatory of Columbia University, Palisades, NY, USA; NASA Goddard Institute of Space Studies, New York, NY, USA

M. Tekman, Alfred Wegener Institute, Helmholtz Center for Polar and Marine Research, Bremerhaven, Germany

R. L. Thoman, NOAA, National Weather Service, Alaska Region, Anchorage, AK, USA

M. -L. Timmermans, Yale University, New Haven, CT, USA

H. Tømmervik, Norwegian Institute for Nature Research, Tromsø, Norway

M. Tretiakov, Arctic and Antarctic Research Institute, St. Petersburg, Russia

M. Tschudi, Aerospace Engineering Sciences, University of Colorado, Boulder, CO, USA

D. van As, Geological Survey of Denmark and Greenland, Copenhagen, Denmark

R. S. W. van de Wal, Institute for Marine and Atmospheric Research Utrecht, Utrecht University, Utrecht, The Netherlands

D. Walker, Institute of Arctic Biology, University of Alaska Fairbanks, AK, USA

J. E. Walsh, International Arctic Research Center, University of Alaska Fairbanks, Fairbanks, AK, USA

M. Wang, Joint Institute for the Study of the Atmosphere and Ocean, University of Washington, Seattle, WA, USA

M. Webster, NASA Goddard Space Flight Center, Greenbelt, MD, USA